NOTE TO USERS

ELEMENTAL PERIODIC SOLUTIONS OF THE CIRCULAR RESTRICTED 3-BODY PROBLEM

Volodymyr Romanov

A Thesis

in the Department of Computer Science

Presented in Partial Fulfilment of the Requirements

for the Degree of Master of Computer Science

Concordia University

Montréal, Quebéc, Canada

June 29, 2005

Your file Votre référence
ISBN: 0-494-10295-0
Our file Notre référence
ISBN: 0-494-10295-0

ABSTRACT

Elemental Periodic Solutions of the Circular Restricted 3-Body Problem

Volodymyr Romanov

In this thesis, the continuation and bifurcation software AUTO is used to investigate elemental periodic orbits, certain secondary bifurcating orbit families, and homoclinic orbits, associated with the libration points of the Circular Restricted 3-Body Problem, for values of the mass ratio between 0 and 0.5. Periodic solution families for representative values of the mass ratio, and corresponding bifurcation diagrams, are studied in detail.

To understand the solution structure of the Circular Restricted 3-Body Problem better, a new data visualization package, DR Orbits, has been developed. It reads AUTO data files and creates solution diagrams. The package may be useful for space mission design. This new graphics package has good rendering speed, flexibility, and display quality. A user-friendly interface makes DR Orbits easy to use.

Acknowledgments

I would like to express my sincerest appreciation to my supervisor professor Eusebius J. Doedel for his support, guidance, patience, and valuable insight, which have made the completion of my thesis possible.

Contents

List of Figures

List of Tables

Chapter 1

Introduction

This thesis presents results obtained for a famous classical problem of Celestial Mechanics: the Circular Restricted 3-Body Problem (CR3BP). The CR3BP can be traced back to the time of Sir Isaac Newton. This problem has not been solved completely, despite the efforts of many famous mathematicians such as G.-L. Lagrange, K. Jacobi, H. Poincaré, G. Birkhoff, *etc.*, who have spent much time investigating it. In more recent years, the problem has attracted special interest in connection with satellite mission design. Certain periodic orbits of the CR3BP are very suitable for this design.

We calculated numerically all the primary periodic orbit families associated with the libration points, as well as some secondary periodic orbit families bifurcating from the primary ones, for all possible values of the mass ratio μ. To achieve this goal, we used AUTO, an established tool for bifurcation analysis of ordinary differential equations.

1.1 Organization of the thesis

This thesis is organized as follows:

Chapter 2. A brief description of the general N-Body Problem of Celestial Mechanics, including the particular case of the 3-Body Problem, is presented at the beginning of Chapter 2. We also present a short review of analytical and numerical solutions (classical and modern) of the general problem and of some

particular cases. A review of the CR3BP in this chapter includes the analysis of the system of differential equations, the stability of its libration points, its primary periodic solutions, and its application to satellite mission design.

Chapter 3. This chapter contains a review of the numerical continuation method used in AUTO for ODE bifurcation analysis. We describe briefly how this method can be used to study the global solution behavior of dynamical systems, including periodic solutions, their bifurcations, and homoclinic orbits. Use of continuation to compute the families of periodic orbits that emanate from a libration point in the CR3BP is also described.

Chapter 4. This chapter presents the results of our numerical investigation of the CR3BP for the Earth-Moon system for $\mu = 0.01215$. We give a detailed bifurcation diagram of this system and brief descriptions and images of many types of orbit families, namely, "elemental" periodic orbits associated with the five libration points, *i.e.*, the families of periodic orbits that bifurcate from these libration points, and certain secondary bifurcating families.

Chapter 5. This chapter presents the results of our numerical investigation of the CR3BP for all values of the mass ratio μ. For this case, we also give an overview of our results for "elemental" periodic orbits. We also consider homoclinic orbits that are limits of families of elemental periodic orbits. Furthermore, using extended boundary value systems, we determine how certain branch points in the CR3BP depend on the value of the mass ratio μ. This allows us to give a rather complete classification of all primary families and of some secondary bifurcating families for all values of μ in the interval $(0 < \mu < 0.5)$. For completeness, our description includes various families of periodic orbits and branch points whose existence is well-known for certain specific values of the value of μ.

Chapter 6. This chapter contains a description of the design and the development of the new program, DR Orbits, for the visualization of periodic orbit families of the CR3BP.

Chapter 7. This chapter contains concluding remarks and gives some directions for

future investigation.

Appendices. Appendix 1 contains the user manual for the DR Orbits program, while Appendix 2 explains briefly how one can use AUTO for computing periodic solutions of the CR3BP.

Chapter 2

Elements of Celestial Mechanics and Space Dynamics

2.1 The N-Body Problem

The N-body Problem and its particular cases, the 3-Body Problem and the Circular Restricted 3-Body Problem, are described in detail in many books on Classical Mechanics, Celestial Mechanics, and Space Dynamics: [92, 93, 112, 86, 43, 94, 5, 59, 102, 53, 22, 113, 110, 100], and in books, dedicated to these problems exclusively [107, 80, 79, 14, 61, 79]. In this chapter we present a brief review of the N-body problem; this is needed for a better understanding of the main results of this thesis.

Suppose we have a system of N bodies (material points or centro-symmetric spherical rigid bodies having small radii) with masses $m_1, m_2, ..., m_N$, interacting according to the Newtonian law of gravity. If there is an inertial frame of reference $O\xi\eta\zeta$, having orthogonal axes $O\xi$, $O\eta$, and $O\zeta$ with an arbitrarily located origin, such that $\mathbf{r}_i = (\xi_i, \eta_i, \zeta_i)$ is a radius vector of the i-th body with mass m_i $(i = 1, 2, ..., N)$, then the distance between the bodies m_i and m_j can be written as

$$r_{ij} \;=\; \| \mathbf{r}_i - \mathbf{r}_j \| \;=\; [(\xi_i - \xi_j)^2 \;+\; (\eta_i - \eta_j)^2 \;+\; (\zeta_i - \zeta_j)^2]^{1/2} \; . \qquad (2.1)$$

The gravitational force exerted on the mass m_i by another one, m_j, is

$$\mathbf{f}_{ij} \;=\; G \; \frac{m_i m_j}{r_{ij}^2} \; \frac{\mathbf{r}_i - \mathbf{r}_j}{r_{ij}} \; , \qquad (2.2)$$

where G is the gravitational constant ($G \approx 6.67259 \cdot 10^{-11} m^3 s^{-2} kg^{-1}$).

Using Newton's second law, we can write a system of N differential equations for the motion of the bodies m_i ($i = 1, 2, ..., N$), moving in the gravitational field of the other $N - 1$ bodies, namely,

$$\frac{d^2\mathbf{r}_i}{dt^2} = -G \sum_{\substack{j=1 \\ j \neq i}}^{N} m_j \frac{\mathbf{r}_i - \mathbf{r}_j}{r_{ij}^3} \ . \tag{2.3}$$

Equation (2.3) is a system of $3N$ second order differential equations.

The goal of the "solution" of the system (2.3) is to determine the motion of each of the N bodies; in other words, the dependence of the coordinates of each body on time t:

$$\mathbf{r}_i = \mathbf{r}_i(t) \ , \tag{2.4}$$

when the coordinates $\mathbf{r}_i$ and the velocities $\mathbf{v}_i \equiv \dfrac{d\mathbf{r}_i}{dt}$ of all the bodies are known at a starting time $t = t_0$:

$$\mathbf{r}_{i0} = \mathbf{r}_i(t_0), \quad \mathbf{v}_{i0} = \left.\frac{d\mathbf{r}_i}{dt}\right|_{t=t_0} \ , \tag{2.5}$$

$i = 1, 2, ..., N$. Having a solution of Eq.(2.3), with starting conditions (2.5), we can determine any characteristic of our N-body system (coordinates, velocities, accelerations, energies, *etc.*) at any moment of time. Below we will describe general properties of the system (2.3), and list some useful relations.

The system (2.3) can be rewritten using the gravitational potential function U of the system of N masses [43, 59]:

$$U = \frac{1}{2} G \sum_{i=1}^{N} \sum_{\substack{j=1 \\ j \neq i}}^{N} \frac{m_i m_j}{r_{ij}} \ . \tag{2.6}$$

Since

$$\nabla_i U = -G m_i \sum_{j=1}^{N} m_j \frac{\mathbf{r}_i - \mathbf{r}_j}{r_{ij}^3} \ , \tag{2.7}$$

where gradient vector is defined as

$$\nabla_i \equiv \left(\mathbf{i} \frac{\partial}{\partial \xi_i} \ , \ \mathbf{j} \frac{\partial}{\partial \eta_i} \ , \ \mathbf{k} \frac{\partial}{\partial \zeta_i} \right) , \tag{2.8}$$

and **i**, **j**, **k** are orthonormal vectors coinciding with the axes of the inertial frame of reference $O\xi, O\eta$, and $O\zeta$, resp., we can rewrite the system (2.3) as

$$m_i \frac{d^2\mathbf{r}_i}{dt^2} = \nabla_i U \ , \tag{2.9}$$

where $i = 1, 2, ..., N$. This is the Newtonian representation of the N-Body Problem. These equations can also be rewritten in canonical or Hamiltonian form, if we define generalized coordinate vectors and linear momenta as

$$\mathbf{q}_i \equiv \mathbf{r}_i \ , \quad \mathbf{p}_i \equiv m_i \frac{d\mathbf{r}_i}{dt} \ , \tag{2.10}$$

and the Hamiltonian

$$H \equiv \frac{1}{2} \sum_{i=1}^{N} \frac{\mathbf{p}^2{}_i}{m_i} - U \ , \tag{2.11}$$

where the gravitational potential function U is written as:

$$U = \frac{1}{2} \, G \sum_{i=1}^{N} \sum_{\substack{j=1 \\ j \neq i}}^{N} \frac{m_i m_j}{||\mathbf{q}_i - \mathbf{q}_j||} \ , \tag{2.12}$$

$i = 1, 2, ..., N$. Then the Hamiltonian equations for the N-Body Problem are

$$\begin{aligned} \frac{d\mathbf{q}_i}{dt} &= \frac{\partial H}{\partial \mathbf{p}_i} \ , \\ \\ \frac{d\mathbf{p}_i}{dt} &= -\frac{\partial H}{\partial \mathbf{q}_i} \ . \end{aligned} \tag{2.13}$$

The Hamiltonian H, which is the total energy of the N-body system, is preserved:

$$\frac{dH}{dt} \ = \ \sum_{i=1}^{N} \left(\frac{\partial H}{\partial \mathbf{q}_i} \frac{d\mathbf{q}_i}{dt} + \frac{\partial H}{\partial \mathbf{p}_i} \frac{d\mathbf{p}_i}{dt} \right) \ = \ \sum_{i=1}^{N} \left(\frac{\partial H}{\partial \mathbf{q}_i} \frac{\partial H}{\partial \mathbf{p}_i} + \frac{\partial H}{\partial \mathbf{p}_i} \left(-\frac{\partial H}{\partial \mathbf{q}_i} \right) \right) \ \equiv \ 0 \ . \tag{2.14}$$

The potential function U of Eq. (2.6) depends only on mutual distances between the bodies, (*i.e.*, on the differences between the coordinates of each pair of bodies); it does not depend directly on their coordinates. This means [43, 59] that

$$\sum_{i=1}^{N} \nabla_i U \ = \ 0 \ . \tag{2.15}$$

We can rewrite Eq.(2.15) using Eq.(2.9), as

$$\sum_{i=1}^{N} m_i \frac{d^2\mathbf{r}_i}{dt^2} \ = \ 0 \ , \tag{2.16}$$

Equations (2.16) are easily integrated, and we have three integrals, one for each of three projections on the axes:

$$\sum_{i=1}^{N} m_i \frac{d\mathbf{r}_i}{dt} = \mathbf{a}_1 , \tag{2.17}$$

where $\mathbf{a}_1 = (a_{11}, a_{12}, a_{13})$ is the vector of constants of the first integration. Integrating once more, we obtain

$$\sum_{i=1}^{N} m_i \mathbf{r}_i = \mathbf{a}_1 t + \mathbf{a}_2 , \tag{2.18}$$

where $\mathbf{a}_2 = (a_{21}, a_{22}, a_{23})$ is the vector of constants of the second integration. The radius vector $\mathbf{R} = (\Xi, H, Z)$ of the barycenter of the system of the N masses is

$$\mathbf{R} = \frac{1}{M} \sum_{i=1}^{N} m_i \mathbf{r}_i , \tag{2.19}$$

and we have

$$M\mathbf{R} = \mathbf{a}_1 t + \mathbf{a}_2 . \tag{2.20}$$

The velocity of the barycenter is also constant:

$$V = \left\| \frac{d\mathbf{R}}{dt} \right\| = \frac{1}{M} (a_{11}^2 + a_{12}^2 + a_{13}^2)^{1/2} , \tag{2.21}$$

and the trajectory of the barycenter is the following straight line

$$\frac{M\Xi - a_{21}}{a_{11}} = \frac{MH - a_{22}}{a_{12}} = \frac{MZ - a_{23}}{a_{13}} . \tag{2.22}$$

Thus, we can conclude that the barycenter of the N masses, interacting via the Newtonian gravitational law, moves in space with constant velocity (2.21) along a straight line (2.22).

Any rotation of the axes of the inertial frame of reference does not change the distances between the bodies of the N masses, so the potential function U does not depend on rotation of the frame either. Let us take an inertial frame of reference $O\xi'\eta'\zeta'$, with the same origin as $O\xi\eta\zeta$, such that axes $O\zeta$ and $O\zeta'$ coincide, but other axes of $O\xi'\eta'\zeta'$ are rotated around the axes $O\zeta$ at a fixed angle φ_0. (The frame $O\xi'\eta'\zeta'$ is inertial so it is not rotating permanently: it is simply rotated over a constant angle.) Thus, the transition from one frame of reference to another one can be written as

$$\begin{aligned} \xi_i' &= \xi_i \cos\varphi_0 - \eta_i \sin\varphi_0 , \\ \eta_i' &= \xi_i \sin\varphi_0 + \eta_i \cos\varphi_0 , \\ \zeta_i' &= \zeta_i . \end{aligned} \tag{2.23}$$

Then we have

$$\frac{\partial U}{\partial \varphi_0} = \sum_{i=1}^{N} \frac{\partial U}{\partial \xi_i'} \frac{d\xi_i'}{d\varphi_0} + \sum_{i=1}^{N} \frac{\partial U}{\partial \eta_i'} \frac{d\eta_i'}{d\varphi_0} + \sum_{i=1}^{N} \frac{\partial U}{\partial \zeta_i'} \frac{d\zeta_i'}{d\varphi_0} = 0. \tag{2.24}$$

However, from (2.23)

$$\frac{d\xi_i'}{d\varphi_0} = -\eta_i', \quad \frac{d\eta_i'}{d\varphi_0} = \xi_i', \quad \frac{d\zeta_i'}{d\varphi_0} = 0. \tag{2.25}$$

we can rewrite (2.24) as

$$\sum_{i=1}^{N} \left(\xi_i' \frac{\partial U}{\partial \eta_i'} - \eta_i' \frac{\partial U}{\partial \xi_i'} \right) = 0. \tag{2.26}$$

Considering rotation around the other two axes $O\xi$ and $O\eta$, and using (2.9), we can generalize (2.26) as

$$\sum_{i=1}^{N} \left(\mathbf{r}_i \times \frac{d^2 \mathbf{r}_i}{dt^2} \right) = 0 , \tag{2.27}$$

where $\times$ denotes the cross product. Equation (2.27) can be integrated once:

$$\sum_{i=1}^{N} \left(\mathbf{r}_i \times \frac{d\mathbf{r}_i}{dt} \right) = \mathbf{a}_3, \tag{2.28}$$

where $\mathbf{a}_3 = (a_{31}, a_{32}, a_{33})$ is a vector of integration constants. Equation (2.28) represents the three integrals of conservation of the angular momentum of the system of N masses.

Finally, if we multiply Eq.(2.3) by $d\mathbf{r}_i/dt$, we obtain

$$\sum_{i=1}^{N} m_i \left(\frac{d^2 \mathbf{r}_i}{dt^2} \frac{d\mathbf{r}_i}{dt} \right) = \sum_{i=1}^{N} \left((\nabla_i U) \frac{d\mathbf{r}_i}{dt} \right) , \tag{2.29}$$

or

$$\frac{1}{2} \frac{d}{dt} \sum_{i=1}^{N} m_i \left(\frac{d\mathbf{r}_i}{dt} \right)^2 = \frac{dU}{dt} . \tag{2.30}$$

After integration of Eq.(2.30), we obtain

$$T = U + C , \tag{2.31}$$

where

$$T = \sum_{i=1}^{N} m_i \left(\frac{d\mathbf{r}_i}{dt} \right)^2 = \sum_{i=1}^{N} m_i \mathbf{v}_i^2 \tag{2.32}$$

is the kinetic energy of the system of N masses, and C is the energy constant (the constant of integration). Equation (2.31) shows that the sum of the kinetic and the

potential energy of the system of N masses is a constant (the *conservation of energy* law).

Therefore, we can conclude that for the $6N$ equations represented by Eq.(2.3), for the general N-Body Problem, we have ten integrals (six integrals of motion of the barycenter, three integrals of the conservation of the angular momentum, and one integral for the conservation of energy). Thus, the full number of equations in Eq. (2.3) can be reduced by ten, to a system of $6N-10$ second order differential equations [59, 43]. This reduction procedure is useful for analysis of the N-Body Problem for small N, especially for the case $N = 3$. Unfortunately, general integration of Eq. (2.3) has not been done for any $N \geq 3$; moreover, the mathematical difficulties of the N-Body Problem grow rapidly when N is increased. At the same time, there are many numerical and combined analytical-numerical methods which give an approximate solution of Eq. (2.3), *i.e.*, the coordinates and the velocities of the N bodies for any time interval with acceptable accuracy for use in Astronomy and Space Dynamics [59, 43].

2.2 The 3-Body Problem

For the two special cases $N = 1$ and $N = 2$, the N-Body Problem was solved completely about 300 years ago by Sir Isaac Newton, who based his research on the previous work of Galileo Galilei, Johannes Kepler, and others. Modern versions of Newton's solution of 1-Body and 2-Body Problems can be found in at most any book on General Physics or Classical Mechanics. However, the next step, the 3-Body Problem, has required titanic efforts of the greatest mathematicians of the post-Newtonian Age, and so far it has not been solved completely. Below we will discuss briefly some specific features of this problem.

If we have only three masses m_1, m_2, and m_3, with radius vectors $\mathbf{r}_1 = (\xi_1, \eta_1, \zeta_1)$, $\mathbf{r}_2 = (\xi_2, \eta_2, \zeta_2)$, and $\mathbf{r}_3 = (\xi_3, \eta_3, \zeta_3)$, resp., we can rewrite Eq.(2.3) explicitly as nine

second order differential equations of order 18:

$$\begin{aligned}
\frac{d^2\mathbf{r}_1}{dt^2} &= -Gm_2\frac{\mathbf{r}_1-\mathbf{r}_2}{r_{12}^3}+Gm_3\frac{\mathbf{r}_1-\mathbf{r}_3}{r_{13}^3}\,,\\
\frac{d^2\mathbf{r}_2}{dt^2} &= -Gm_1\frac{\mathbf{r}_2-\mathbf{r}_1}{r_{12}^3}+Gm_3\frac{\mathbf{r}_2-\mathbf{r}_3}{r_{23}^3}\,,\\
\frac{d^2\mathbf{r}_3}{dt^2} &= -Gm_1\frac{\mathbf{r}_3-\mathbf{r}_1}{r_{13}^3}+Gm_2\frac{\mathbf{r}_3-\mathbf{r}_2}{r_{23}^3}\,,
\end{aligned} \tag{2.33}$$

where r_{ij}, for $i,j=1,2,3$, is given in Eq.(2.1). The six integrals of motion of the barycenter of the three masses are

$$\begin{aligned}
m_1\frac{d\mathbf{r}_1}{dt}+m_2\frac{d\mathbf{r}_2}{dt}+m_3\frac{d\mathbf{r}_3}{dt} &= \mathbf{a}_1,\\
m_1\mathbf{r}_1+m_2\mathbf{r}_2+m_3\mathbf{r}_3 &= \mathbf{a}_1 t+\mathbf{a}_2,
\end{aligned} \tag{2.34}$$

and the three integrals of conservation of angular momentum are given by

$$m_1\left(\mathbf{r}_1\times\frac{d\mathbf{r}_1}{dt}\right)+m_2\left(\mathbf{r}_2\times\frac{d\mathbf{r}_2}{dt}\right)+m_3\left(\mathbf{r}_3\times\frac{d\mathbf{r}_3}{dt}\right) = \mathbf{a}_3. \tag{2.35}$$

Note that the plane passing through the barycenter, perpendicularly to the vector $\mathbf{a}$, preserves its orientation in space. This plane is called the Laplace invariant plane.

The energy integral of the system of three masses is

$$\frac{1}{2}m_1\mathbf{v}_1^2+\frac{1}{2}m_2\mathbf{v}_2^2+\frac{1}{2}m_3\mathbf{v}_3^2 = U+C, \tag{2.36}$$

where

$$U = G\left(\frac{m_1m_2}{r_{12}}+\frac{m_1m_3}{r_{13}}+\frac{m_2m_3}{r_{23}}\right). \tag{2.37}$$

The ten integrals (2.34) - (2.36) allow to reduce the full order of the Eqs.(2.33) by 10 and to solve the system of the eighth order. In practice, only the six first integrals are used to reduce the order of the system by six. It is easy to switch to the barycentric frame of reference $O'\xi'\eta'\zeta'$, with the origin O' at the barycenter of the three masses, which is defined in the old frame $O\xi\eta\zeta$ by the equation

$$m_1\mathbf{r}_1'+m_2\mathbf{r}_2'+m_3\mathbf{r}_3' = 0\,, \tag{2.38}$$

and we can exclude the coordinates of one mass from Eqs.(2.33):

$$\mathbf{r}_1' = -\frac{1}{m_1}(m_2\mathbf{r}_2'+m_3\mathbf{r}_3'), \tag{2.39}$$

and rewrite Eq.(2.33) in the barycentric frame as a system of six scalar differential equations of second order

$$\begin{aligned}
\frac{d^2\xi_2'}{dt^2} &= -G\frac{(m_1+m_2)\xi_2' + m_3\xi_3'}{R_{21}^3} + Gm_3\frac{(\xi_3'+\xi_2')}{R_{23}^3}\ , \\
\frac{d^2\eta_2'}{dt^2} &= -G\frac{(m_1+m_2)\eta_2' + m_3\eta_3'}{R_{21}^3} + Gm_3\frac{(\eta_3'+\eta_2')}{R_{23}^3}\ , \\
\frac{d^2\zeta_2'}{dt^2} &= -G\frac{(m_1+m_2)\zeta_2' + m_3\zeta_3'}{R_{21}^3} + Gm_3\frac{(\zeta_3'+\zeta_2')}{R_{23}^3}\ , \\
\frac{d^2\xi_3'}{dt^2} &= -G\frac{(m_1+m_3)\xi_2' + m_2\xi_3'}{R_{31}^3} + Gm_3\frac{(\xi_3'+\xi_2')}{R_{23}^3}\ , \\
\frac{d^2\eta_3'}{dt^2} &= -G\frac{(m_1+m_3)\eta_2' + m_2\eta_3'}{R_{31}^3} + Gm_3\frac{(\eta_3'+\eta_2')}{R_{23}^3}\ , \\
\frac{d^2\zeta_3'}{dt^2} &= -G\frac{(m_1+m_3)\zeta_2' + m_2\zeta_3'}{R_{31}^3} + Gm_3\frac{(\zeta_3'+\zeta_2')}{R_{23}^3}\ ,
\end{aligned} \tag{2.40}$$

where the relative distances between the masses are defined by

$$\begin{aligned}
R_{21} &= \left[\left(\frac{(m_1+m_2)\xi_2' + m_3\xi_3'}{m_1}\right)^2 + \left(\frac{(m_1+m_2)\eta_2' + m_3\eta_3'}{m_1}\right)^2 + \right. \\
&\quad \left.\left(\frac{(m_1+m_2)\zeta_2' + m_3\zeta_3'}{m_1}\right)^2\right]^{1/2}\ , \\
R_{31} &= \left[\left(\frac{(m_1+m_3)\xi_3' + m_2\xi_2'}{m_1}\right)^2 + \left(\frac{(m_1+m_3)\eta_3' + m_2\eta_2'}{m_1}\right)^2 + \right. \\
&\quad \left.\left(\frac{(m_1+m_3)\zeta_3' + m_2\zeta_2'}{m_1}\right)^2\right]^{1/2}\ ,
\end{aligned} \tag{2.41}$$

$$R_{23} = [(\xi_3'-\xi_2')^2 + (\eta_3'-\eta_2')^2 + (\zeta_3'-\zeta_2')^2]^{1/2}\ .$$

Equations (2.40) have only four first integrals: three integrals of angular momentum (2.35) and one integral of energy (2.36). These integrals can be rewritten in the barycentric frame using Eq. (2.39). Other ways to decrease the order of Eq.(2.33) of the 3-Body Problem are described in books on Celestial Mechanics, classical and

as well as recent: [92, 93, 112] and [86, 43, 94, 5]), Spacecraft Dynamics [99, 53, 22, 100, 110, 113, 59, 102], and in books dedicated specifically to the 3-Body Problem [79]. Usually, methods for decreasing the order of Eq.(2.3) or Eq.(2.33) are useful for theoretical investigations of the N-Body Problem or for constructing approximations to it [86, 43].

A review of classical and modern results, questions, and hypotheses for the 3-Body Problem is given in [79]. This book described the achievements of the last century and discusses conjectures and possible future work on stability, singularities, regularization, periodic motions, asymptotic behavior, *etc.*, of the 3-Body system, as described by Eq.(2.33).

2.3 Analytical and numerical solutions of the N-Body Problem

Unfortunately, even for the 3-Body Problem we do not know any other integrals than the ten classical first integrals. At the end of the nineteenth century, Henri Poincaré [92, 93] proved that a general solution of the 3-Body Problem cannot be expressed in terms of simple transcendental functions of coordinates and velocities of the bodies, and Eqs.(2.33) cannot be integrated completely. Thus we cannot obtain a general solution of the Eqs.(2.33). However, as long ago as 1772, J.-L. Lagrange noted that the 3-Body problem can be solved for some simple cases. The first case is the motion of three bodies of arbitrary masses along a straight line; such motions are called collinear. This problem was solved by L. Euler earlier in 1767, and it is called Euler's case of the 3-Body Problem. We can describe Euler's solution as a motion of three arbitrary masses along a Keplerian orbit, such that the three bodies lie on a straight line at all times (Fig. 2.1, left). This configuration is invariant under permutation of the bodies, so we can find three solutions for Euler's case. In 1772, Lagrange solved the second case, where the three bodies form an equilateral triangle and move with respect to each other and with respect to the barycenter along Keplerian orbits (Fig. 2.1, right). The equilateral configuration is preserved during the motion. Also, for this case we have two solutions obtained by permutation of any two bodies. Therefore,

only five partial analytical solutions of the 3-Body Problem are known so far. There is also the case where one mass is much larger than other two masses: this problem can be reduced to two independent 2-Body Problems, where each of the two has an exact solution.

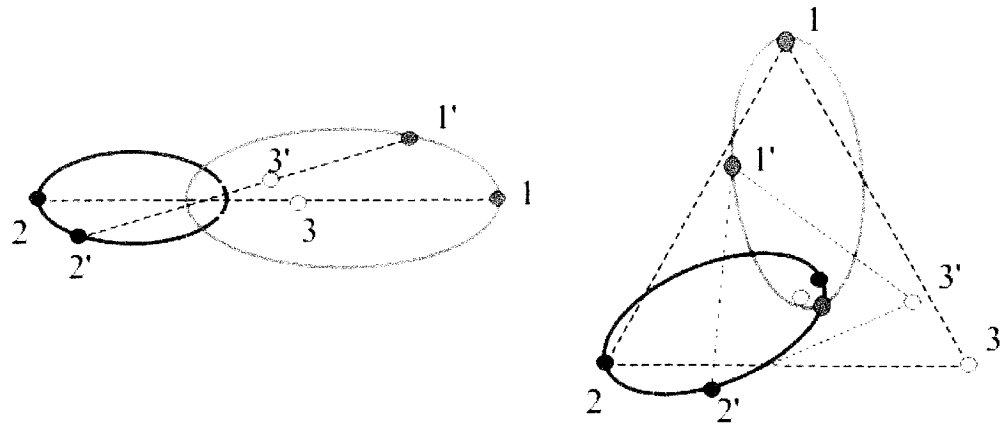

Figure 2.1: Euler (Left) and Lagrange (Right) solutions of the 3-Body Problem. **Left:** The bodies move along an elliptical Keplerian orbit, such that all three lie on a straight line. **Right:** Three bodies moving along ellipses form at each moment of time an equilateral triangle. The numbers 1, 2, and 3 and 1', 2', and 3' show the configurations of the three bodies at different moments of time.

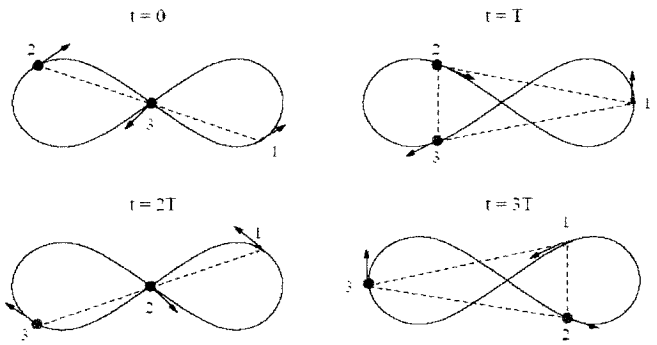

Figure 2.2: The Chenciner-Montgomery orbit. T is 1/12 of the full period. (From [17]).

In 1912, K. Sundman found a solution of the N-Body Problem as an infinite con-

verging series. Unfortunately, the rate of convergence of these series is not sufficient, even for modern supercomputers, to evaluate the series to appropriate accuracy. In the 1990's, W. Q. Dong tried to improve convergence of the series representing solutions of the N-Body Problem, but her series still converge slowly [59, 43].

At the end of the 1990's, new types of periodic solutions of the N-Body Problem were found. In [19], A. Chenciner and R. Montgomery proved the existence of a planar figure-8 periodic solution for the 3-Body Problem, where the bodies have equal masses: $m_1 = m_2 = m_3$ (Fig. 2.2). The proof in [19, 17] uses variational arguments: after certain reductions the action integral is minimized over a restricted set of symmetric arcs. Further, C. Simó ([104, 105, 106]) numerically computed this remarkable solution with high accuracy and confirmed stability of this solution. Simó also discovered many other single-curve planar periodic solutions for the N-Body Problem, with N as high as 799 [18]. He called these solutions "choreographies" (Fig. 2.3). In [40], E. J. Doedel with co-authors generalized computations for the 3-Body Problem for different masses: the mass of one body varied from 0 to 1, while the other two bodies have masses 1. Such three-dimensional solutions, as dependent on the mass of the third particle, are represented in Fig. 2.4.

2.4 The Circular Restricted 3-Body Problem

2.4.1 The system of differential equations in the rotating frame

In many practical problems of Celestial Mechanics, and especially in Satellite Dynamics, the mass of one of three bodies is very small compared to the other two masses; for example, the problem of the motion of a comet under the gravitational forces of the Sun and Jupiter in the solar system, the problem of the motion of a satellite in the Earth-Moon system, *etc.* In such cases, the small or infinitesimal mass has no perceptible influence on the two large masses. If so, then we can neglect the terms in (2.33) that have the infinitesimal mass as a factor. This gives an approximate equation for the 3-Body Problem describing the motion of a zero-mass body under the gravitational force of two bodies of arbitrary mass. This problem was referred to by H. Poincaré as *the Restricted 3-Body Problem* [92, 93].

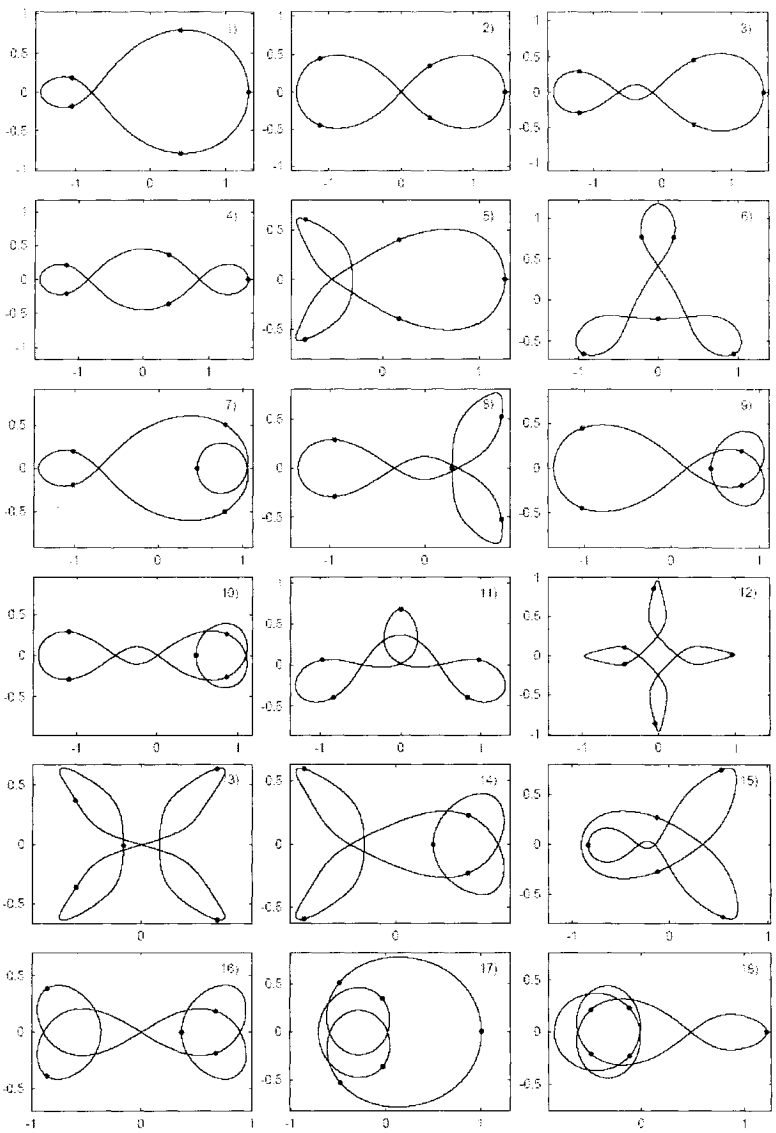

Figure 2.3: Different Simó choreographies for $N = 5$. (From [18])

Differential equations for this problem can be obtained directly from Eq. (2.33), if we take, for example, $m_3 \equiv 0$. In this case, it is easy to show that the system (2.33) splits into two independent systems. One describes the Keplerian motion of two bodies of finite masses m_1 and m_2, and the other defines the motion of the infinitesimal body, having zero mass, formerly m_3, in the gravitational field of two finite masses. The bodies m_1 and m_2 in the Restricted 3-Body Problem are called

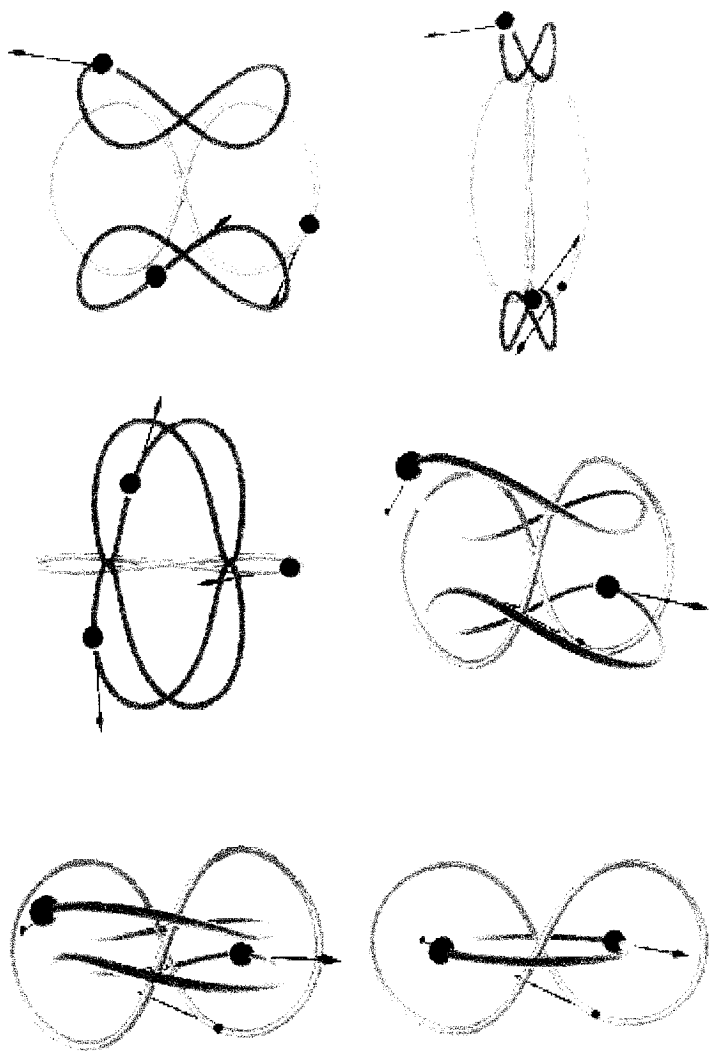

Figure 2.4: Non-planar periodic solutions of the 3-Body problem. (From [40])

the primary bodies, or *primaries*.

Suppose that the reference frame $O\xi\eta\zeta$ has the origin at the barycenter of the primaries, and that the plane $O\xi\eta$, coincides with the plane of their Keplerian motion (Fig. 2.5). Suppose that the infinitesimal body δm has coordinates (ξ, η, ζ), and the two primaries m_1 and m_2 have coordinates $(\xi_1, \eta_1, 0)$ and $(\xi_2, \eta_2, 0)$, resp. Note that the primaries will remain in the plane $O\xi\eta$ at all time. Thus, we have a system of

three differential equations:

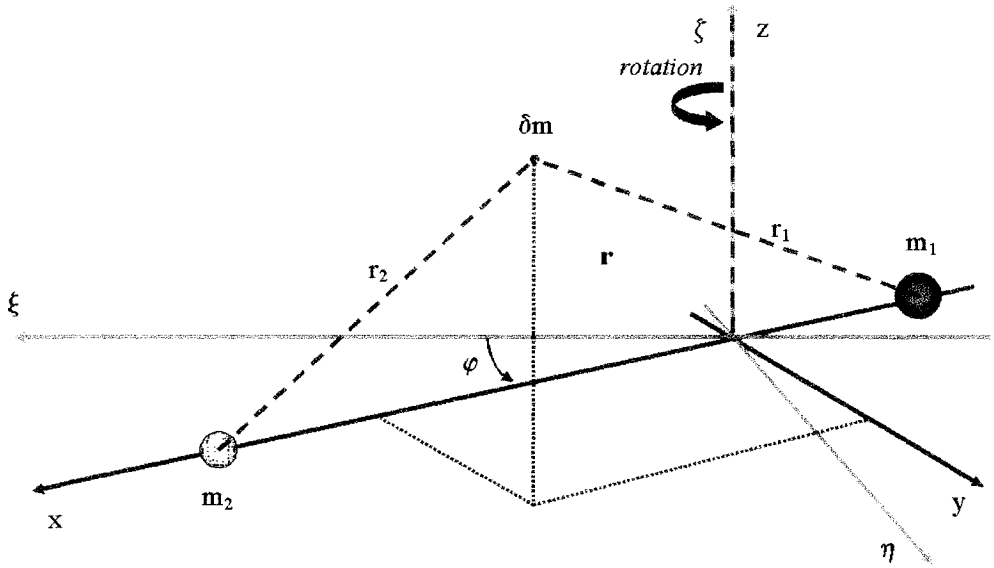

Figure 2.5: Reference frames and positions of the bodies for the CR3BP.

$$\begin{aligned}
\frac{d^2\xi}{dt^2} &= -Gm_1\frac{\xi-\xi_1}{r_1^3} - Gm_2\frac{\xi-\xi_2}{r_2^3}\ , \\
\frac{d^2\eta}{dt^2} &= -Gm_1\frac{\eta-\eta_1}{r_1^3} - Gm_2\frac{\eta-\eta_2}{r_2^3}\ , \\
\frac{d^2\zeta}{dt^2} &= -Gm_1\frac{\zeta}{r_1^3} - Gm_2\frac{\zeta}{r_2^3}\ ,
\end{aligned} \tag{2.42}$$

where the mutual distances are

$$\begin{aligned}
r_1 &= [(\xi-\xi_1)^2 + (\eta-\eta_1)^2 + \zeta^2]^{1/2}\ , \\
r_2 &= [(\xi-\xi_2)^2 + (\eta-\eta_2)^2 + \zeta^2]^{1/2}\ .
\end{aligned} \tag{2.43}$$

The coordinates of the primaries are defined by equations

$$\begin{aligned}
(m_1+m_2)\xi_1 &= -m_2 r_0\cos\varphi\ , \\
(m_1+m_2)\eta_1 &= -m_2 r_0\sin\varphi\ , \\
(m_1+m_2)\xi_1 &= m_1 r_0\cos\varphi\ , \\
(m_1+m_2)\xi_1 &= m_1 r_0\sin\varphi\ ,
\end{aligned} \tag{2.44}$$

where $r_0 = r_0(t)$ is the distance between the primaries, and $\varphi = \varphi(t)$ is the angle between direction from m_1 to m_2 and the positive direction of the axis $O\xi$. The values of r_0 and φ are well-known functions [43, 59] of the Keplerian motion of primaries. For example, the Keplerian orbit of the mass m_2 is given by equation

$$r_0 = \frac{p}{1 + e\cos\varphi}\,, \tag{2.45}$$

where p is the parameter of the conic section [43] of the Keplerian orbit, and e is its excentricity. Such an orbit can be a circle ($e = 0$), an ellipse ($e < 0$), a parabola ($e = 1$), or a hyperbola ($e > 1$), depending on the value of the starting velocity of the primary m_2 with respect to m_1. Therefore, in Celestial Mechanics the next three cases can be discerned [1] :

1. The Hyperbolic Restricted 3-Body Problem, for which the orbit of m_2 is a hyperbola with focus at m_1.

2. The Elliptical Restricted 3-Body Problem, where the mass m_2 describes an ellipse around m_1 with focus at m_1.

3. The CR3BP, for which the mass m_2 has a strictly circular orbit, centered at m_1.

In this thesis, we limit ourselves to the classical CR3BP. Thus, we consider the case where the primary m_2 describes a circle around m_1, with a constant angular velocity ω, such that $\varphi = \omega t$.

For simplicity we choose the units of measurement such that: 1) the gravitational constant G is equal to one; 2) the mass of the larger primary is $m_1 \equiv 1 - \mu$ and the sum of the masses is equal to one: $m_1 + m_2 = 1$, so $m_2 = \mu$; the distance between primaries is equal to one: $r_0 = 1$. The value $\mu = (m_1 + m_2)/m_1$ so μ is called *the mass ratio*. Moreover, in these units of measurement the angular velocity of the primaries is also equal to one:

$$\omega \equiv \frac{\sqrt{GM}}{r_0} = 1\,. \tag{2.46}$$

[1] It is also possible to define a Parabolic Restricted 3-Body Problem and a Linear Restricted 3-Body Problem [43]

Then the system of differential equations (2.42) can be rewritten as

$$\begin{aligned}
\frac{d^2\xi}{dt^2} &= -(1-\mu)\frac{\xi-\xi_1}{r_1^3} - \mu\frac{\xi-\xi_2}{r_2^3}\ , \\
\frac{d^2\eta}{dt^2} &= -(1-\mu)\frac{\eta-\eta_1}{r_1^3} - \mu\frac{\eta-\eta_2}{r_2^3}\ , \\
\frac{d^2\zeta}{dt^2} &= -(1-\mu)\frac{\zeta}{r_1^3} - \mu\frac{\zeta}{r_2^3}\ .
\end{aligned} \tag{2.47}$$

Now we turn from the inertial reference frame $O\xi\eta\zeta$ to the rotating non-inertial reference frame $Oxyz$, having the origin at the barycenter O, so that the plane Oxy coincides with the plane $O\xi\eta$, and the axis Oz coincides with the axis $O\zeta$. Suppose that the frame $Oxyz$ rotates around the axis Oz with constant angular velocity $\omega = 1$. The corresponding transformation from the $O\xi\eta\zeta$ frame to the $Oxyz$ frame is given by

$$\begin{aligned}
\xi &= x\cos t - y\sin t\ , \\
\eta &= x\sin t + y\cos t\ , \\
\zeta &= z.
\end{aligned} \tag{2.48}$$

We can also assume that $O\xi\eta\zeta$ and $Oxyz$ coincide at $t = 0$.

By substituting the second derivatives of (2.48) in (2.47) we obtain

$$\begin{aligned}
&\left(\frac{d^2x}{dt^2} - 2\frac{dy}{dt} - x\right)\cos t - \left(\frac{d^2y}{dt^2} + 2\frac{dx}{dt} - y\right)\sin t \ = \\
&-\left((1-\mu)\frac{x-x_1}{r_1^3} + \mu\frac{x-x_2}{r_2^3}\right)\cos t - \left((1-\mu)\frac{y-y_1}{r_1^3} + \mu\frac{y-y_2}{r_2^3}\right)\sin t\ , \\
&\left(\frac{d^2x}{dt^2} - 2\frac{dy}{dt} - x\right)\sin t - \left(\frac{d^2y}{dt^2} + 2\frac{dx}{dt} - y\right)\cos t \ = \\
&-\left((1-\mu)\frac{x-x_1}{r_1^3} + \mu\frac{x-x_2}{r_2^3}\right)\sin t - \left((1-\mu)\frac{y-y_1}{r_1^3} + \mu\frac{y-y_2}{r_2^3}\right)\cos t\ , \\
&\frac{d^2z}{dt^2} = -(1-\mu)\frac{z}{r_1^3} - \mu\frac{z}{r_2^3}\ .
\end{aligned} \tag{2.49}$$

Multiplying the first two equations (2.49) by $\cos t$ and $\sin t$, respectively, and then by

$-\sin t$ and $\cos t$, we obtain the system

$$\begin{aligned}
\frac{d^2x}{dt^2} &= 2\frac{dy}{dt} + x - (1-\mu)\frac{x-x_1}{r_1^3} - \mu\frac{x-x_2}{r_2^3} \,, \\
\frac{d^2y}{dt^2} &= -2\frac{dy}{dt} + y - (1-\mu)\frac{y-y_1}{r_1^3} - \mu\frac{y-y_2}{r_2^3} \,, \\
\frac{d^2z}{dt^2} &= -(1-\mu)\frac{z}{r_1^3} - \mu\frac{z}{r_2^3} \,.
\end{aligned} \tag{2.50}$$

In the rotating frame $Oxyz$, the coordinates of the primaries are $(-\mu, 0, 0)$ and $(1-\mu, 0, 0)$ for $m_1 = 1-\mu$ and $m_2 = \mu$, resp. Thus, we can rewrite the system (2.50) as

$$\begin{aligned}
\ddot{x} &= 2\dot{y} + x - (1-\mu)\frac{x+\mu}{r_1^3} - \mu\frac{x-1+\mu}{r_2^3} \,, \\
\ddot{y} &= -2\dot{x} + y - (1-\mu)\frac{y}{r_1^3} - \mu\frac{y}{r_2^3} \,, \\
\ddot{z} &= -\frac{z}{r_1^3} - \mu\frac{z}{r_2^3} \,,
\end{aligned} \tag{2.51}$$

where

$$\begin{aligned}
r_1 &= [(x+\mu)^2 + y^2 + z^2]^{1/2} \,, \\
r_2 &= [(x-1+\mu)^2 + y^2 + z^2]^{1/2} \,,
\end{aligned} \tag{2.52}$$

and the dot means d/dt. This is a 6-th order system.

The system (2.51) describes the motion of the infinitesimal body only, because it does not include the dependence of the coordinates of the primaries on time. However, even for this simple system of differential equations, we cannot obtain an exact solution of the form $\mathbf{r} = \mathbf{r}(t)$.

If the infinitesimal body moves in the plane Oxy (*i.e.*, $z = \dot{z} = 0$), then the order of the system can be reduced to 4 [86], and the plane Oxy is an invariant subspace of planar orbits. There are also various symmetries that follow from (2.51). First, if (x, y, z) is a solution of (2.51) so is $(x, y, -z)$. Second, if (x, y, z) is a solution so is $(x, -y, z)$, provided time is reversed. Eq. (2.51) also has a symmetry with respect to μ: if (x, y, z) is a solution for $\mu = \mu_0$ then $(-x, y, z)$ is a solution for $\mu = 1 - \mu_0$, if time is reversed.

The system (2.51) has one integral derived by Jacobi in 1836. Indeed, for a potential function

$$U = \frac{x^2+y^2}{2} + \frac{1-\mu}{r_1} + \frac{\mu}{r_2}\ , \tag{2.53}$$

the system (2.51) can be rewritten as

$$\begin{aligned} \ddot{x} - 2\dot{y} &= \frac{\partial U}{\partial x}\ , \\ \ddot{y} + 2\dot{x} &= \frac{\partial U}{\partial y}\ , \\ \ddot{z} &= \frac{\partial U}{\partial z}\ . \end{aligned} \tag{2.54}$$

By multiplying these equations by d/dx, d/dy, and d/dz, resp., and adding them, we obtain an expression that can be integrated:

$$\dot{x}^2 + \dot{y}^2 + \dot{z}^2 = 2U - C, \tag{2.55}$$

where C is a constant of integration. The left-hand side of this equation is the squared velocity v^2 of the zero-mass body, and we have

$$v^2 = x^2 + y^2 + 2\frac{1-\mu}{r_1} + 2\frac{\mu}{r_2} - C\ , \tag{2.56}$$

This formula is known as *the Jacobi integral* and the constant C is called *the Jacobi constant.*

Note that the system (2.51) describes the motion of an infinitesimal body for any mass ratio μ of the primaries, with $0 \leq \mu \leq 1/2$. For example, for the Earth-Moon system (which can be considered circular, in first approximation), $\mu = 0.01215$, for the Sun-Earth system $\mu = 3.0359 \cdot 10^{-6}$, and for the Sun-Jupiter case we have $\mu = 0.00095$. Higher values of the mass ratio μ exists for some other planetary systems and double star systems.

2.4.2 Libration points

Analysis of many complex dynamical systems starts with obtaining their equilibrium points, *i.e.*, the points where the forces in the system balance each other. It is well-known that for each value of μ, Eq. (2.51) has five equilibrium points, called *the*

Lagrange points or *libration points*. We note, that these libration points exist only in a rotating frame, *i.e.*, for Eq. (2.51), but not in the inertial frame, Eq.(2.42), because Eq. (2.42) contains an explicit time dependence on the coordinates of the primaries, and there are no equilibria.

Thus, to find the libration points we must set the velocity and acceleration components equal to zero. This leads to the following three equations:

$$\begin{aligned} x - (1-\mu)\frac{x+\mu}{r_1^3} - \mu\frac{x-1+\mu}{r_2^3} &= 0 \,, \\ y - (1-\mu)\frac{y}{r_1^3} - \mu\frac{y}{r_2^3} &= 0 \,, \\ \frac{z}{r_1^3} - \mu\frac{z}{r_2^3} &= 0 \,. \end{aligned} \tag{2.57}$$

From the third equation we obtain immediately that $z = 0$; so, all libration points lie in the orbit plane of the primaries Oxy. The second equation of Eq. (2.57) divides the solution space into two parts: 1) $y = 0$ defines three collinear libration points, *i.e.*, lying on the straight line, and 2) $y \neq 0$ defines two other libration points. We start with the case where $y = 0$. Then the first equation of Eq. (2.57) can be written, using Eq.(2.52), as the fifth order nonlinear equation:

$$x - (1-\mu)\frac{x+\mu}{((x+\mu)^2)^{3/2}} - \mu\frac{x-1+\mu}{((x-1+\mu)^2)^{3/2}} = 0 \,. \tag{2.58}$$

This equation can be rewritten separately for each of three cases:

1. For $x \leq 1-\mu$, Eq. (2.58) has the form

$$x - \frac{1-\mu}{(x+\mu)^2} + \frac{\mu}{(x-1+\mu)^2} = 0 \,, \tag{2.59}$$

   which defines the libration point L1, lying between the two primaries.

2. For $x \leq 1-\mu$, Eq. (2.58) has the form

$$x - \frac{1-\mu}{(x+\mu)^2} - \frac{\mu}{(x-1+\mu)^2} = 0 \,, \tag{2.60}$$

   which defines the libration point L2, lying to the right of the second primary.

3. For $x \leq -\mu$, Eq. (2.58) has the form

$$x + \frac{1-\mu}{(x+\mu)^2} + \frac{\mu}{(x-1+\mu)^2} = 0 \,, \tag{2.61}$$

which defines the libration point L3, lying to the left of the first primary.

Equations (2.59) - (2.61) can be solved numerically for any value of μ. The coordinates of the libration points L1, L2, and L3 as a functions of the value of μ, are shown in Fig.(2.6).

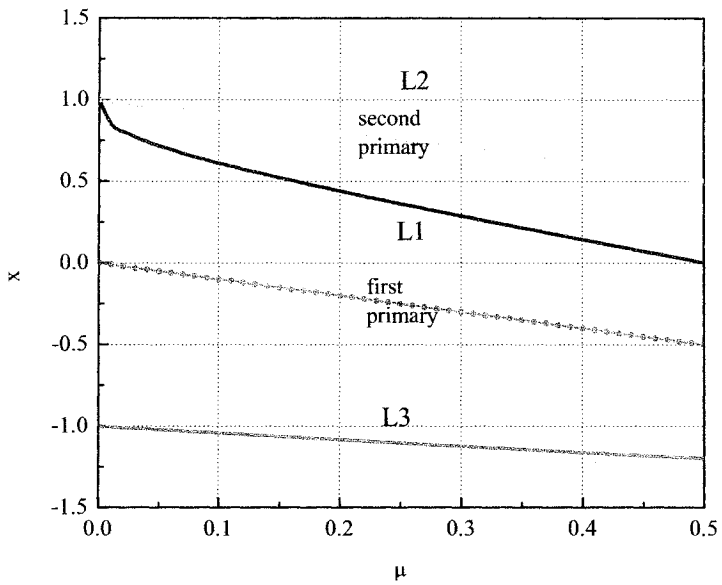

Figure 2.6: The x-coordinate of the collinear libration points L1, L2, and L3 as a function of μ. The locations of the primaries are also shown.

For the case $y \neq 0$, the first two equations of Eq. (2.57) can be transformed into the equations

$$\begin{aligned} (x-1+\mu)^2 + y^2 &= 1 \,, \\ (x+\mu)^2 + y^2 &= 1 \,, \end{aligned} \tag{2.62}$$

which have two exact solutions:

$$x = \frac{1}{2} - \mu \,, \quad y = -\frac{\sqrt{3}}{2} \,, \tag{2.63}$$

defining the libration point L4; and

$$x = \frac{1}{2} - \mu \,, \quad y = \frac{\sqrt{3}}{2} \,, \tag{2.64}$$

defining the libration point L5. Note that the libration points L4 and L5 form two equilateral triangles with the primaries, for any μ value. The position of all libration points in the Oxy plane for two different values of μ is shown in Fig.2.7 . Figure 2.8 shows the coordinates of the libration points as a function of μ, for $0 \leq \mu \leq 1$. L1, L2, and L3 lie on a single, planar S-shaped curve that connects the circles of equilibria which exist at $\mu = 0$ and at $\mu = 1$. L1 and L2 coalesce as $\mu \to 0$ and L1 and L3 coalesce as $\mu \to 1$. L4 and L5 lie on straight lines that also connect the circles.

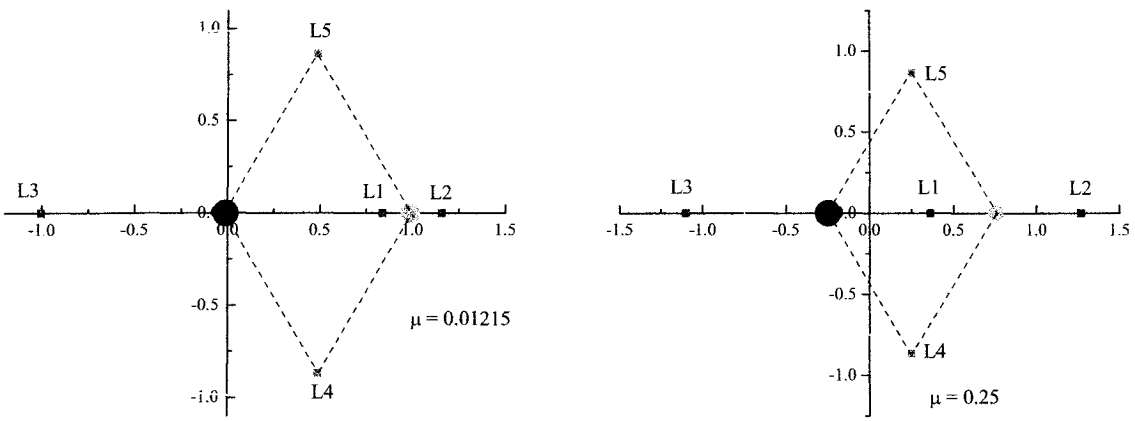

Figure 2.7: Relative position of the libration points L1, L2, L3, L4, and L5 (small red and blue squares) for the Earth-Moon system ($\mu = 0.01215$) (left), and for the system with $\mu = 0.25$ in the rotating reference frame $Oxyz$. Dashed equilateral triangles are formed by the primaries (blue and yellow circles) and libration points L4 and L5. The big circle is the orbit of the second primary.

The CR3BP is a good approximation to several celestial pairs in the solar system such as: 1) the Earth-Moon system, 2) the Sun-Earth system, 3) the Sun-Jupiter system. In reality, these systems are not circular, but the deviation of their real orbits from the circular ones is only about 10%.

It is interesting to note that until 1906, the existence of the libration points in the CR3BP was accepted as a curious mathematical fact. However, in 1906 the first asteroids were discovered. These asteroids were called Trojan asteroids and they moved in orbits at the libration points L4 and L5 of the Sun-Jupiter system. At the present time, many Trojan asteroids have been found for the Sun-Jupiter system

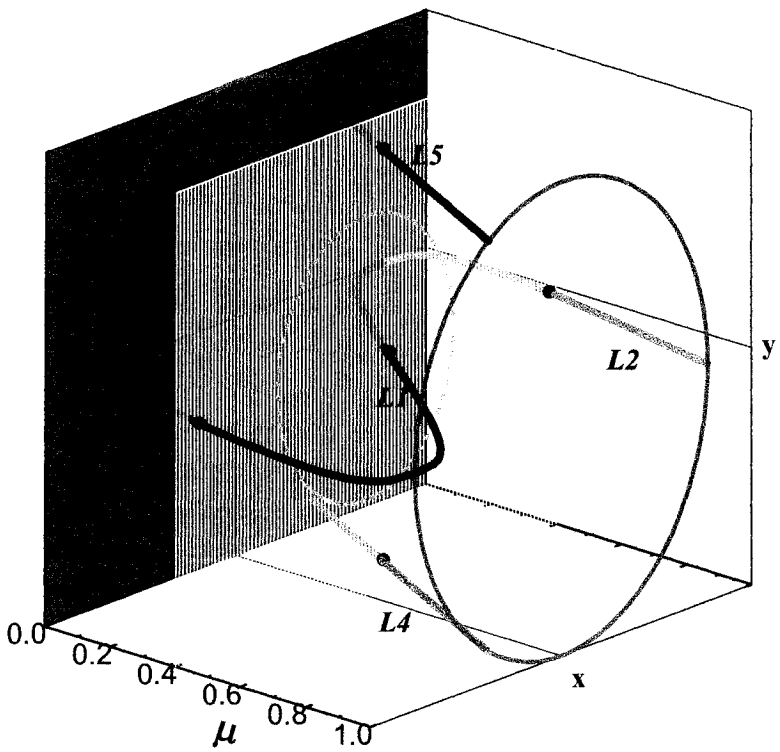

Figure 2.8: The libration points as a function of μ. The transparent plane at $\mu = 0.4$ shows the position of the libration points as dark dots for that value of μ.

[15] (962 near L4 named the Greeks, and 603 near L5 named the Trojans); others have been found for the Sun-Mars (1 at L4, 5 at L5) and for the Sun-Neptune (1 at L4) systems. (See [85] for a discussion of stability of Trojan asteroids of Saturn, Uranus and Neptune.) The existence of the libration points may be essential for cosmology, because these points can serve as centers capturing and accumulating small bodies. Thus, the libration points of double stars can become centers for new stars or planetoids in the process of their formation.

2.4.3 Stability of the libration points

The mathematical problem of stability of the libration points can be reformulated as follows: If the infinitesimal body mass starts out near a libration point, will it remain in the vicinity or will it wander off over time? A detailed analysis of this problem is presented in many books on Celestial Mechanics and, especially, Spacecraft Dynamics [80, 100, 81]. As a rule, such analysis is based on linearization of Eq. (2.51) and subsequent checking whether or not any eigenvalues of the Jacobian of the linearized system have positive real components [5, 4, 103, 75]. This is the problem of linear stability of the libration points.

A general system of n differential equations

$$\begin{aligned} \dot{\mathbf{x}}_1 &= f_1(x_1, x_2, ..., x_n) \ , \\ \dot{\mathbf{x}}_2 &= f_2(x_1, x_2, ..., x_n) \ , \\ &\cdots \\ \dot{\mathbf{x}}_n &= f_n(x_1, x_2, ..., x_n) \ , \end{aligned} \tag{2.65}$$

where $f_i : \Re^n \to \Re$, and $x_i \in \Re$, $i = 1, 2, ..., n$, can be rewritten in a vector form as

$$\dot{\mathbf{x}} = \mathbf{f}(\mathbf{x}) \ , \tag{2.66}$$

where $\mathbf{f} : \Re^n \to \Re^n$ and $\mathbf{x} \in \Re^n$, and $\Re$ is a set of real numbers. Eq. (2.66) is called autonomous because $\mathbf{f}(\mathbf{x})$ does not depend directly on the time t. An equilibrium point (critical point, stationary point, rest point, or libration point for the Restricted 3-Body problem) is a point $\mathbf{x}' \in \Re^n$ such that $\mathbf{f}(\mathbf{x}') = 0$. Let us shift the coordinate system such that $\mathbf{x}' = 0$ for simplicity.

By definition, an equilibrium point $\mathbf{x} = 0$ of Eq. (2.66) is stable (or Lyapunov stable) if for any $\epsilon > 0$ there exists $\delta > 0$ (which depends only on ϵ and does not depend on the time t) such that for any $\mathbf{x}_0$ with $||\mathbf{x}_0|| < \delta$ a solution $\mathbf{X}(t)$ of Eq. (2.66) with starting condition $\mathbf{X}(0) = \mathbf{x}_0$ exists for $t > 0$ and satisfies to the inequality $||\mathbf{X}(t)|| < \epsilon$ for all $t > 0$.

Finally, the rest point $\mathbf{x} = 0$ of Eq. (2.66) is asymptotically stable if it is Lyapunov stable (corresponding to the previous definition) and

$$\lim_{t \to +\infty} \mathbf{X}(t) = 0 \tag{2.67}$$

for any solution with starting condition $\mathbf{X}(0)$ lying in a sufficiently small vicinity of $\mathbf{x} = 0$.

Analysis of the stability of an equilibrium point starts with the analysis of the linearized Eq. (2.66):

$$\dot{\mathbf{x}} \;=\; J \cdot \mathbf{x} + \mathbf{g}(\mathbf{x}), \tag{2.68}$$

where J is the Jacobian of Eq. (2.66):

$$J \equiv \left.\frac{\partial \mathbf{f}}{\partial \mathbf{x}}\right|_{\mathbf{x}\,=\,0} = \begin{pmatrix} \left.\frac{\partial f_1}{\partial x_1}\right|_{x_1=0} & \left.\frac{\partial f_1}{\partial x_2}\right|_{x_2=0} & \cdots & \left.\frac{\partial f_1}{\partial x_n}\right|_{x_n=0} \\ \left.\frac{\partial f_2}{\partial x_1}\right|_{x_1=0} & \left.\frac{\partial f_2}{\partial x_2}\right|_{x_2=0} & \cdots & \left.\frac{\partial f_2}{\partial x_n}\right|_{x_n=0} \\ \cdots & \cdots & \cdots & \cdots \\ \left.\frac{\partial f_n}{\partial x_1}\right|_{x_1=0} & \left.\frac{\partial f_n}{\partial x_2}\right|_{x_2=0} & \cdots & \left.\frac{\partial f_n}{\partial x_n}\right|_{x_n=0} \end{pmatrix}, \tag{2.69}$$

and $\mathbf{g}(\mathbf{x}) = \mathbf{f}(\mathbf{x}) - J \cdot \mathbf{x}$; so $\mathbf{g}(0) = 0$, and $\partial \mathbf{g}/\partial \mathbf{x}|_{\mathbf{x}=0} = 0$. All nonlinear terms of Eq. (2.66) are contained in $\mathbf{g}(\mathbf{x})$.

There is a basic theorem about the stability in the linear approximation. Let all eigenvalues σ of the Jacobian J lie in the left complex semi-plane: $Re\ \sigma < 0$. Then the equilibrium point is stable. It is possible to prove that, if the real part of one or more eigenvalues σ is positive, then the equilibrium point is unstable. In the case of purely imaginary σ's, stability of the equilibrium point depends on the nonlinear term $\mathbf{g}(\mathbf{x})$. Indeed, from the theory of linear differential equations with constant coefficients, the linearized equation $\dot{\mathbf{x}} = J \cdot \mathbf{x}$ near an equilibrium point has solutions which contain terms like $\exp(\sigma t)$, where σ is an eigenvalue of J. Then we can conclude that the equilibrium point is stable in a linear approximation if and only if the Jacobian J has no eigenvalues with a positive real part.

We have to note here that this case (purely imaginary eigenvalues) is more interesting: if the Jacobian at an equilibrium point has purely imaginary eigenvalues (more precisely M pairs of conjugate purely imaginary eigenvalues), then in a vicinity of the equilibrium point there exists families of periodic solutions (orbits), *i.e.*, M solution

families $\mathbf{X}_m(t)$, where $m = 1, 2, ..., M$ such that for each of them

$$\mathbf{X}_m(t) \;=\; \mathbf{X}_m(t + T_m) \tag{2.70}$$

for any t. The value T_m is a period of the m^{th} solution. These periodic orbits can be stable or unstable.

For our calculations with AUTO, we need to carry out stability analysis and compute the eigenvalues of the Jacobian. We can rewrite Eq. (2.51) as a system of six first order differential equations, like Eqs. (2.65) and (2.66)

$$\begin{cases} \dot{u} &= 2v + x - (1-\mu)\dfrac{x+\mu}{((x+\mu)^2+y^2+z^2)^{3/2}} - \mu\dfrac{x-1+\mu}{((x-1+\mu)^2+y^2+z^2)^{3/2}}\,, \\ \dot{v} &= -2u + y - (1-\mu)\dfrac{y}{((x+\mu)^2+y^2+z^2)^{3/2}} - \mu\dfrac{y}{((x-1+\mu)^2+y^2+z^2)^{3/2}}\,, \\ \dot{w} &= -\dfrac{z}{((x+\mu)^2+y^2+z^2)^{3/2}} - \mu\dfrac{z}{((x-1+\mu)^2+y^2+z^2)^{3/2}}\,, \\ \dot{x} &= u\,, \\ \dot{y} &= v\,, \\ \dot{z} &= w\,, \end{cases} \tag{2.71}$$

where u, v, and w are new independent variables defined by the last three equations. Let

$$\begin{aligned} f_1(x,y,z) &\equiv -(1-\mu)\frac{x+\mu}{((x+\mu)^2+y^2+z^2)^{3/2}} - \mu\frac{x-1+\mu}{((x-1+\mu)^2+y^2+z^2)^{3/2}}\,, \\ f_2(x,y,z) &\equiv -(1-\mu)\frac{y}{((x+\mu)^2+y^2+z^2)^{3/2}} - \mu\frac{y}{((x-1+\mu)^2+y^2+z^2)^{3/2}}\,, \\ f_3(x,y,z) &\equiv -\frac{z}{((x+\mu)^2+y^2+z^2)^{3/2}} - \mu\frac{z}{((x-1+\mu)^2+y^2+z^2)^{3/2}}\,. \end{aligned} \tag{2.72}$$

The stationary equations for Eq. (2.71) are

$$\begin{cases} 2v + x - f_1(x,y,z) = 0\,, \\ -2u + y - f_2(x,y,z) = 0\,, \\ f_3(x,y,z) = 0\,, \\ u = 0\,, \\ v = 0\,, \\ w = 0\,. \end{cases} \tag{2.73}$$

The Jacobian of the Eq. (2.71) is

$$J = \begin{pmatrix} 0 & 2 & 0 & \frac{\partial f_1}{\partial x} & \frac{\partial f_1}{\partial y} & \frac{\partial f_1}{\partial z} \\ -2 & 0 & 0 & \frac{\partial f_2}{\partial x} & \frac{\partial f_2}{\partial y} & \frac{\partial f_2}{\partial z} \\ 0 & 0 & 0 & \frac{\partial f_3}{\partial x} & \frac{\partial f_3}{\partial y} & \frac{\partial f_3}{\partial z} \\ 1 & 0 & 0 & 0 & 0 & 0 \\ 0 & 1 & 0 & 0 & 0 & 0 \\ 0 & 0 & 1 & 0 & 0 & 0 \end{pmatrix}, \tag{2.74}$$

where $f_1 \equiv f_1(x,y,z)$, $f_2 \equiv f_2(x,y,z)$, and $f_3 \equiv f_3(x,y,z)$.

Consider the collinear libration points L1, L2, L3. Keeping in mind that for all of them $y = 0$ and $z = 0$, we obtain

$$\frac{\partial f_1}{\partial x} = 1 - \frac{1-\mu}{((x+\mu)^2)^{3/2}} - \frac{\mu}{((x-1+\mu)^2)^{3/2}} + \frac{3(1-\mu)(x+\mu)^2}{((x+\mu)^2)^{5/2}} + \frac{3\mu(x-1+\mu)^2}{((x-1+\mu)^2)^{5/2}}\,,$$

$$\frac{\partial f_1}{\partial y} = 0\,, \quad \frac{\partial f_1}{\partial z} = 0\,,$$

$$\frac{\partial f_2}{\partial y} = 1 - \frac{1-\mu}{((x+\mu)^2)^{3/2}} - \frac{\mu}{((x-1+\mu)^2)^{3/2}}\,, \quad \frac{\partial f_2}{\partial x} = 0\,, \quad \frac{\partial f_2}{\partial z} = 0\,,$$

$$\frac{\partial f_3}{\partial z} = \frac{1-\mu}{((x+\mu)^2)^{3/2}} - \frac{\mu}{((x-1+\mu)^2)^{3/2}}\,, \quad \frac{\partial f_2}{\partial x} = 0\,, \quad \frac{\partial f_2}{\partial y} = 0\,. \tag{2.75}$$

Thus, the Jacobian for this case is

$$J_{123} = \begin{pmatrix} 0 & 2 & 0 & \frac{\partial f_1}{\partial x} & 0 & 0 \\ -2 & 0 & 0 & 0 & \frac{\partial f_2}{\partial y} & 0 \\ 0 & 0 & 0 & 0 & 0 & \frac{\partial f_3}{\partial z} \\ 1 & 0 & 0 & 0 & 0 & 0 \\ 0 & 1 & 0 & 0 & 0 & 0 \\ 0 & 0 & 1 & 0 & 0 & 0 \end{pmatrix} , \tag{2.76}$$

and its eigenvalues σ_i $(i = 1, 2, ..., 6)$ can be found from the equation

$$det\ (J_{123} - \sigma I) =$$

$$det \begin{pmatrix} -\sigma & 2 & 0 & \frac{\partial f_1}{\partial x} & 0 & 0 \\ -2 & -\sigma & 0 & 0 & \frac{\partial f_2}{\partial y} & 0 \\ 0 & 0 & -\sigma & 0 & 0 & \frac{\partial f_3}{\partial z} \\ 1 & 0 & 0 & -\sigma & 0 & 0 \\ 0 & 1 & 0 & 0 & -\sigma & 0 \\ 0 & 0 & 1 & 0 & 0 & -\sigma \end{pmatrix} = 0 , \tag{2.77}$$

where I is an identity matrix. After calculating the determinant of Eq. (2.77) we derive two nonlinear equations:

$$\begin{cases} \sigma^2 - \frac{\partial f_3}{\partial z} = 0 , \\ \\ \sigma^4 + \sigma^2 \left(4 - \frac{\partial f_1}{\partial x} - \frac{\partial f_2}{\partial y} \right) + \frac{\partial f_1}{\partial x} \frac{\partial f_2}{\partial y} = 0 . \end{cases} \tag{2.78}$$

The first equation of Eq. (2.78) has two conjugate purely imaginary roots if $\partial f_3/\partial z$ is negative. For the libration point L1 we have

$$\frac{\partial f_3}{\partial z} = -\frac{1-\mu}{(x+\mu)^3)} + \frac{\mu}{(x-1+\mu)^3)} , \tag{2.79}$$

but for this point $(x + \mu) \geq 0$ and $(x - 1 + \mu) \leq 0$, therefore we find that for L1 the value of $\partial f_3/\partial z \leq 0$ for all μ values. Similarly, we can prove that $\partial f_3/\partial z \leq 0$ for

the libration points L2 and L3. As for the second equation of Eq. (2.79), it has four solutions

$$\sigma^2 = \frac{1}{2}\left(-\left(4-\frac{\partial f_1}{\partial x}-\frac{\partial f_2}{\partial y}\right)\pm\sqrt{\left(4-\frac{\partial f_1}{\partial x}-\frac{\partial f_2}{\partial y}\right)^2-4\frac{\partial f_1}{\partial x}\frac{\partial f_2}{\partial y}}\right) . \quad (2.80)$$

Calculated numerically, the right part of Eq. (2.80) is shown in Fig. (2.9) for all collinear libration points. Thus, we can conclude for this case, that the Jacobian of Eq. (2.76) for each collinear libration point has among its six eigenvalues one real positive eigenvalue. This means that all collinear libration points are unstable (in the linear approximation). Moreover, the collinear libration points are equilibrium points *saddle* × *center* × *center* [103, 75]. This type of the equilibrium point gives for each libration points two types of periodic orbits. For these points we have two pairs of conjugate purely imaginary eigenvalues as well.

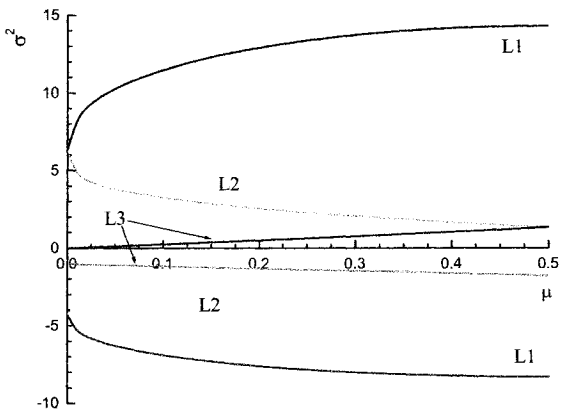

Figure 2.9: The right part of Eq. (2.80) depending on the value of μ for the collinear libration points L1, L2, and L3. One can see that for each of them, for any μ value, we have one negative and one positive value of σ^2.

For the triangular libration points L4 and L5 we have only $z = 0$, and the Jacobian

Eq. (2.73) for these points is

$$J_{45} = \begin{pmatrix} 0 & 2 & 0 & \frac{\partial f_1}{\partial x} & \frac{\partial f_1}{\partial y} & 0 \\ -2 & 0 & 0 & \frac{\partial f_2}{\partial x} & \frac{\partial f_2}{\partial y} & 0 \\ 0 & 0 & 0 & 0 & 0 & \frac{\partial f_3}{\partial z} \\ 1 & 0 & 0 & 0 & 0 & 0 \\ 0 & 1 & 0 & 0 & 0 & 0 \\ 0 & 0 & 1 & 0 & 0 & 0 \end{pmatrix} , \tag{2.81}$$

and the equations for its eigenvalues σ are

$$\begin{cases} \sigma^2 - \dfrac{\partial f_3}{\partial z} = 0 , \\ \\ \sigma^4 + \sigma^2 \left(4 - \dfrac{\partial f_1}{\partial x} - \dfrac{\partial f_2}{\partial y} \right) + 2\sigma \left(\dfrac{\partial f_1}{\partial y} - \dfrac{\partial f_2}{\partial x} \right) - \dfrac{\partial f_2}{\partial x}\dfrac{\partial f_1}{\partial y} + \dfrac{\partial f_1}{\partial x}\dfrac{\partial f_2}{\partial y} = 0 . \end{cases} \tag{2.82}$$

Using Eq. (2.72), and Eqs. (2.62)-(2.64) we find

$$\begin{aligned} \frac{\partial f_1}{\partial x} &= \frac{3}{4} , \quad \frac{\partial f_1}{\partial y} = \pm \left(\frac{3}{2} - \mu \right) \frac{\sqrt{3}}{2} , \\ \\ \frac{\partial f_2}{\partial x} &= \pm \left(\frac{3}{2} - \mu \right) \frac{\sqrt{3}}{2} , \quad \frac{\partial f_2}{\partial y} = \frac{3}{4} , \\ \\ \frac{\partial f_3}{\partial z} &= -1 , \end{aligned} \tag{2.83}$$

where the sign "$\pm$" shows that we need to choose "$-$" for L4 and "$+$" for L5. Thus, we can rewrite Eq. (2.82) as

$$\begin{cases} \sigma^2 = -1 , \\ \\ \sigma^4 + \sigma^2 + \dfrac{27}{4}\mu(1-\mu) = 0 . \end{cases} \tag{2.84}$$

The first equation of Eq. (2.84) has two conjugate purely imaginary roots. The second one has two pairs of conjugate pure imaginary roots only if

$$27\mu^2 - 27\mu + 1 \geq 0 , \tag{2.85}$$

or if $0 \leq \mu \leq \mu_2 \approx 0.03852089$; otherwise this equation has four complex roots consisting of real and imaginary parts. Thus, we can conclude that for $0 \leq \mu \leq \mu_2$ the points L4 and L5 are stable in the linear approximation. In 1962, A. Leontovich, using results of A. Kolmogorov and V. Arnold, showed [80] that the libration points L4 and L5 are stable in general for planar motion in the Oxy-plane except possibly for a discrete set of μ values. Later, in 1967-1969, A. Deprit and B. Deprit [25] proved that this set contains only two values:

$$\mu' = \frac{15 - \sqrt{213}}{30} \approx 0.01351160 \ , \quad \mu'' = \frac{45 - \sqrt{1883}}{90} \approx 0.0242938 \ . \tag{2.86}$$

In the general (nonlinear) case of non-planar motion we definitely have instability at $\mu = \mu'$ and $\mu = \mu''$ and possibly for a few other μ values [80]. For all other μ such that $0 < \mu < \mu_2 \approx 0.03852089$ we have stability (in other words, if L4 and L5 are unstable then this instability is extremely weak). It was shown that for $\mu = \mu_2$ the libration points L4 and L5 are stable. For $\mu > \mu_2$ we have instability, as for the collinear libration points.

2.4.4 Periodic solutions of the Restricted 3-Body Problem

For the case where the Jacobian J has purely imaginary eigenvalues we cannot draw any conclusion about the stability, and we must analyze the nonlinear equations.

As long ago as 1892, Poincaré emphasized the fundamental role of periodic orbits (solutions) in the N-Body Problem: they are "the only opening through which we can penetrate the stronghold" (citing from [100]). Moreover, periodic orbits organize the "skeleton" [28] around which other orbits are formed. Thus, after 1892, much effort on the (Circular) Restricted 3-Body Problem has been spent on finding periodic orbits [107, 14, 61, 29, 69, 70, 87, 89, 88, 115, 116, 12]. We note that some families (or groups) of periodic orbits were calculated numerically, whereas others were found using complicated analytical methods.

As mentioned above, each of the libration points has in its vicinity a few families of periodic solutions, because the Jacobian (2.74) at these points has a corresponding number of pairs of conjugate purely imaginary eigenvalues. Thus, the collinear points L1, L2, L3, for which J has two pairs of such eigenvalues, have in their vicinities two

different families of periodic orbits. The triangular libration points L4 and L5 for $\mu \leq \mu_2$ have three families each, while for $\mu > \mu_2$ they have only one family each.

H. Poincaré conjectured that periodic orbits are dense in the set of all possible solutions of the problem that are bounded in the 6N-dimensional phase space formed by the components of the coordinates and the velocities of the N bodies. For the 6-dimensional phase space of the CR3BP where we have only three coordinates and three velocities of the body with zero mass, it means that if $\mathbf{X}(t)$ is a solution of the equation

$$\dot{\mathbf{x}} = \mathbf{f}(\mathbf{x}) , \tag{2.87}$$

where $\mathbf{f} : \Re^6 \rightarrow \Re^6, \mathbf{x} \in \Re^6$, with starting conditions $\mathbf{X}(t_0) = \mathbf{X}_0$, then exists a periodic solution $\tilde{\mathbf{x}}(t) : \tilde{\mathbf{x}}(t) = \tilde{\mathbf{x}}(t+T)$ of Eq. (2.87) with a period T, such that this periodic orbit at all times is as close to $\mathbf{X}(t)$ as we want (though, the period T may be infinite), *i.e.*:

$$||\mathbf{X}(t) - \tilde{\mathbf{x}}(t)|| < \delta \tag{2.88}$$

for any $0 \leq t < +\infty$, where $\delta > 0$ may very small. This fundamental result for the Restricted 3-Body Problem can be paraphrased as follows: For any point of the phase space there always exists a point belonging to a periodic orbit when the distance between the points is infinitely small. This theorem is very useful for building numerical methods of finding periodic orbits [80].

Another method is analytical continuation: it is possible to solve the problem for $\mu = 0$ and then to perform analytical continuation of this solution for any μ value in the interval $[0, 0.5]$. Such an approach is the source of most analytical constructions of periodic orbits.

In the fundamental book by V. Szebehely, "Theory of Orbits. The Restricted Problem of Three Bodies" [107], all achievements obtained by 1967, including analytical, numerical and combined approaches, are summarized and reviewed. There are books by A. Bruno [14] and M. Hénon [61], both based on analytical continuation from $\mu = 0$ to finite values of μ. Taking into account recent work [29, 69, 70, 87, 89, 88, 115, 116, 12] and other work, we can see some bones of the "skeleton" of the full set of periodic orbits; however, we cannot see a full and clear picture. In this thesis,

we build such "skeleton", using an original numerical approach [38, 39, 34, 35].

2.4.5 Libration point satellite mission design

The libration points of the Earth-Moon and the Sun-Earth systems, and some of their properties, were already well-known at the beginning of the era of space flights. In the 1960's and 1970's, it was proposed to use periodic orbits near the libration point L2 of the Earth-Moon system [46, 50] for the Apollo project, for uninterrupted communication between the dark side of the Moon and the Earth. Unfortunately, this innovative concept was never implemented. Even before that, regions near the libration points L1 and L2 of the Sun-Earth system were discussed as excellent locations for stationary spacecraft for scientific observations [46] and communication relays [21, 20].

Periodic orbits near libration points are interesting for spacecraft mission design as well: L1 for the investigation of solar wind before influence of the Earth's magnetosphere; L2 for placement of a cosmic telescope, because there is no reflected light from the Earth (from L2 we can see only the night side of the Earth), and the Earth shades the Sun as well. In 1978, the NASA International Sun-Earth Explorer 3 (ISEE-3) became the first spacecraft to orbit the Sun-Earth L1 point, where it traced a Halo orbit [47]. Such orbits were computed with the required accuracy in [46, 50, 48, 49, 13, 97]. Since that time, the European Space Agency (ESA)/NASA SOHO mission and the NASA ACE mission have used Halo orbits about the Sun-Earth L1 point for solar observations [68, 47, 66, 98].

Most of the orbits near L1 and L2 are unstable for any μ value, *i.e.*, if the spacecraft is shifted by a small perturbation, then this shift will increase, at first slowly and then faster and faster. Nevertheless, a spacecraft can remain in the orbit for years by performing small maneuvers every few months [44].

On the other hand, the effect of instability can be used for correcting of the trajectory of a spacecraft: small fuel expenses can give radical changes of trajectory. There exists infinitely many trajectories which converge to this orbit and infinitely many trajectories which diverge from this orbit as well. M. Lo from NASA's Jet Propulsion Laboratory [72, 73] showed, that the form of such trajectories can be very different

while the energy of the spacecraft is almost the same. It is possible to calculate the correction very precisely to obtain a new trajectory of choice. An example of such calculations is shown in Fig. 2.10. Here, after a small (but precisely calculated) changing of the orbit of the spacecraft near L2 (of the Sun-Earth system), the spacecraft is moving on the orbit near the L1 without additional corrections. Such calculations were done, and used for the Genesis mission [72, 73, 77].

Recent libration point mission design has exploited dynamical system theory [5, 103, 75] to compute stable, unstable and center manifolds for libration point orbits [77, 55]. In 2001, the MAP spacecraft was placed in an orbit about the Sun-Earth L2 point [51]. The Genesis mission, launched in 2001, called for the spacecraft to the first orbit the Sun-Earth L1 point, then follow a heteroclinic connection to an orbit around L2, before returning to the Earth [72, 73, 77]. The Genesis spacecraft was designed to collect particles of the solar wind during its mission, and return them to the Earth. The evolution of the Genesis spacecraft is shown on Fig. 2.11 (from http://www.genesismission.org/mission/live_shots.html). A detailed description of the Genesis mission can be find at http://www.genesismission.org.

In Table 1 taken from [49], several missions and future projects are collected. The information about most of the missions from in Table 4.1 can be found at the web site http://highorbits.jhuapl.edu.

We conclude this chapter by noting, that while new trajectories found in the 3-Body Problem were called "choreographies", new missions designed by M. Lo with his colleagues can be called space "acrobatics".

Table 2.1: Past and future libration-point spacecraft missions ([49]). Acronyms: SOHO - Solar heliosphere observatory; ACE - Advanced composition explorer; MAP - Microwave anisotropy probe; NGST - Next generation space telescope; GAILA - Global astrometric interferometer for astrophysics; TPR - terrestrial planet finder.

Mission	Sun-Earth libration points	Date of orbit insertion	Mission purpose
ISEE-3 (NASA)	L1, L2	1978, 1983	Solar wind, cosmic rays,plasma
SOHO (ESA/NASA)	L1	1996	Solar observatory
ASE (NASA)	L1	1997	Solar winds, relativistic particles
WIND (NASA)	L1	1995	Solar wind monitor
MAP (NASA)	L2	2001	Cosmic microwave background
Genesis (NASA)	L1	2001	Solar-wind composition
Hershel (ESA)	L2	2007	Far infrared telescope
Plank (ESA)	L2	2007	Cosmic microwave background
Eddington (ESA)	L2	2008	Stellar observations
NGST (NASA)	L2	2010	Deep space observatory
Constellation-X (NASA)	L2	2011	X-ray astronomy
GAIA (ESA)	L2	2012	Galactic structure, astrometry
TPF (NASA)	L2	2012	Detection of distant planets
Darwin (ESA)	L2	2014	Detection of Earth-like planets

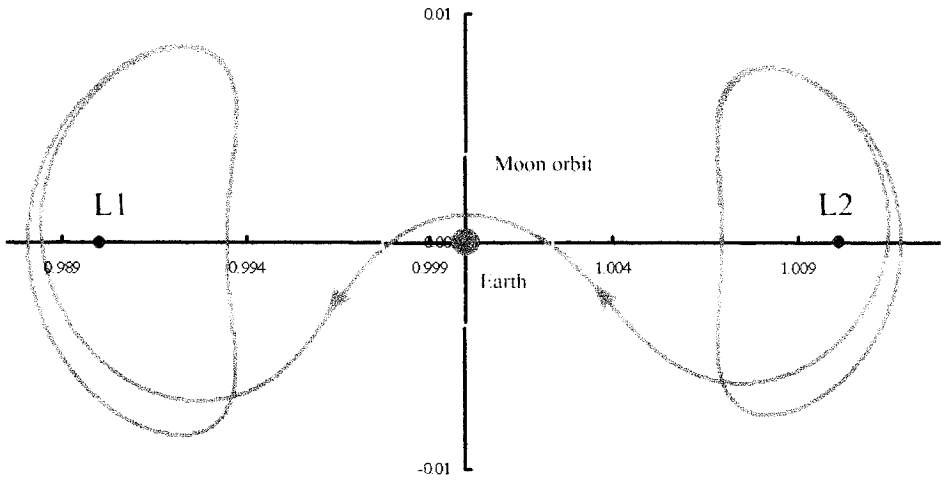

Figure 2.10: Transition of the spacecraft from an orbit near the libration point L2 of the Sun-Earth system to an orbit near L1.

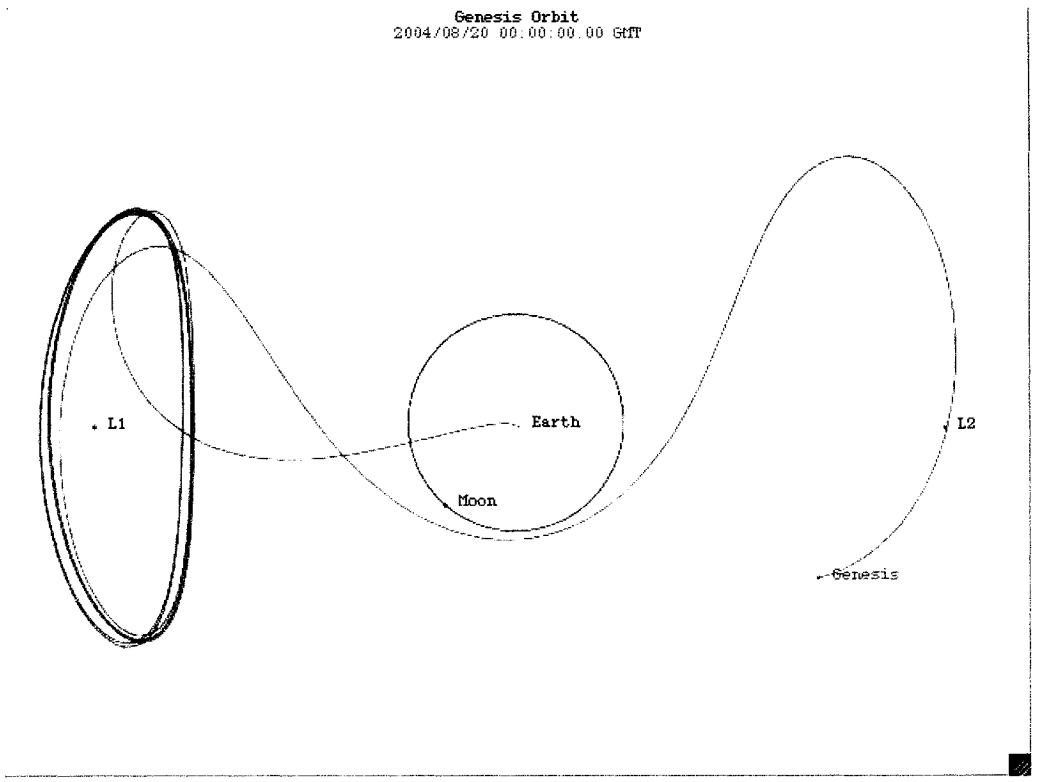

Figure 2.11: Trajectory of the Genesis spacecraft and its position on August 20, 2004. (From the Genesis mission web site)

Chapter 3

Basic Numerical Methods

3.1 Continuation of solutions

Numerical continuation enables the computation of solution manifolds ("*solution families*"). Most existing algorithms are for the computation of one-dimensional solution manifolds ("*solution branches*"), *e.g.*, [1, 11, 38, 39, 96, 103], and [75] (Chapter 10), but continuation algorithms have also been developed for higher-dimensional manifolds [60].

To recall the basic notions of continuation, first consider the finite-dimensional equation

$$F(X) = 0 \ , \qquad F \ : \ \Re^{n+1} \ \rightarrow \ \Re^{n} \ , \tag{3.1}$$

where F is assumed to be sufficiently smooth. This equation has one more variable than it has equations. Given a solution X_0, one has, generically, a locally unique one-dimensional family of solutions that passes through X_0. To compute a next solution, say, X_1, of this family, one can use Newton's method to solve the extended system

$$\begin{aligned} &\text{a)} \quad F(X_1) = 0 \ , \\ &\text{b)} \quad (X_1 - X_0)^* \dot{X}_0 = \Delta s \ . \end{aligned} \tag{3.2}$$

Here $\dot{X}_0$ is the unit tangent to the solution path at X_0, the symbol * denotes transpose, and Δs is a step size in the continuation procedure. The vector $\dot{X}_0$ is, of course, also a null vector of the Jacobian matrix $F_X(X_0)$, and can be computed at little cost [38]. This well-known method, known as the *pseudo-arclength method* [71],

is the basis of vitually all robust continuation algorithms. The size of the pseudo-arclength step size Δs is usually adapted along the solution family, depending, for example, on the convergence of Newton's method.

It can be shown that the above continuation method works near a *regular solution* X_0, *i.e.*, if the null space of $F_X(X_0)$ is one-dimensional. In fact, in this case the Jacobian of Eq. (3.2) evaluated at X_0, *i.e.*, the $n+1$ by $n+1$ matrix

$$\begin{pmatrix} F_X(X_0) \\ \dot{X}_0^* \end{pmatrix} , \tag{3.3}$$

is nonsingular. By the Implicit Function Theorem this guarantees the existence of a locally unique solution family through X_0. This family can be parametrized locally by Δs. Moreover, for Δs sufficiently small, and for sufficiently accurate initial approximation, (*e.g.*, $X_1^{(0)} = X_0 + \Delta s \dot{X}_0$), Newton's method for solving Eq. (3.2) can be shown to converge. Branch points along the solution family correspond to singularity of the Jacobian in Eq. (3.3); such points can be located accurately, and there are standard branch switching algorithms [71].

3.2 Periodic solutions

Here we describe briefly how pseudo-arclength continuation can be used to compute a family of periodic solutions of a dynamical system

$$x'(t) \;=\; f(x(t), \lambda) \;, \qquad f \;:\; \Re^n \times \Re \;\rightarrow\; \Re^n \;, \tag{3.4}$$

where $\lambda \in \Re$ is a physical parameter. In this case the continuation step corresponding to Eq. (3.2) takes the form of the following constrained periodic boundary value

problem:

$$
\begin{aligned}
&a_1) \quad x_1'(t) \;=\; T_1 f(x_1(t), \lambda_1) \;, \\
&a_2) \quad x_1(0) \;=\; x_1(1) \;, \\
&a_3) \quad \int_0^1 x_1(\tau)^*\, x_0'(\tau)\, d\tau \;=\; 0 \;,
\end{aligned}
\tag{3.5}
$$

$$
b) \quad \int_0^1 (x_1(\tau) - x_0(\tau))^* \dot{x}_0(\tau)\, d\tau + (T_1 - T_0)\dot{T}_0 + (\lambda_1 - \lambda_0)\dot{\lambda}_0 \;=\; \Delta s \;.
$$

This equation must be solved for $X_1 = (x_1(\cdot), T_1, \lambda_1)$, given a solution $X_0 = (x_0(\cdot), T_0, \lambda_0)$ and the path tangent $\dot{X}_0 = (\dot{x}_0(\cdot), \dot{T}_0, \dot{\lambda}_0)$. Here $T_1 \in \Re$ is the unknown period. Eq. (3.5a_2) imposes unit periodicity, after rescaling of the independent variable t. Eq. (3.5a_3) is a phase condition, which fixes the phase of the new orbit $x_1(\cdot)$ relative to the given orbit $x_0(\cdot)$. It may be replaced by the classical Poincaré phase condition

$$
a_3') \quad (x_1(0) - x_0(0))^*\, x_0'(0) \;=\; 0 \;.
$$

However, the integral phase condition (3.5a_3) has the desirable property of minimizing phase drift relative to $x_0(\cdot)$, which often allows much bigger continuation steps to be taken. Eq. 3.5b is the functional form of the pseudo-arclength constraint (3.2b). More details on this boundary value approach for computing periodic solutions can be found in [39]; further references include [32, 67, 37].

In each continuation step, Eq. (3.5) is solved by numerical boundary value algorithms. In particular, AUTO uses piecewise polynomial collocation with Gauss-Legendre collocation points ("*orthogonal collocation*") [24, 7, 8], similar to COLSYS [6], and COLDAE [9], with adaptive mesh selection [101]. Combined with continuation, this allows the numerical solution of "difficult" problems, as illustrated by the near-homoclinic and near-collision orbits in this thesis. (For other challenging applications see, for example, [33].) AUTO determines the characteristic multipliers (or Floquet multipliers), that determine asymptotic stability and bifurcation properties, as a by-product of the decomposition of the Jacobian of the boundary value collocation system [39, 45, 78].

3.3 Periodic solutions of the CR3BP

Equation (2.51) describes a *conservative system*, with one conserved quantity, namely the Jacobi constant C defined in Eq. (2.56). In order to use boundary value algorithms, we must introduce an *unfolding term* with corresponding *unfolding parameter*, as discussed in detail in [40] and [83].

First rewrite Eq. (2.51) as a first order system, scale time, so that the period T appears explicitly in the equations, and add periodic boundary conditions and the integral phase constraint, as in Eq. (3.5). As discussed in [40] and theoretically justified in [83], a suitable choice for the unfolding term is $\lambda \nabla E$, where λ is the unfolding parameter. However, this choice is not unique, and for the CR3BP it is more convenient to introduce a simpler unfolding term, namely one that corresponds to "damping". The first order system is then given by

$$\begin{aligned}
x' &= Tv_x \ , \\
y' &= Tv_y \ , \\
z' &= Tv_z \ , \\
v_x' &= T[2v_y + x - (1-\mu)(x+\mu)r_1^{-3} - \mu(x-1+\mu)r_2^{-3}] + \lambda v_x \ , \\
v_y' &= T[-2v_x + y - (1-\mu)yr_1^{-3} - \mu y r_2^{-3}] + \lambda v_y \ , \\
v_z' &= T[-(1-\mu)zr_1^{-3} - \mu z r_2^{-3}] + \lambda v_z \ .
\end{aligned} \tag{3.6}$$

It is important to stress that, while λ is a scalar unknown that is solved for at each continuation step, its value will be zero (up to numerical precision) upon convergence [83].

3.4 Loci of bifurcation points

As is evident from the numerical results reported in this thesis, much insight into the global periodic solution structure can be gained from computing loci of singular points, such as loci of Hopf bifurcations (Fig. 4.1), loci of bifurcation points (*e.g.*, Fig. 5.1), and loci of homoclinic orbits (Fig. 5.38).

3.4.1 Loci of Hopf points

It is well known how to follow Hopf bifurcation points in generic problems; see, for example [38], and references therein. This continuation only involves an algebraic system, and requires two free problem parameters in addition to the period (or frequency) associated with the bifurcation. AUTO uses a so-called "*fully extended system*" for following Hopf bifurcations.

The technique applies without change for following the "Hopf bifurcations" in the CR3BP, provided that the unfolding parameter λ is included in the formulation; *i.e.*, the free problem parameters are μ, λ, and the period T. This standard capability of AUTO was used to compute the curves in Fig. 4.1. In the CR3BP each pair of purely imaginary eigenvalues at a libration point corresponds to a "Hopf bifurcation" in this sense. Actually, this computation simply retraces the equilibria, while tracking one of the periods at the same time.

3.4.2 Loci of homoclinic orbits

There are advanced algorithms for the continuation of homoclinic orbits that include the detection of higher codimension singularities and their continuation. Many such algorithms are included in the HomCont software which is part of AUTO. However, by far the simplest method for following homoclinic orbits is to follow periodic orbits that approximate it. In a generic system one simply fixes the period T at a sufficiently large value, while freeing another problem parameter. Thus such a continuation has two free problem parameters, which is consistent with the codimension of a homoclinic orbit. The approach applies without change to the continuation of homoclinic orbits in the CR3BP, provided the unfolding parameter λ is included in the formulation;

i.e., the free problem parameters are μ and λ. In our calculations we have fixed the value of the period at $T = 500$, although we have also used much higher values of T, for example $T = 10^5$. There is no difficulty in using such high values, since the adaptive high-order discretization used in AUTO allows the computation of such periodic orbits.

3.4.3 Loci of branch points

It is well-known how to compute loci of folds, torus bifurcations, and period-doubling bifurcation in generic dynamical systems. For a recent paper on the theory and the efficient implementation of such algorithms, see [35]. These methods apply equally well to conservative systems such as the CR3BP, given the inclusion of the unfolding parameter λ in the continuation scheme. (Note that there are no genuine folds in the computation of families of periodic orbits in the CR3BP, as all such families are "vertical", *i.e.*, the unfolding parameter λ is always zero. However, one can consider tracking folds with respect to the period T.) Here we present loci of bifurcation orbits. The computation of the loci of period-doubling bifurcations in Fig. (5.7) is accomplished by simply doubling the length of the interval of periodicity from T to $2T$. The locus of period-doubling bifurcations can then be computed as a locus of bifurcation points. Thus we need only consider the computation of bifurcation loci. This continuation is not as standard as the continuation of the generic codimension 1 singularities, and for this reason we describe the algorithm in detail below.

First consider the case of Eq. (3.1), *i.e.*, $F(X) = 0$, where $F : \Re^{n+1} \to \Re^n$. Generically, at a solution X, the Jacobian $F_X(X)$ has full rank, ensuring a locally unique solution family $X(s)$, where s is, for example, the pseudo-arclength parameter ("Δs" in Eq. (3.2)). The simplest non-generic situation is where $F_X(X)$ has a rank drop of one, *i.e.*, rank $F_X(X) = n - 1$, which generically corresponds to a simple bifurcation. In this case the transpose $F_X^*(X)$ has a one-dimensional null space. An

extended system for following a locus of such bifurcations is then given by

$$\begin{aligned} F(X) &= 0 \,, \\ F_X^*(X)\, W &= 0 \,, \\ W^*W - 1 &= 0 \,. \end{aligned} \tag{3.7}$$

Note that Eq. (3.7) comprises $2n+2$ equations, and that it contains $2n+1$ variables, namely, $X \in \Re^{n+1}$ and $W \in \Re^n$. Therefore an additional two variables are needed, say, λ_2 and λ_3, *i.e.*, $F = F(X, \lambda_2, \lambda_3)$. We note that one of the components of X is often considered as a problem parameter, *i.e.*, $X = (x, \lambda_1)$, where $x \in \Re^n$. The tracking of a locus of bifurcations then includes three problem parameters, which is consistent with the codimension of the bifurcation. It can be shown that the resulting system

$$\begin{aligned} a) \quad & F(X, \lambda_2, \lambda_3) = 0 \,, \\ b) \quad & F_X^*(X, \lambda_2, \lambda_3)\, W = 0 \,, \\ c) \quad & W^*W - 1 = 0 \,, \end{aligned} \tag{3.8}$$

is regular at a generic bifurcation point, *i.e.*, that its Jacobian

$$\begin{pmatrix} F_X & O & F_{\lambda_2} & F_{\lambda_3} \\ (F_X^*W)_X & F_X^* & (F_X^*W)_{\lambda_2} & (F_X^*W)_{\lambda_3} \\ 0^* & 2W^* & 0 & 0 \end{pmatrix} , \tag{3.9}$$

has full rank, namely $2n+2$.

The generic setting presented above requires two problem parameters to "find" a bifurcation point, and three parameters to continue a locus of such bifurcations points. In case of symmetries, one often encounters bifurcation points in one-parameter solution families. A locus of such bifurcations then only has two free parameters. However, for numerical purposes one must regularize this continuation through the introduction of an unfolding term with an associated unfolding parameter. The unfolding term

must be chosen so that it "breaks" the bifurcation when the unfolding parameter is non-zero, and such that a solution of the equation only exists (at least locally) if the unfolding parameter is zero. There are many ways to do this; the most general approach is to replace $F(X)$ by $F(X) + \lambda_2 W$, where W is the adjoint null vector in Eq. (3.7). Here λ_2 is the unfolding parameter, which is one of the unknowns in each continuation step, but which will be zero (to numerical precision) upon convergence of the numerical solution procedure.

Now consider the case of bifurcation points for periodic solutions. In this case $X = (x(\cdot), T, \lambda)$, as in Eq. (3.5), and $F(X) = 0$ represents the equations

$$\begin{aligned} x'(t) &= T f(x(t), \lambda_1) \ , \\ x(0) &= x(1) \ , \\ \textstyle\int_0^1 x(\tau)^* \ \hat{x}'(\tau) \ d\tau &= 0 \ , \end{aligned} \tag{3.10}$$

where $\hat{x}(\cdot)$ denotes a reference solution. We need the adjoint F_X^* of the linearized operator F_X. First note that the linear operator F_X acts upon function space elements ("vectors") of the form $(v(\cdot), S, R)$ as follows:

$$F_X \ : \ (v(\cdot), S, R) \rightarrow \begin{cases} v'(t) \ - \ T \ f_x(x(t), \lambda_1) \ v(t) \ - \ S \ f(x(t), \lambda_1) \ - \\ \qquad\qquad\qquad\qquad\qquad\qquad R \ T \ f_{\lambda_1} \ (x(t), \lambda_1) \ , \\ v(0) - v(1) \ , \\ \textstyle\int_0^1 v(\tau)^* \ \hat{x}'(\tau) \ d\tau \ . \end{cases} \tag{3.11}$$

Given this representation, an elementary derivation shows that the adjoint linearized

operator equation corresponding to Eq. (3.8b) is now given by

$$\begin{aligned} w'(t) &= -T\,[f_x^*(x(t),\lambda_1)\,w(t) - \kappa\, f(x(t),\lambda_1)]\,, \\ w(0) - w(1) &= 0\,, \\ \textstyle\int_0^1 w(\tau)^*\, f(x(t),\lambda_1)\, d\tau &= 0\,, \\ \textstyle\int_0^1 w(\tau)^*\, f_{\lambda_1}(x(t),\lambda_1)\, d\tau &= 0\,, \end{aligned} \tag{3.12}$$

where the adjoint variable W in Eq. (3.8) is now given by $W = (v(\cdot), \kappa)$, with $\kappa \in \Re$. The normalization corresponding to Eq. (3.8c) becomes

$$\textstyle\int_0^1 w(\tau)^*\, w(\tau)\, d\tau + \kappa^2 - 1 = 0\,. \tag{3.13}$$

The complete extended system for computing a locus of bifurcation points for periodic solutions now consists of Equations (3.10)-(3.13), which together comprise $2n$ first order ODEs, with $2n$ periodicity boundary conditions, and subject to an additional 4 integral constraints. The unknowns to be solved for in each continuation step are the functions $x(\cdot)$ and $w(\cdot)$, and the five scalar variables T, κ, and $\lambda \equiv (\lambda_1, \lambda_2, \lambda_3) \in \Re^3$. In the generic case, λ represents three problem parameters. The extended system consisting of Eqs. (3.10)-(3.13) then gives a one-dimensional solution family, which can be computed using standard pseudo-arclength continuation. In the non-generic case one must introduce an unfolding term that perturbs the bifurcation. In this case one of the components of λ, say, λ_2 corresponds to the unfolding parameter.

The extended system (3.10)-(3.13) can also be used for tracking bifurcation points in a conservative system, provided that λ_1 corresponds to an appropriate unfolding parameter. For completeness we give the extended system for the CR3BP in detail. First note that Eq. (1.51), with unfolding parameter λ_1 (see Eq. (3.6)), can be written in the form

$$\begin{aligned} x'(t) &= T\, v(t)\,, \\ v'(t) &= T[g(x(t), v(t)) + \lambda_1 v(t)]\,, \end{aligned} \tag{3.14}$$

subject to the periodicity equations

$$x(0) - x(1) \;=\; 0\;, \qquad v(0) - v(1) \;=\; 0\;, \tag{3.15}$$

and the phase constraint

$$\int_0^1 x(\tau)^*\;\hat{x}'(\tau) + v(\tau)^*\;\hat{v}'(\tau)\;d\tau \;=\; 0\;, \tag{3.16}$$

where, as before, $\hat{x}(\cdot)$ denotes a reference solution. Denote the adjoint variables corresponding to $x(\cdot)$ and $v(\cdot)$ as $\tilde{x}(\cdot)$ and $\tilde{v}(\cdot)$, respectively. The adjoint equations are then given by

$$\begin{pmatrix} \tilde{x}'(t) \\ \tilde{v}'(t) \end{pmatrix} = -T\left[\begin{pmatrix} O & g_x(x(t),v(t))^* \\ I & (g_v(x(t),v(t)) + \lambda_1 I)^* \end{pmatrix}\begin{pmatrix} \tilde{x}(t) \\ \tilde{v}(t) \end{pmatrix} - \kappa\begin{pmatrix} v(t) \\ g(x(t),v(t)) + \lambda_1 v(t) \end{pmatrix}\right]\;, \tag{3.17}$$

with adjoint periodicity equations

$$\tilde{x}(0) - \tilde{x}(1) = 0\;, \qquad \tilde{v}(0) - \tilde{v}(1) = 0\;. \tag{3.18}$$

integral constraints

$$\begin{aligned} &\int_0^1 v(\tau)^*\tilde{v}(\tau)\,d\tau = 0\;, \\ &\int_0^1 \{v(\tau)^*\tilde{x}(\tau) + [g(x(\tau),v(\tau)) + \lambda_1 v(\tau)]\tilde{v}(\tau)\}\,d\tau = 0\;, \end{aligned} \tag{3.19}$$

and normalization

$$\int_0^1 [\tilde{x}(\tau)^*\tilde{x}(\tau) \;+\; \tilde{v}(\tau)^*\tilde{v}(\tau)]\,d\tau + \kappa^2 \;= 1\;. \tag{3.20}$$

As in Eqs. (3.10)-(3.13), the above extended system for computing bifurcation loci for the CR3BP comprises $2n$ first order ODEs and $2n$ periodicity boundary conditions, with $n = 6$, and 4 integral constraints. The unknowns to be solved for in each continuation step are the functions $x(\cdot)$, $v(\cdot)$, the adjoint functions $\tilde{x}(\cdot)$, $\tilde{v}(\cdot)$, and the five scalar variables μ, T, κ, and $\lambda \equiv (\lambda_1, \lambda_2) \in \Re^2$. Here μ is the mass-ratio parameter in the CR3BP, λ_1 is the unfolding parameter for conservative systems, and

λ_2 is the additional unfolding parameter introduced to perturb bifurcation points. As before, the unfolding parameters λ_1 and λ_2 are solved for in each continuation step, but they remain zero, up to numerical precision.

It was already noted that the number of differential equations in these extended systems is double the number in the original system. After discretization, and upon application of Newton's method, the resulting linear systems have a very special matrix structure, that can be taken advantage of in the numerical linear algebra.

Alternatively, one can also derive *minimally extended systems* for following branch points, where the number of differential equations remains the same, but where certain auxiliary computations are required. Such minimally extended systems have been considered in detail in [36], for the case of branch points along periodic solution families. The treatment there includes the case where two unfolding parameters are needed, as in Section 3.3 above for the CR3BP.

Chapter 4

Periodic Solutions of the Earth-Moon System

4.1 Periodic orbits that emanate from the libration points

If Eq. (2.51) is rewritten as a first order system in $\Re^6$, then its Jacobian evaluated at the libration points L1, L2, and L3, has two pairs of purely imaginary eigenvalues, which give rise to well-known families of periodic orbits, namely the planar *Lyapunov orbits*, **L**1, **L**2, and **L**3, and the *Vertical orbits*, **V**1, **V**2, and **V**3. (See Table 4.1 for a glossary of abbreviations.) The Jacobian at the libration points L4 and L5 has at least one pair of purely imaginary eigenvalues, for all μ, which gives rise to the families **V**4 and **V**5 of Vertical orbits from L4 and L5, respectively. For μ less than the critical value $\mu_2 \approx 0.0385$, the Jacobian at the libration point L4 and L5 has an additional two pairs of purely imaginary eigenvalues, that give rise to two families of planar orbits, for both L4 and L5 [65]. (For a list of *critical* μ-values see Table 5.1.) For the libration point L4 these families are called the *Long-Period* family and the *Short-Period* family, and similarly for the libration point L5. The Long-Period families that emanate from L4 and L5 are called **L**4 and **L**5, respectively, while the Short-Period families from L4 and L5 actually constitute a single connected family, which we shall refer to as **S**3.

For the Earth-Moon case, the above-mentioned families of periodic orbits, along

with various other families, are represented in the schematic bifurcation diagram in Fig. 4.2, which will be explained in more detail in Sec. 4.2 below. Corresponding periodic orbits are shown in Figs. 4.3-4.25. Bifurcation diagrams for other representative values of μ, as shown in Figs. 5.13-5.25, will be described in Chapter. 5, with periodic orbits from some additional families shown in Figs. 5.26-5.37.

Figure 4.1 shows the limiting value of the period T at the libration points, for each emanating family of periodic orbits. This period satisfies $T = 2\pi/\omega$, where ω is the imaginary part of the corresponding purely imaginary eigenvalues of the Jacobian. In accordance with the summary above, counting double curves, there are eight curves for $\mu_2 < \mu \leq 1/2$, and twelve curves for $0 < \mu < \mu_2$.

The critical value μ_2, already referred to above, corresponds to the fold on the curve in the right-hand panel of Figure 4.1, where two pairs of purely imaginary eigenvalues collide. This critical point is an example of a *Hamiltonian Hopf bifurcation.* The upper portion of the curve that passes through the fold, corresponds to the bifurcating Long-Period families **L**4 (or **L**5), while the lower portion corresponds to the bifurcating Short-Period family **S**3.

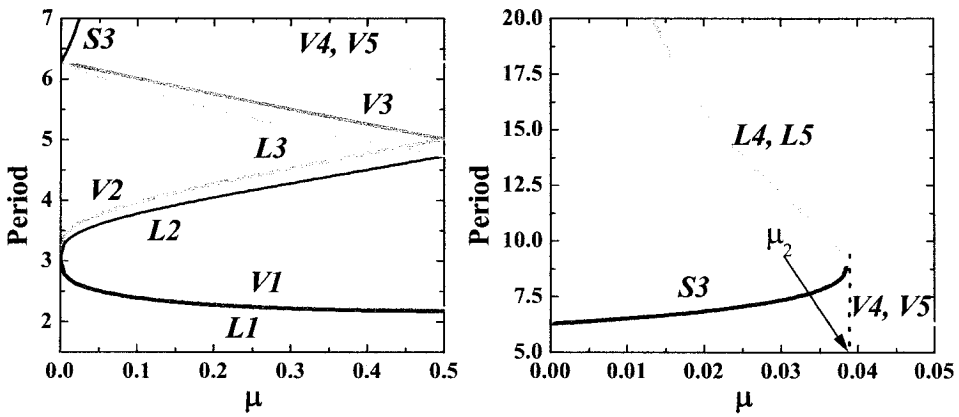

Figure 4.1: The period at the libration points for each emanating family of periodic orbits. The two panels show different details of the diagram. The fold at $\mu_2 \approx 0.0385$ in the panel on the right, corresponds to a Hamiltonian Hopf bifurcation. Due to symmetry, several curves coincide in the diagram; however, the curves for **L**1 and **V**1, although close to each other, do not coincide.

Table 4.1: Abbreviations used for orbit families, branch points and their loci. (Some of these only occur for certain values of μ.)

Symbol	Definition	Example
Li	Libration Point, ($i = 1, \cdots, 5$; red cubes in Fig. 4.2)	Fig. 4.2
Ai	The Axial family from **L**i at Li2, ($i = 1, 2, 3$)	Fig. 4.2
Bi	The Backflip family from **V**i at Vi2, ($i = 1, 2, 3$)	Fig. 4.2
Ci	The planar "Circular" family, ($i = 1, 2$)	Fig. 4.2
D1	The **D**1-family	Fig. 4.2
E1	The **E**1-family from **D**1 at D12	Fig. 4.2
Hi	The Halo family from **L**i at Li1, ($i = 1, 2, 3$)	Fig. 4.2
Ki	The **K**-families from **L**1 at L15-L18, ($i = 1, \cdots, 4$)	Fig. 5.25
Li	The planar Lyapunov family from Li, ($i = 1, 2, 3$)	Fig. 4.2
Li	The Long-Period planar family from Li, ($i = 4, 5$)	Fig. 4.2
R2	The **R**2-family from **L**2 at L24	Fig. 4.2
Si	The planar families from **L**i at Li3, ($i = 1, 2$)	Fig. 5.25
T1	The **T**1-family from **L**1 at L14	Fig. 5.18
T2	The **T**2-family from **L**2 at L25	Fig. 5.16
Vi	The Vertical family from Li, ($i = 1, \cdots, 5$)	Fig. 4.2
Wi	The **W**4/**W**5-family connecting V41 to V51	Fig. 4.2
Xi	The **X**4/**X**5-family from **V**4/**V**5 at V42/V52	Fig. 5.25
Zij	Branch point j along family **Z**i, where **Z** = **L**, **V**, $\cdots$	Fig. 4.2
Zij	Locus of branch points Zij	Fig. 5.1

4.2 Periodic Solutions of the Earth-Moon System

In this section we give an overview of families of elemental periodic orbits for the Earth-Moon system, as represented in the schematic bifurcation diagram in Fig. 4.2. This bifurcation diagram is more complete than that given in [40], and it is accompanied by diagrams that show examples of the actual orbits, namely, in Figs. 4.3-4.25. In Sec. 5.1 we will explain how the bifurcation picture changes with μ.

Each point on a curve in the bifurcation diagram in Fig. 4.2 represents a periodic solution, with its associated period. The notation used to denote orbit families and branch points is summarized in Table 4.1. Along the families of periodic solutions there are various branch points. In this thesis we use the term *branch point* to denote transcritical and pitch-fork bifurcations, thereby excluding period-doubling, torus, and subharmonic bifurcations. At a branch point, distinct periodic solution families intersect, with identical orbit and identical minimal period at the point of intersection. Apart from some special cases, we do not present results on solution families that bifurcate from period-doubling and subharmonic bifurcations. However, the solution structure that we present can be viewed as a "skeleton", from which many other solutions may be reached [27].

The orbits shown in Figs. 4.3-4.25 are represented by colored curves. Orbits that correspond to branch points in the bifurcation diagram ("*branching orbits*") appear annotated and colored differently; such orbits belong to two different families. The pink cubes denote the libration points, and the gray disk represents the Moon's orbit. The standard rotating barycentric coordinate system for the CR3BP is used. We note that the Earth and the Moon are not drawn on scale.

The diagram in Fig. 4.2 is qualitatively correct for the Earth-Moon system, for which $\mu = 0.01215$, and for neighboring μ-values, as explained in Sec. 5.1. Many features of the bifurcation diagram in Fig. 4.2 are, in fact, qualitatively correct for all μ-values, $(0 < \mu < 1/2)$; however, there are certain features that depend on μ, as specified in detail in Sec. 5.1.

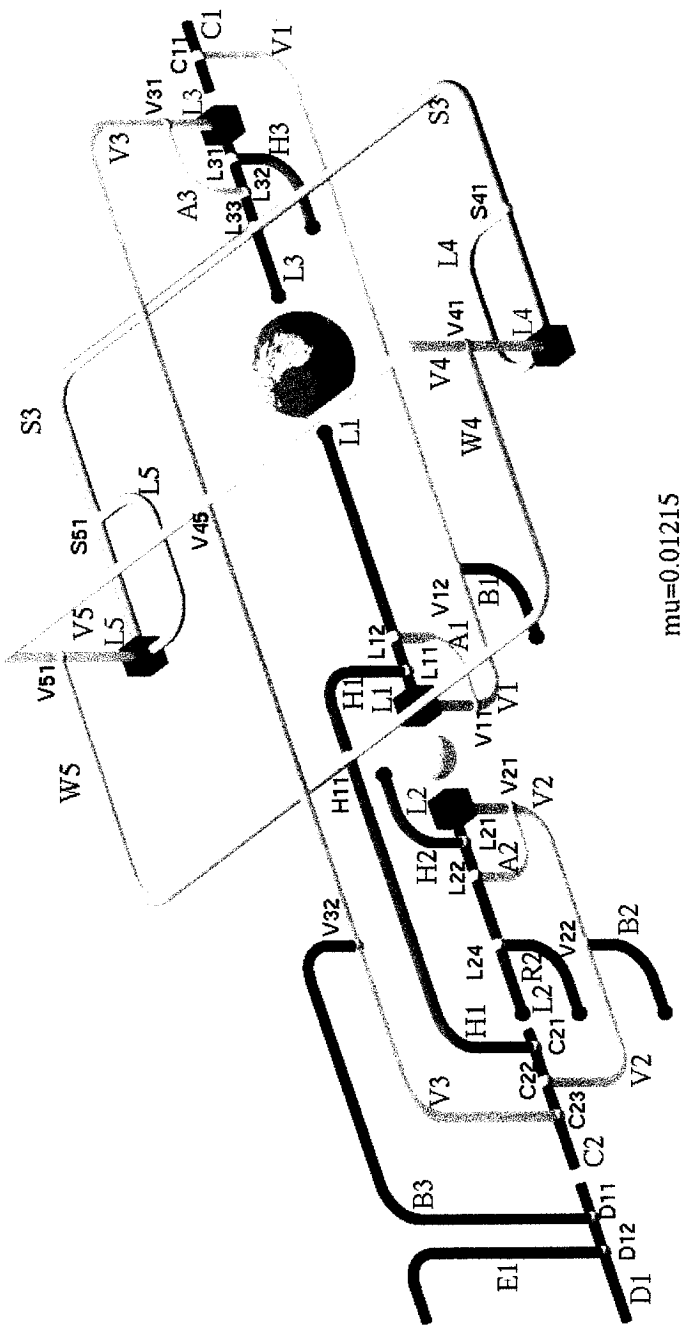

Figure 4.2: Bifurcation diagram for the Earth-Moon system ($\mu = 0.01215$), showing families of periodic orbits that emanate from the libration points and from subsequent branch points. The red cubes are libration points. Small white spheres denote branch points, and small dark-red spheres denote collision orbits. The planar families **C1**, **C2**, and **D1**, are only partially represented. A glossary of the notation used is given in Table 4.1

4.2.1 The Planar Lyapunov families

As mentioned in Sec. 4.1, the families of planar Lyapunov orbits are represented by the curves **L**1, **L**2, and **L**3 in Fig. 4.2, where the family **L**i emanates from the libration point Li, respectively, ($i = 1, 2, 3$). Actual orbits from the planar Lyapunov families are shown in Figs. 4.3-4.5. The Lyapunov families **L**1, **L**2, **L**3 terminate in orbits that collide with the primaries. Such collision orbits are denoted by small dark-red spheres in Fig. 4.2.

Figure 4.2 shows two branch points along the planar Lyapunov family **L**1, and three branch points along each of the Lyapunov families **L**2 and **L**3. The branch points along the family **L**1 are denoted L11 and L12, and branch points along other solution families are designated similarly.

4.2.2 The Long-Period and Short-Period planar Lyapunov families

For $0 < \mu < \mu_2$ (see Table 5.1), and in particular for the Earth-Moon system, there are two planar Lyapunov families that emanate from the libration point L4; these families are referred to as the "Long-Period" family and the "Short-Period" family.

The Short-Period family **S**3 connects the libration point L4 to the libration point L5, while half-way it connects to the **L**3 family at the branch point L33. Orbits along one-half of the **S**3 family are shown in Fig. 4.6, namely, orbits between the libration point L4 and the branch point L33.

The Long-Period family from L4 is denoted **L**4, and orbits along this family are shown in Fig. 4.7. There are no branch points along the Long-Period family **L**4, except for the end point S41, where **L**4 reconnects to the Short-Period family **S**3. The precise nature of this connection depends on μ; for the Earth-Moon system it corresponds to a period-quadrupling bifurcation.

By the $(x, y, z) \rightarrow (x, -y, z)$ symmetry, the same happens to the libration point L5: a Long-Period family (**L**5) and the Short-Period family (**S**3) emanate from L5, and the Long-Period family reconnects to the Short-Period family at the branch point S51. Corresponding Long-Period and Short-Period orbits can be obtained by reflection across the $x - z$-plane of orbits in Fig. 4.6 and Fig. 4.7.

4.2.3 The Vertical families

The families of Vertical orbits are represented by **V**1-**V**5 in Fig. 4.2, where the family **V**i emanates from the libration point Li, respectively, ($i = 1, ..., 5$). Corresponding orbits appear in Figs. 4.8-4.11. As shown in the bifurcation diagram (Fig. 4.2), the Vertical families that emanate from L4 and L5 are smoothly connected, and they can be considered as a single family, referred to as the **V**4/**V**5 family.

Along the Vertical family **V**1 there are three branch points, denoted V11, V12, and C11. Along the Vertical family **V**2 there are also three branch points, namely, V21, V22, and C22. Note, however, that there are four branch points along the Vertical family **V**3, namely, V31, V32, C23, and the branch point denoted V45, where the Vertical family **V**3 connects to the Vertical family **V**4/**V**5. Along the Vertical family **V**4/**V**5 there are the branch points V41 and V51, and the above-mentioned branch point V45, located at the midpoint.

The Vertical families **V**1, **V**2, and **V**3 connect to "circular" planar orbits at the branch points C11, C22, and C23, respectively. These branch points correspond to "reverse period-doubling" bifurcations. For the Vertical families **V**1 and **V**2 the reverse period-doubling bifurcations C11 and C22 correspond to the third branch point along the family away from the libration point, whereas for the Vertical family **V**3 the reverse period-doubling bifurcation C23 corresponds to the fourth branch point. The planar orbits corresponding to C22 and C23 encompass both primaries, and both belong to the Circular family **C**2. The planar orbit corresponding to C11 encompasses the larger primary only, and belongs to the Circular family **C**1.

4.2.4 The Halo families

The Halo families **H**i bifurcate from the Lyapunov families **L**i at the branch point Li1, for $i = 1, 2, 3$. At this branch point the North-South symmetry is broken, and so, for each i, there are actually two Halo families **H**i, namely the so-called Northern and Southern Halo families. In the solution diagrams in Figs. 4.12-4.14 only the Northern Halo families are shown.

The Halo families **H**2 and **H**3 terminate in collision orbits. The Halo family **H**1

that bifurcates from the Lyapunov family **L**1 at the branch point L11, connects to the planar family **C**2 at the branch point C21. Along the Halo family **H**1 there is another branch point, denoted H11, from which the **W**4/**W**5 family bifurcates, which in turn connects to the Vertical family **V**4 at the branch point V41, and to its symmetry partner **V**5 at V51.

4.2.5 The Axial families

The Axial families **A**i that bifurcate from the Lyapunov families **L**i at the branch points Li2, connect at their other end to the Vertical families **V**i at the branch points Vi1, respectively, ($i = 1, 2, 3$). Representative Axial orbits can be seen in Figs. 4.15-4.17. These orbits are invariant under the reflection $(x, y, z) \rightarrow (x, -y, -z)$ and intersect the x-axis at two points, which explains the name of these families. Each of the Axial families **A**i consists, in fact, of two families, related by a reflection across the $x - z$-plane. Note that the limiting branching orbits Li2 and Vi1 are invariant under this reflection.

4.2.6 The Backflip families

The branch points Vi2 along the Vertical families **V**i give rise to the non-planar Backflip families, **B**i, ($i = 1, 2, 3$), whose orbits are shown in Figs. 4.18-4.20. The Backflip family **B**1 undergoes rather complicated transitions, which are described in detail in [31]. The orbits are named after the so-called "Backflip maneuver" described in [108]. Both of the Backflip families **B**1 and **B**2 end in collision orbits, while the Backflip family **B**3 connects to the planar family **D**1.

Each of the Backflip families **B**i ($i = 1, 2, 3$) consists of two families, related by a reflection across the $x - y$-plane, and originating from a pitchfork bifurcation at the branching orbits Vi2, which themselves are invariant under such reflection.

4.2.7 The W4/W5 family

Along the Vertical family **V**4 there is a pitchfork bifurcation at the branch point V41, resulting in two families, both denoted **W**4, and related by a reflection across

the $x-y$-plane. Symmetrically with respect to the $x-z$-plane the same happens at the branch point V51 on the Vertical family **V**5, leading to two families, both denoted **W**5. The Northern parts of **W**4 and **W**5 connect to each other and to the Northern Halo family **H**1 at the branch point H11. Similarly the Southern parts of **W**4 and **W**5 (not shown in Fig. 4.2) connect to each other and to the Southern Halo family **H**1 at the Southern partner of H11. Figure 4.21 shows orbits along the Northern part of **W**4, between the branch points V41 and H11, thereby covering one quarter of the complete **W**4/**W**5 family. The remaining three parts of **W**4/**W**5 can be obtained by applying the above-mentioned symmetry operations.

4.2.8 The Circular families

The reverse period-doubling orbit C11 at the end of the Vertical family **V**1, belongs to a family of planar circular orbits, called **C**1. Orbits along the Circular family **C**1 encompass the Earth only, as shown in Fig. 4.22.

The reverse period-doubling orbits C22 and C23 at the end of the Vertical families **V**2 and **V**3, respectively, both belong to a second family of planar "circular" orbits, namely, **C**2. Orbits along the Circular family **C**2 encompass both primaries, as shown in Fig. 4.23.

4.2.9 The D1 family

Another family of planar orbits can be reached via the Backflip family **B**3. This family, called **D**1, is only partially shown in the bifurcation diagram in Fig. 4.2. Some of its orbits can be seen in Fig. 4.24. Along the family **D**1, there is another branch point, namely D12, from which the **E**1 family bifurcates. Actually, the **D**1 family bifurcates from the **C**1 family via a period-doubling bifurcation, as indicated by a dashed arrow in Fig. 4.22, although this connection is not shown in the bifurcation diagram.

4.2.10 The E1 family

Two families originate from a pitchfork bifurcation at the branch point D12 along **D**1. These two families, both denoted by **E**1, are related by a reflection across the $x-y$-plane. Some representative orbits along one of the **E**1 families are shown in Fig. 4.25.

4.2.11 The R2 family

At the branch point L24 there is a pitchfork bifurcation, resulting in two bifurcating families, both denoted by **R**2, and related by a reflection across the $x-y$-plane. The orbits along one of these families are shown in Fig. 4.26.

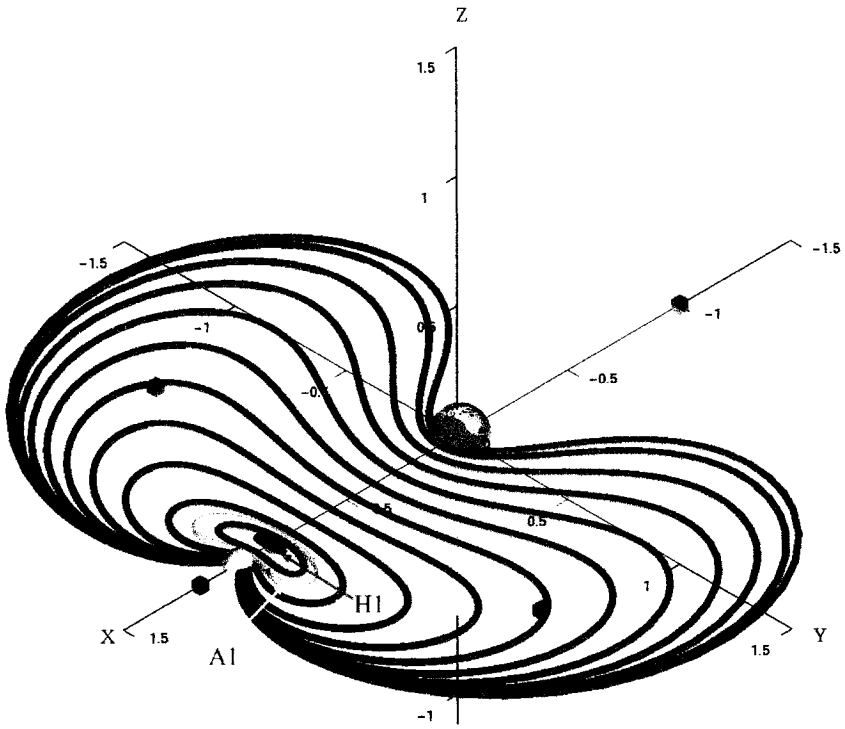

Figure 4.3: The planar Lyapunov family **L1** of the Earth-Moon system.

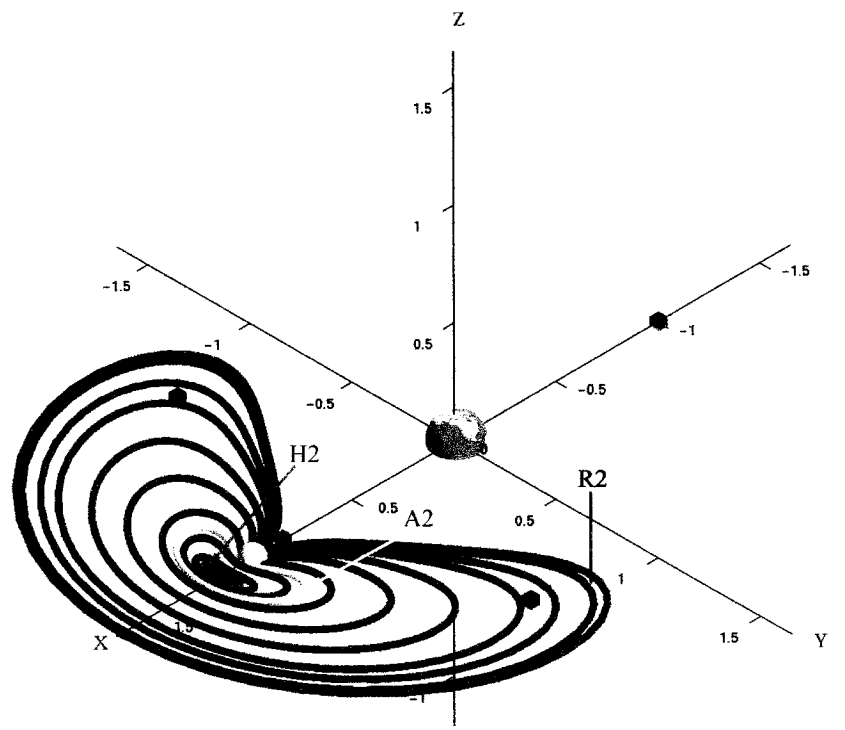

Figure 4.4: The planar Lyapunov family **L2** of the the Earth-Moon system.

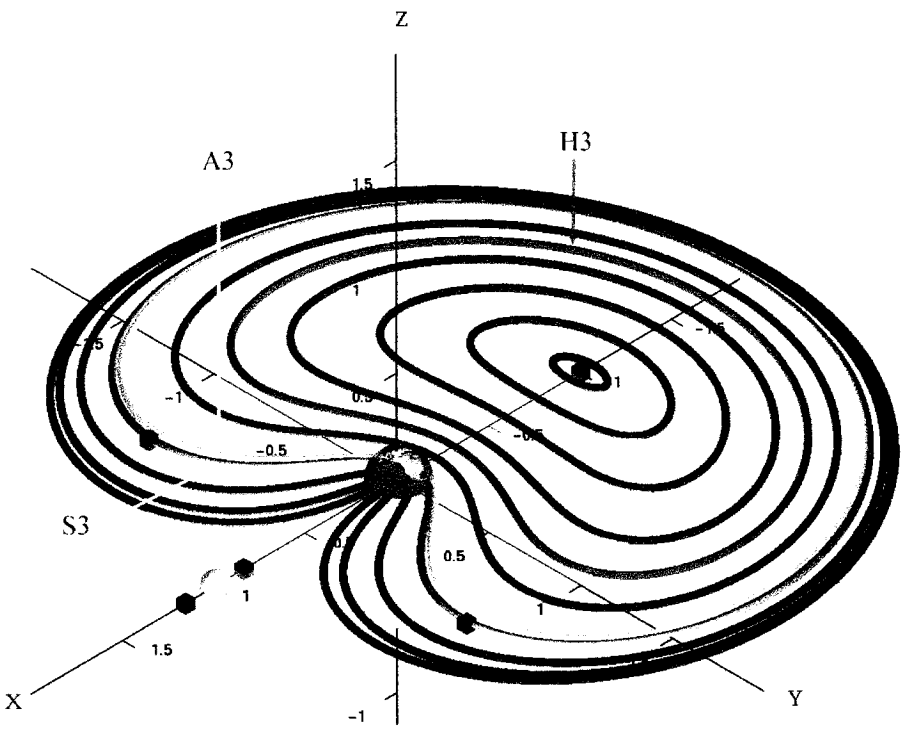

Figure 4.5: The planar Lyapunov family **L3** of the Earth-Moon system.

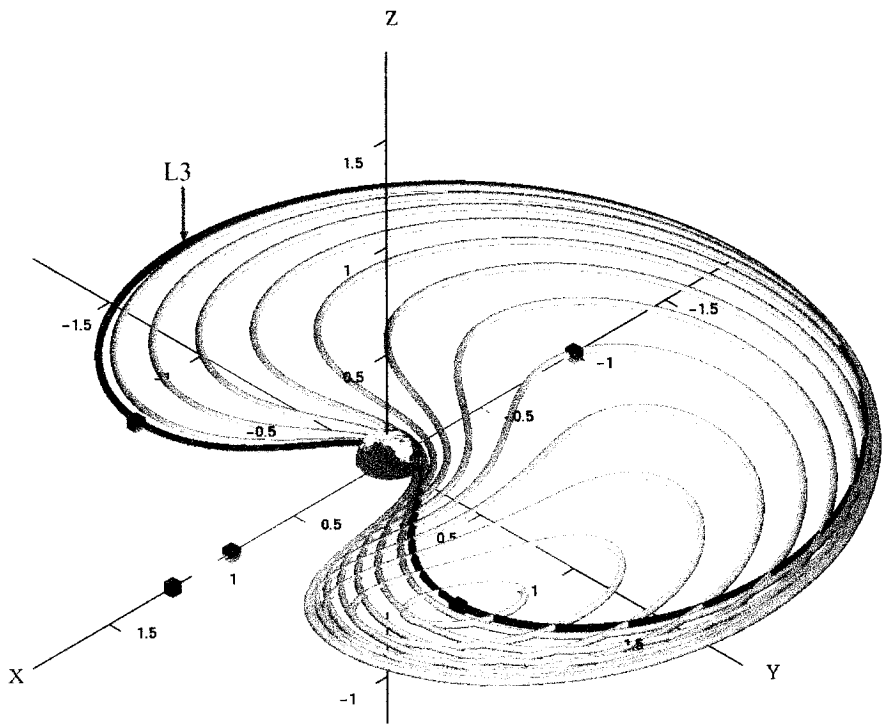

Figure 4.6: The planar Short-Period family **S3** of the Earth-Moon system.

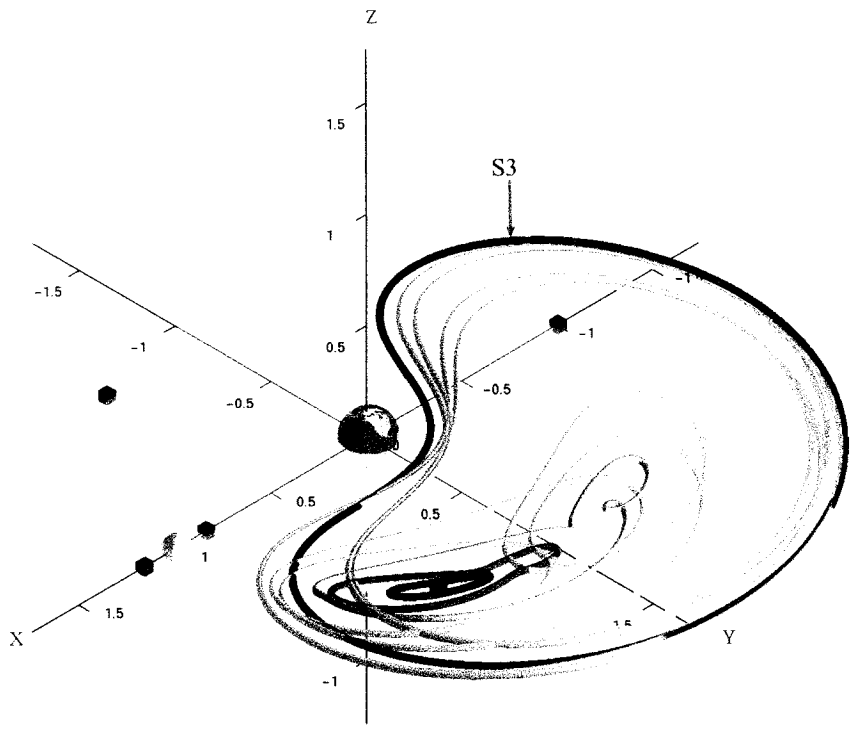

Figure 4.7: The planar Long-Period family **L4** of the Earth-Moon system.

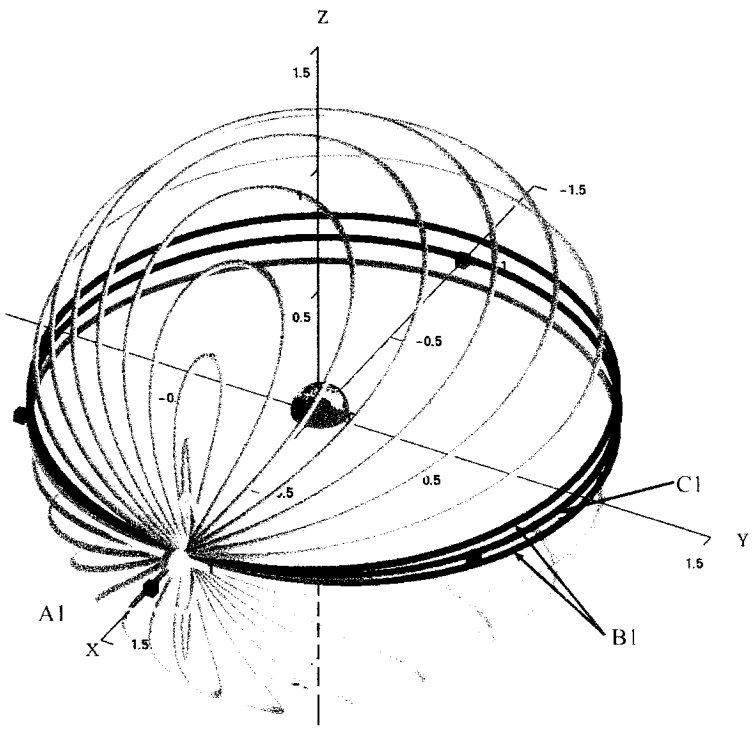

Figure 4.8: The Vertical family **V1** of the Earth-Moon system.

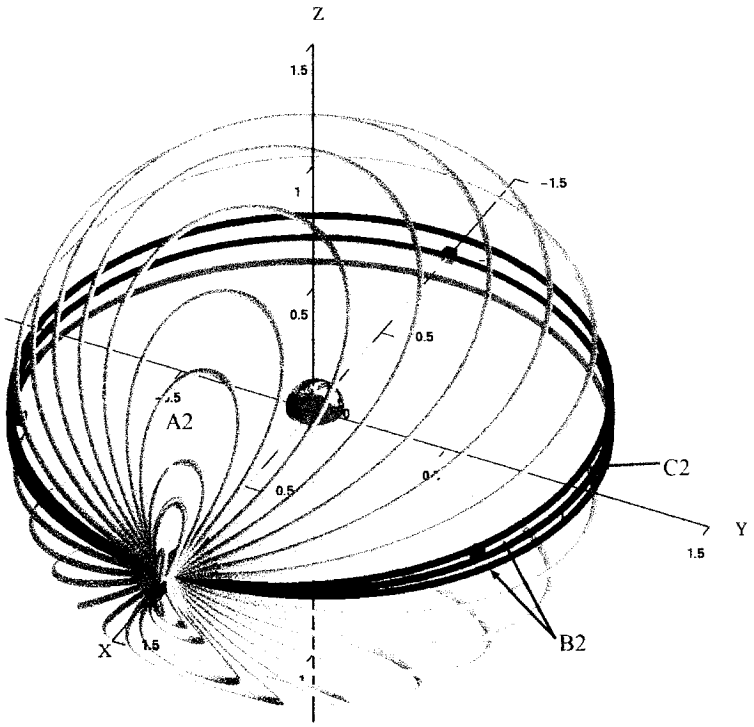

Figure 4.9: The Vertical family **V2** of the Earth-Moon system.

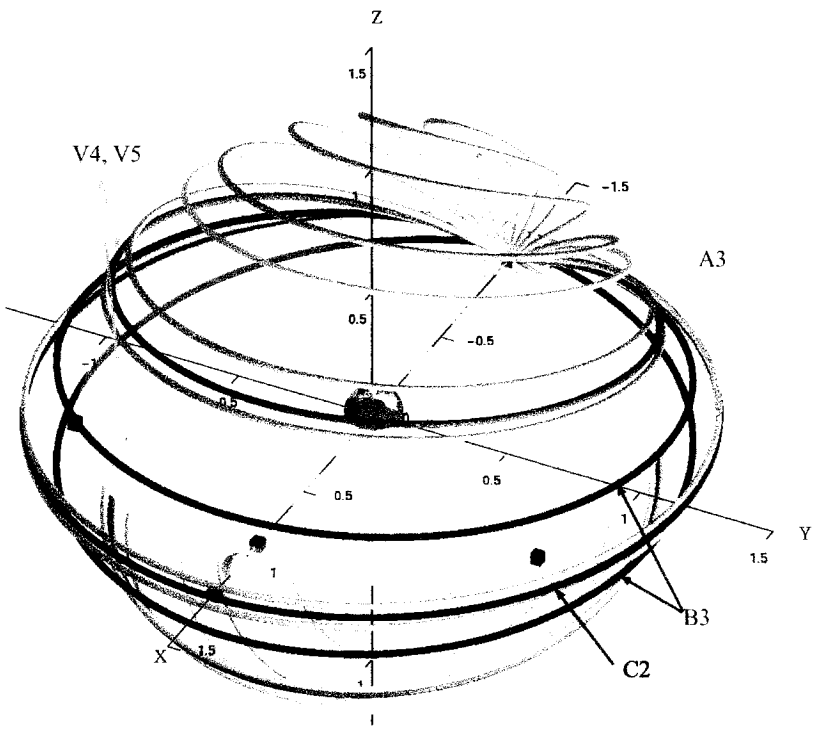

Figure 4.10: The Vertical family **V3** of the Earth-Moon system.

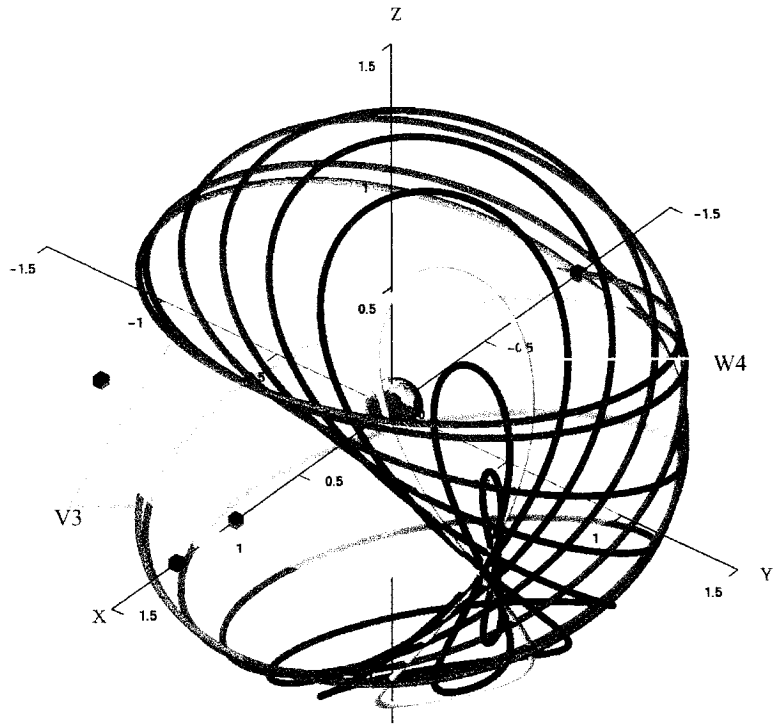

Figure 4.11: The Vertical family **V4** of the Earth-Moon system.

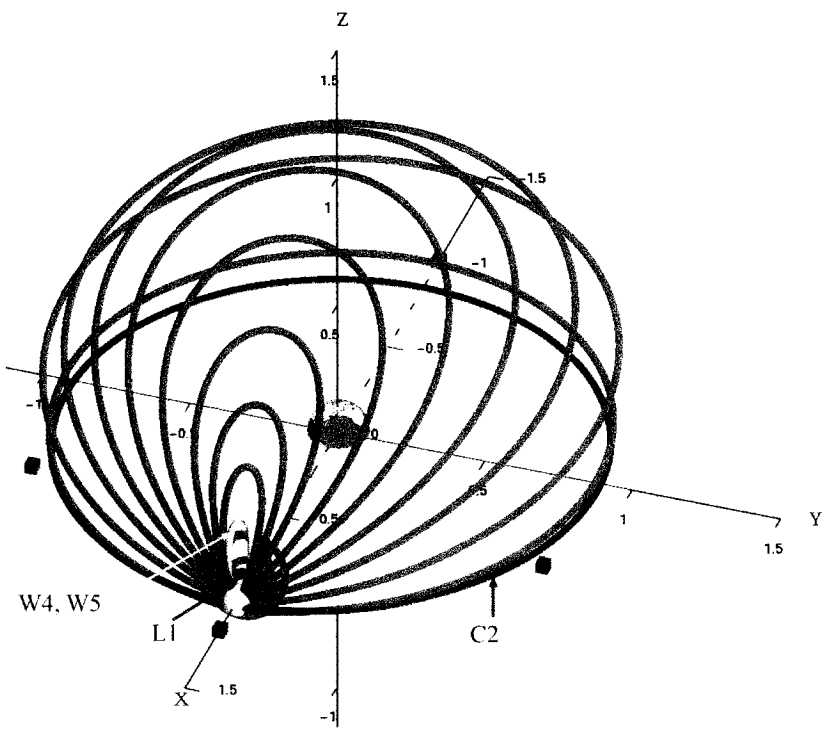

Figure 4.12: The Northern Halo family **H1** of the Earth-Moon system.

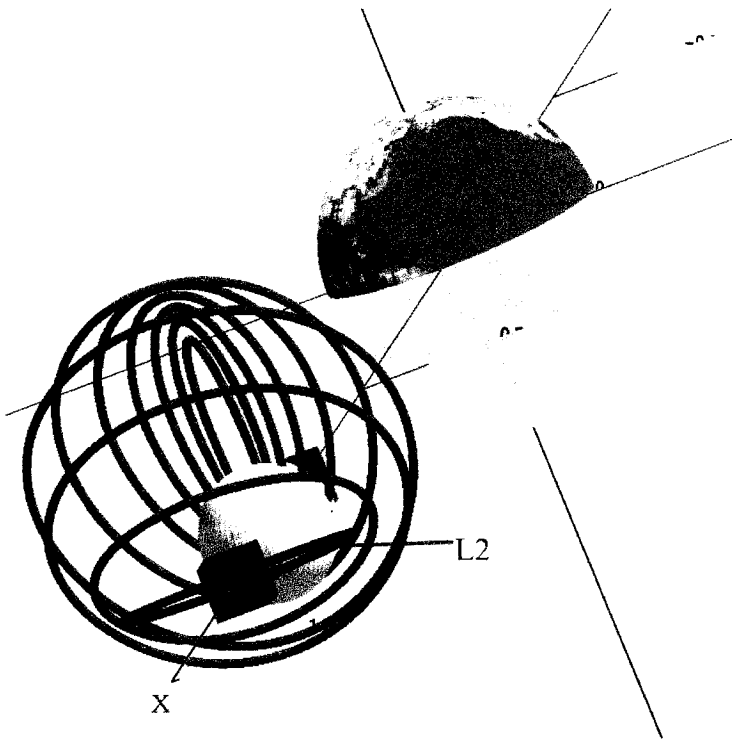

Figure 4.13: The Northern Halo family **H2** of the Earth-Moon system.

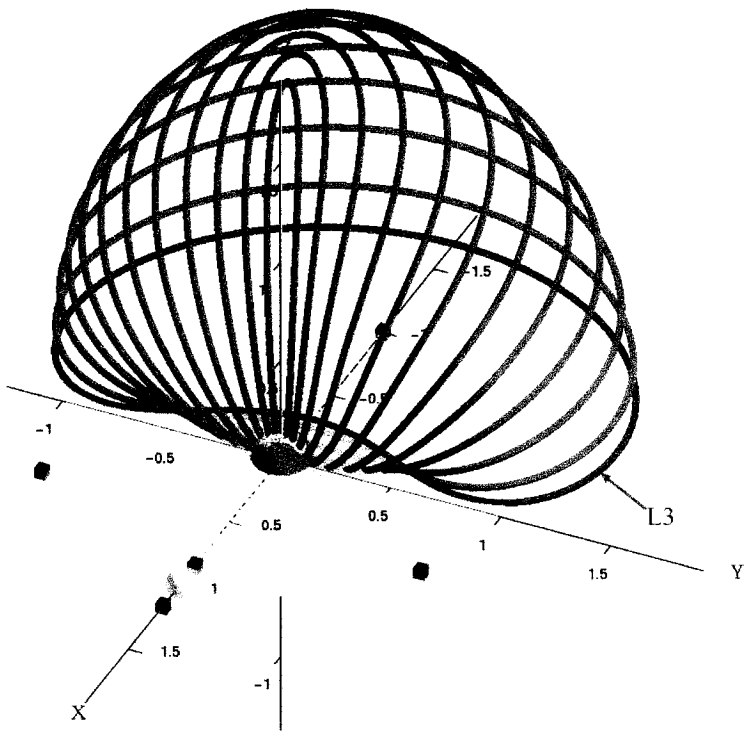

Figure 4.14: The Northern Halo family **H3** of the Earth-Moon system.

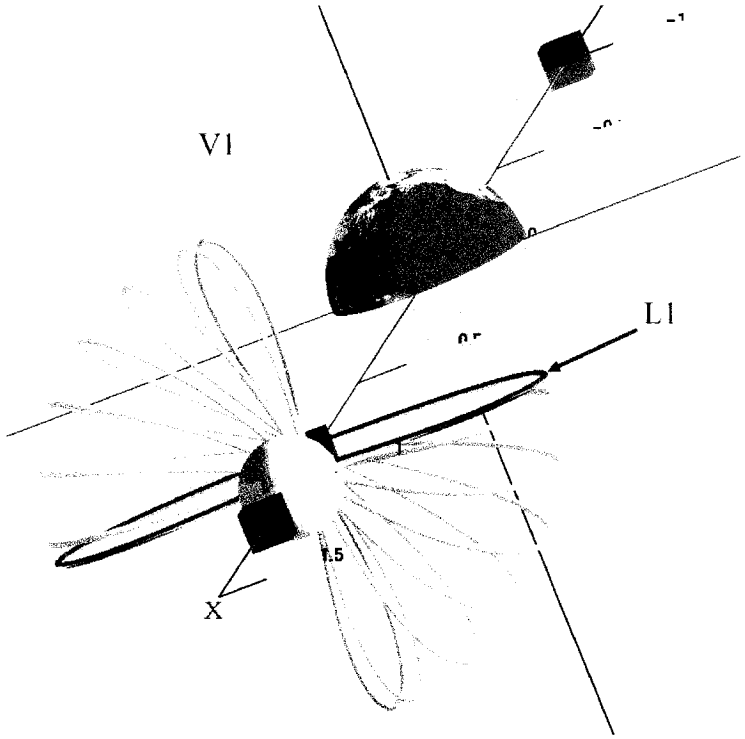

Figure 4.15: The Axial family **A1** of the Earth-Moon system.

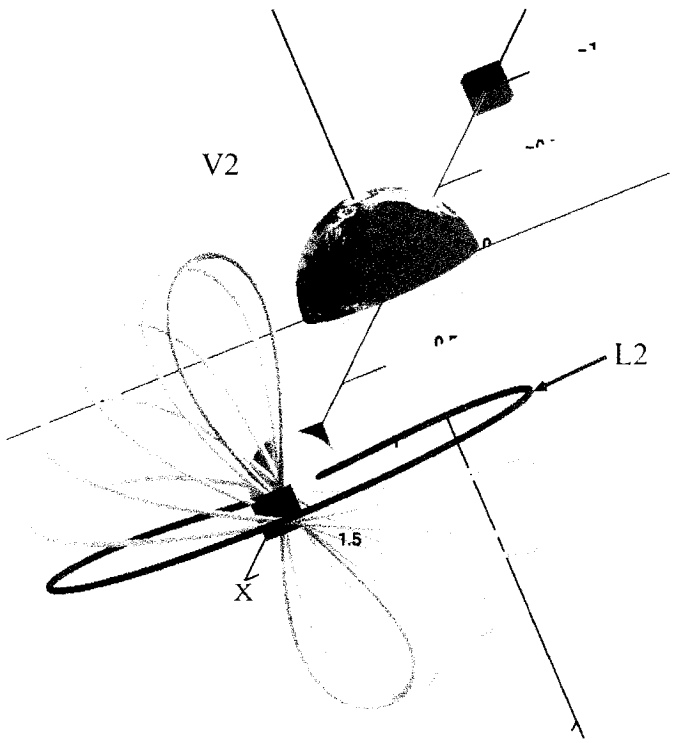

Figure 4.16: The Axial family **A2** of the Earth-Moon system.

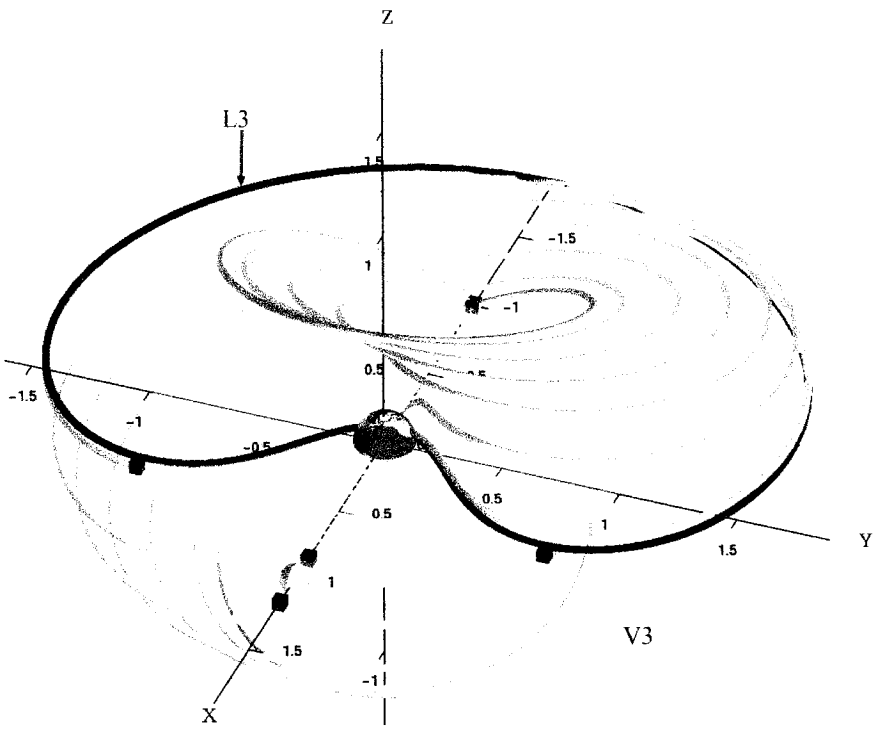

Figure 4.17: The Axial family **A3** of the Earth-Moon system.

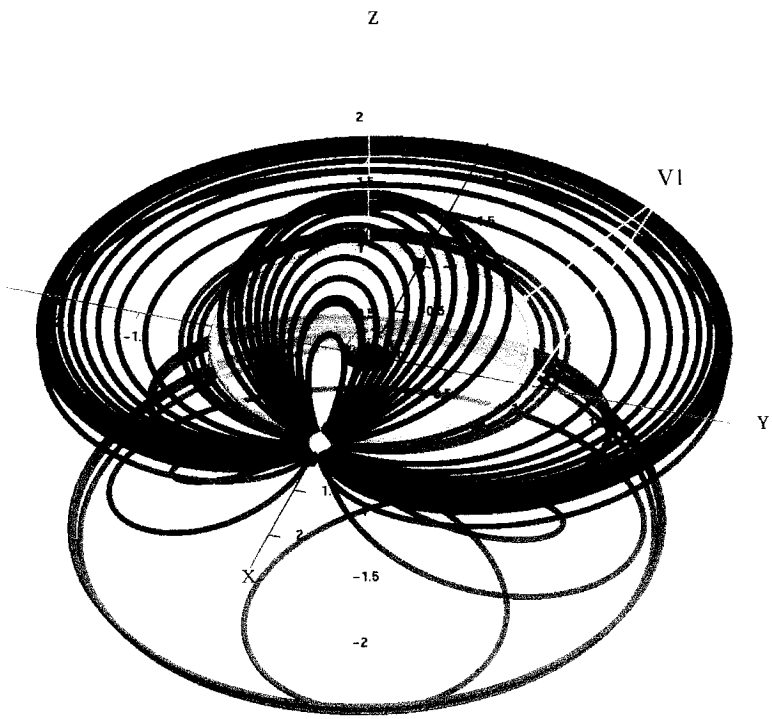

Figure 4.18: The Northern part of the **B1** family of the Earth-Moon system.

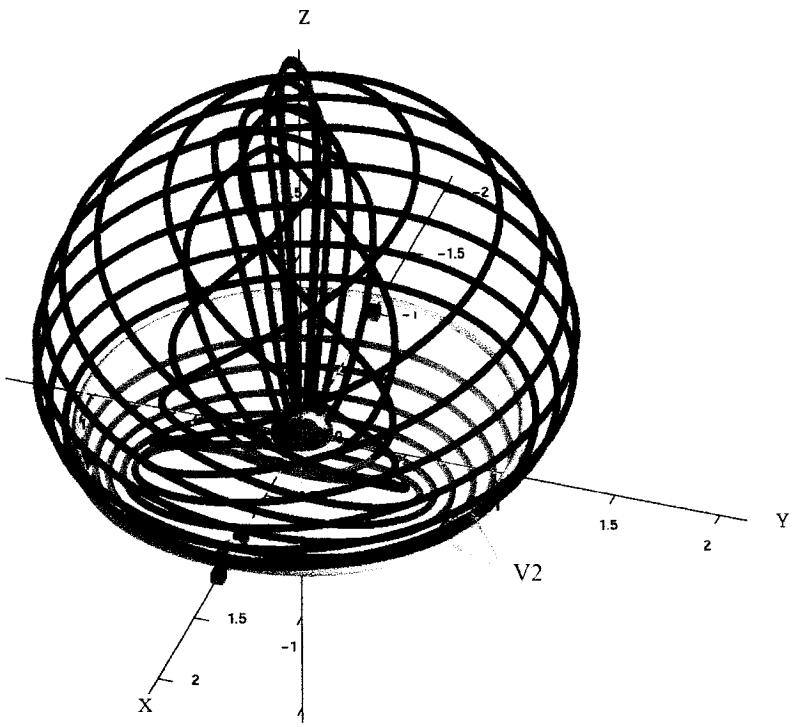

Figure 4.19: The Northern part of the **B2** family of the Earth-Moon system.

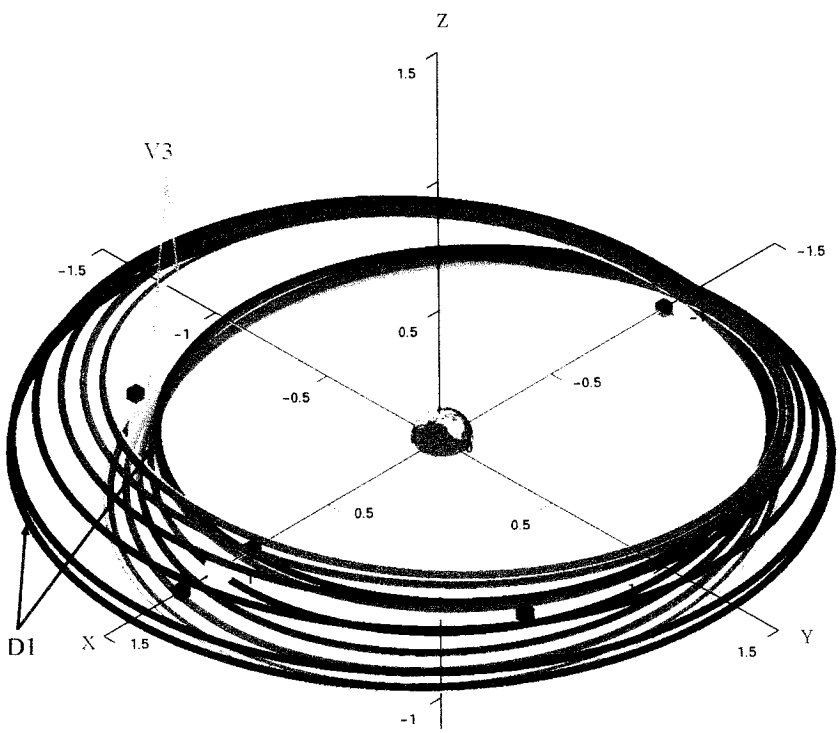

Figure 4.20: The Northern part of the **B3** family of the Earth-Moon system..

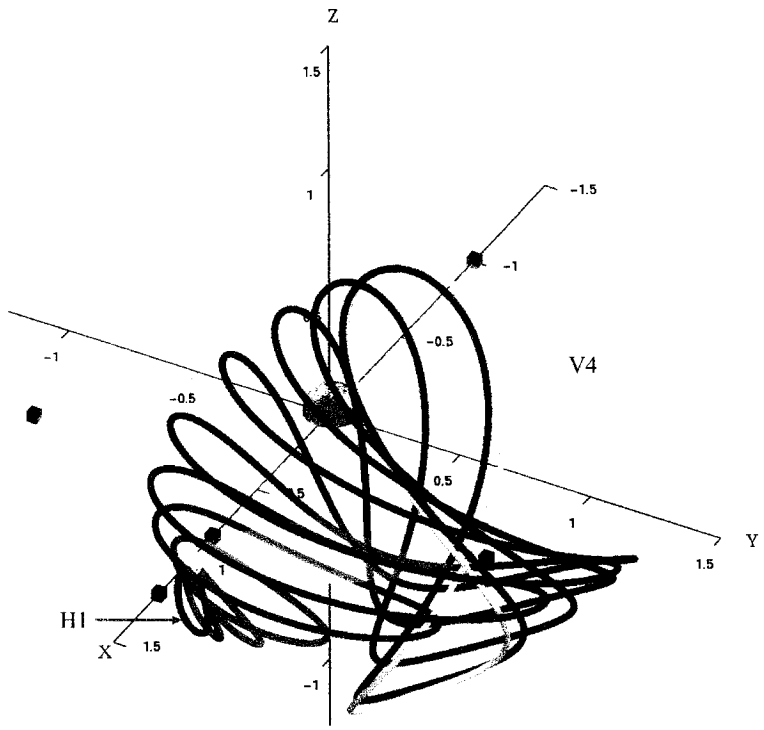

Figure 4.21: One-half of the Northern part of the **W4** family of the Earth-Moon system.

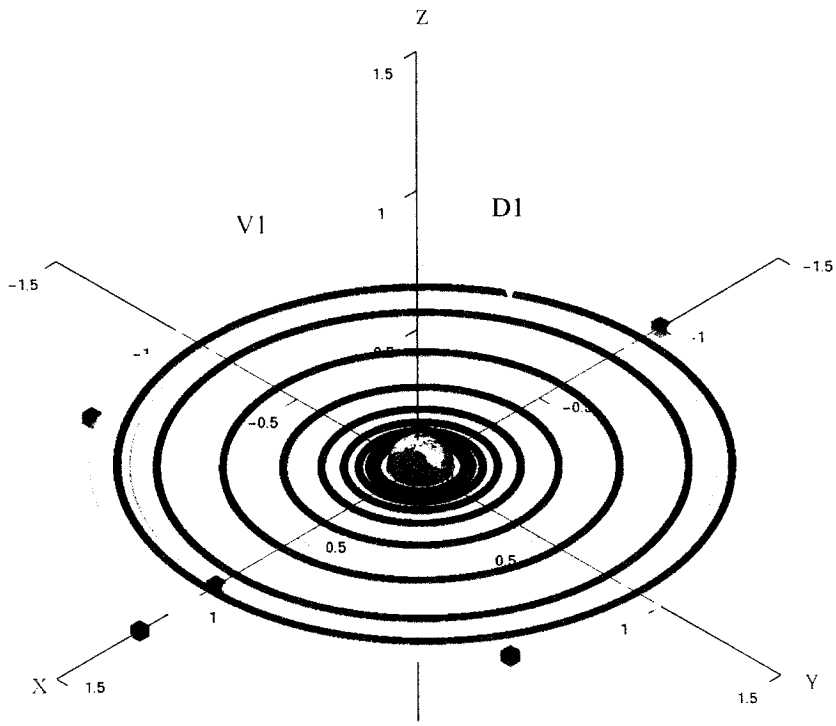

Figure 4.22: The "Circular" family **C1** of the Earth-Moon system.

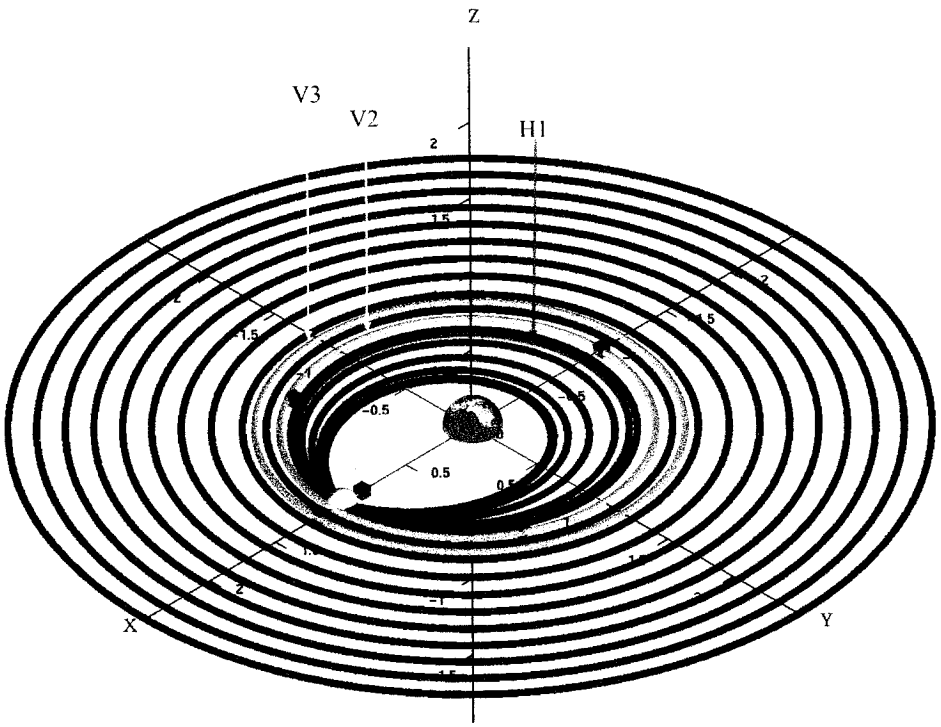

Figure 4.23: The "Circular" family **C2** of the Earth-Moon system.

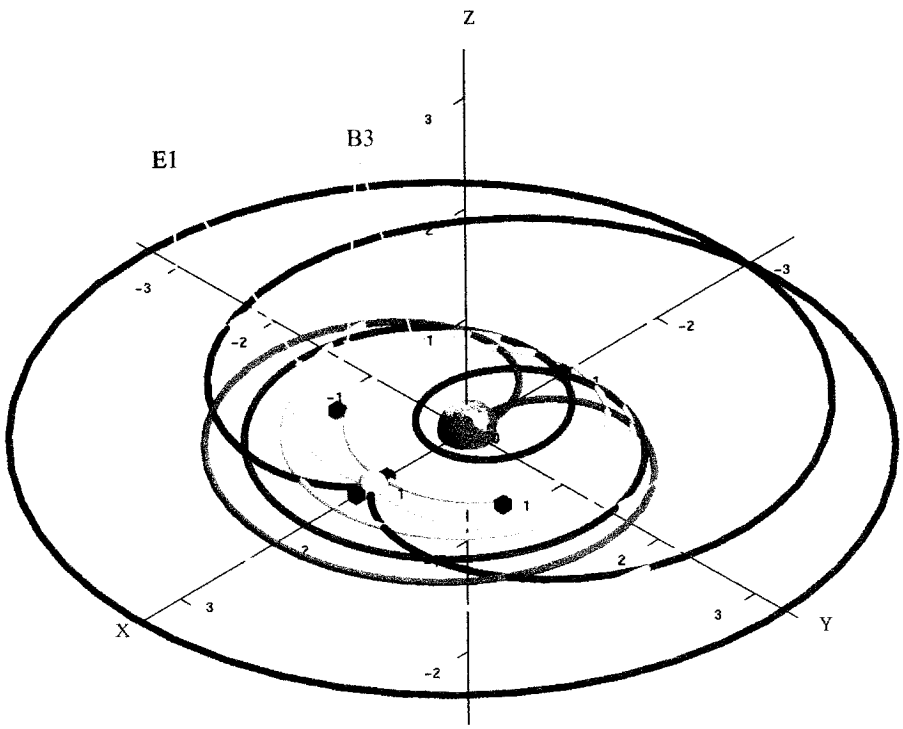

Figure 4.24: The family **D1** of the Earth-Moon system.

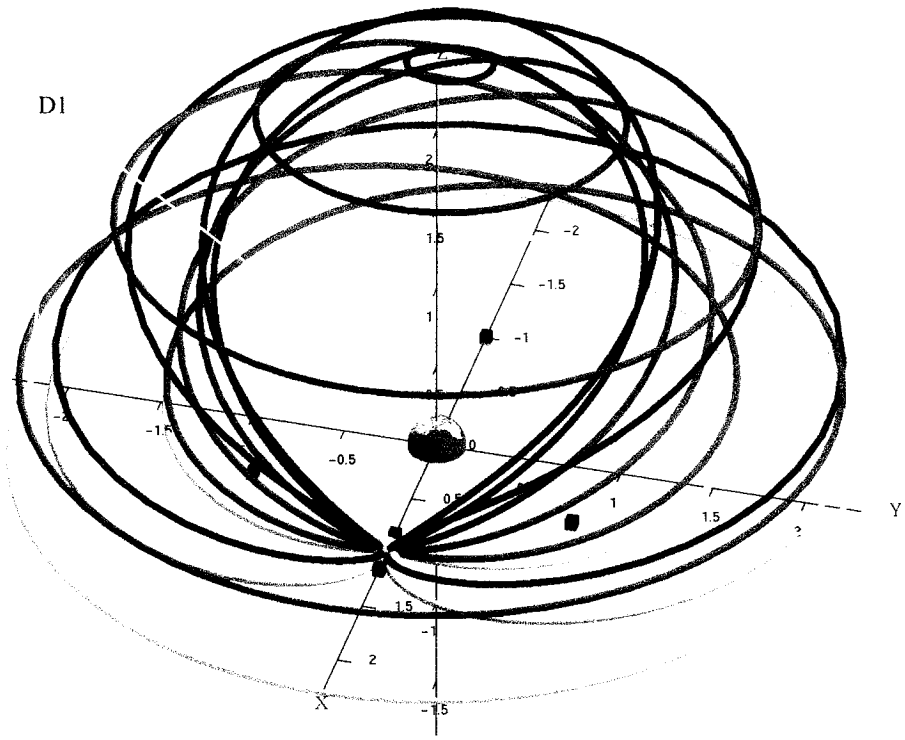

Figure 4.25: The Northern part of the **E1** family of the Earth-Moon system.

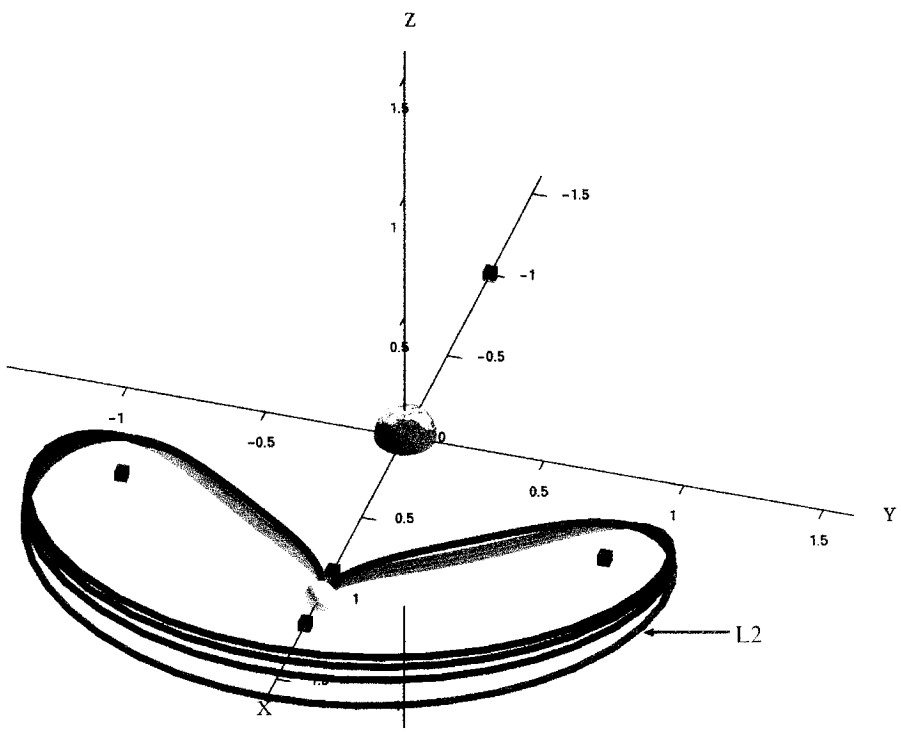

Figure 4.26: The family **R2** of the Earth-Moon system.

Chapter 5

Periodic solutions for general values of μ

5.1 Loci of Branch Points

In this chapter we describe how the bifurcation diagram for the Earth-Moon system, as shown in Fig. 4.2, changes when the mass-ratio parameter μ changes. Many features of the bifurcation diagram remain qualitatively the same; however, there are also some qualitative changes. Our main numerical tool in this investigation is a continuation algorithm for branch points, as described in Chapter 3, which allows the computation of a family (or *locus*) of branch points, for varying μ, as shown in Figs. 5.1-5.12, where the energy E and the period T of branching orbits are plotted versus the mass-ratio parameter μ. Note that, due to the symmetry about $\mu = 1/2$, it suffices to show these curves for μ in the interval $[0, 1/2]$

Additional information on the persistence of periodic solution families, as μ is varied, can be deduced from the persistence of the homoclinic orbits that terminate some of these families, as will be discussed separately in Sec. 5.2.

The loci of branch points, as well as the loci of homoclinic orbits discussed in Sec. 5.2, contain *critical points*. These are special points (higher order singularities) that correspond to structural changes in the bifurcation diagram, and consequently in phase space.

As an example, consider the curve **L**13 in Fig. 5.1, which represents the locus of branch points L13 along the Lyapunov family **L**1. As can be seen in Fig. 5.1, the curve **L**13 contains a fold, namely, at the critical value $\mu = \mu_5$, where $\mu_5 \approx 0.066$. The corresponding structural changes in the bifurcation diagram can be observed by comparing the bifurcation diagrams for μ-values near the critical value μ_5, as shown in Fig. 5.17 and Fig. 5.18. One observes the appearance of two new branch points, namely, L13 and L14, in Fig. 5.18, in accordance with the fold on the locus **L**13 in Fig. 5.1.

In order to highlight the change between the bifurcation diagram in Fig. 5.17 and the bifurcation diagram in Fig. 5.18, we use a bright-red color for the families bifurcating from the new bifurcation points L13 and L14. (These families are called **S**1 and **T**1, respectively.) Changes between other consecutive bifurcation diagrams are highlighted in a similar fashion.

Table 5.1 contains a list of critical μ-values, also indicating the μ-diagram in which the critical point appears, and indicating bifurcation diagrams for nearby μ-values, in which the qualitative changes corresponding to a critical point can be observed.

Below we describe the implications that can be deduced from features of the computed loci of branch points. To some extent our discussion follows the order in which the μ-diagrams appear, *i.e.*, from Fig. 5.1 to Fig. 5.12.

5.1.1 Branch points along the Lyapunov family L1

The number of branch points along the Lyapunov family **L**1 depends on the value of the mass-ratio parameter μ, as can be seen in Fig. 5.1, which displays loci of branch points along this family, computed using the extended boundary value system described in Chapter 3.

In Fig. 5.1, note that the locus **L**11, which corresponds to bifurcations to Halo orbits, extend over the entire interval. Similarly, the bifurcations to the families of Axial orbits, represented by the locus **L**12, exist for all μ. Thus, the numerical evidence indicates that the Halo bifurcations and the bifurcations to the Axial orbits are always present along the Lyapunov family **L**1.

However, the locus **L**13 contains a fold located at the critical value μ_5, as can be

seen in Fig. 5.1. We conclude that the branch point L13 ceases to exist for μ less than μ_5. On the other hand, the fold also implies the existence of another bifurcation from **L**1, namely at the branch point L14, whose locus **L**14 is the continuation of the locus **L**13 past the fold in Fig. 5.1. As μ decreases past the critical value μ_5, the branch points L13 and L14 approach and annihilate each other.

Fig. 5.1 also shows that, whereas the locus of branch points **L**13 exists for all μ greater than or equal to μ_5, the locus **L**14 terminates at a value μ_8, where the branching orbit L14 collides with one of the primaries.

Additional loci, labeled **L**15-**L**18 appear near $\mu = 1/2$ in Fig. 5.1. These curves originate from folds at the critical points μ_{13} and μ_{14}, and imply an additional four branch points, namely, L15, L16, L17, and L18, which can be seen in the bifurcation diagram for $\mu = 0.45$ in Fig. 5.25. We refer to the four bifurcating families as the **K**-families. Representative orbits along the **K**-families can be seen in Figs. 5.32-5.36.

5.1.2 Branch points along the Lyapunov family L2

First observe that the loci **L**21 and **L**22 extend over the entire μ-interval in Fig. 5.2. Thus, as was the case for the family **L**1, the Halo bifurcations and the Axial bifurcations are always present along the Lyapunov family **L**2.

Also similar to the case of the family **L**1 is that the locus **L**23 contains a fold, namely, at the critical value μ_3, where $\mu_3 \approx 0.049$, as seen in Fig. 5.2. It follows that the branch point L23 does not exist for μ less than μ_3.

The fold implies another bifurcation from **L**2, namely L25, whose locus **L**25 in Fig. 5.2 is the continuation of the locus **L**23 past the fold. The locus **L**25 ends at the critical value μ_4, where the branching orbit L25 becomes a collision orbit.

Another locus of branch points appears in Fig. 5.2, namely, **L**24, bounded at both ends by collision orbits at the critical values μ_1 and μ_{11}. Thus, for example, for μ less than μ_1 the branch point L24 is not present along **L**2, as in Fig. 5.13. Also note that, in accordance with Fig. 5.2, the branch points L23 and L25 are also absent in Fig. 5.13.

As can also be observed in Fig. 5.2, all three branch points, L23, L24, and L25, are present in a narrow interval of μ-values, namely, between the critical values μ_3

and μ_4, as illustrated in the bifurcation diagram for the value $\mu = 0.055$, which lies inside this interval, in Fig. 5.16.

5.1.3 Branch points along the Lyapunov family L3

Similar to the case of the family **L**1 and the family **L**2, the Halo bifurcations and the Axial bifurcations are always present along the Lyapunov family **L**3, as can be seen in Fig. 5.3, where their loci, **L**31 and **L**32, extend over the entire μ-interval.

In Fig. 5.3, we also observe that the branch point L33, from which the planar family **S**3 bifurcates, also exists for all values of μ.

Table 5.1: Critical μ-values, and nearby μ-values with their bifurcation diagrams

Critical value	Definition	Locus	Nearby μ-value	Nearby Diagram
			0.0005	Fig. 5.13
$\mu_1 \approx 0.001$	collision on **L**24	Fig. 5.2		
			0.020	Fig. 5.14
$\mu_2 \approx 0.038$	Hamiltonian Hopf	Fig. 5.38		
			0.045	Fig. 5.15
$\mu_3 \approx 0.049$	fold on **L**23	Fig. 5.2		
			0.055	Fig. 5.16
$\mu_4 \approx 0.057$	collision on **L**25	Fig. 5.2		
			0.063	Fig. 5.17
$\mu_5 \approx 0.066$	fold on **L**13	Fig. 5.1		
			0.073	Fig. 5.18
$\mu_6 \approx 0.080$	fold on **S**2∞	Fig. 5.38		
			0.090	Fig. 5.19
$\mu_7 \approx 0.104$	fold on **D**11	Fig. 5.12		
			0.120	Fig. 5.20
$\mu_8 \approx 0.142$	collision on **L**14	Fig. 5.1		
			0.145	Fig. 5.21
$\mu_9 \approx 0.147$	fold on **S**1∞	Fig. 5.38		
			0.190	Fig. 5.22
$\mu_{10} \approx 0.230$	collision on **S**1∞	Fig. 5.38		
			0.280	Fig. 5.23
$\mu_{11} \approx 0.332$	collision on **L**24	Fig. 5.2		
			0.360	Fig. 5.24
$\mu_{12} \approx 0.399$	singular point	Fig. 5.6		
$\mu_{13} \approx 0.427$	fold on **L**15	Fig. 5.1		
$\mu_{14} \approx 0.433$	fold on **L**17	Fig. 5.1		
			0.450	Fig. 5.25

5.1.4 Branch points along the Vertical family V1

Along the Vertical family **V**1 there are three branch points, that exist for all values of μ.

The first branch point encountered along **V**1 is V11. At V11 the Axial family **A**1, which bifurcates from the Lyapunov family **L**1 at the branch point L12, meets the Vertical family **V**1. The locus **V**11 can be seen in Fig. 5.4.

The second branch point along **V**1 is V12, which corresponds to the bifurcation to the so-called "Backflip orbits". Its locus, **V**12, also appears in Fig. 5.4

At the the third branch point along **V**1, namely C11, the Vertical family **V**1 connects to the planar family **C**1 of "circular" orbits via a "reverse period-doubling bifurcation". The planar orbit C11 encompasses the larger primary only. The locus **C**11 of this reverse period-doubling bifurcation is shown in Fig. 5.7. Evidently, C11 also exists for all μ.

5.1.5 Branch points along the Vertical family V2

There are also three branch points along the Vertical family **V**2, for all values of μ, namely the branch point V21, where the Axial family **A**2 from branch point L22 meets **V**2; the branch point V22, where the Backflip family **B**2 bifurcates; and the reverse period-doubling bifurcation C22, where **V**2 connects to the Circular family **C**2. Orbits along **C**2, and in particular the branching orbit C22, encompass both primaries. The loci **V**21 and **V**22 are shown in Fig. 5.5, while the locus **C**22 appears in Fig. 5.7.

In Fig. 5.7, note that the locus **C**22 meets the locus **C**23 at $\mu = 1/2$. The significance of this will be discussed in more detail in Sec. 5.3.

5.1.6 Branch points along the Vertical family V3

The family **V**3 emanates from the libration point L3. There are four branch points along **V**3, of which the first branch point, denoted V31, gives rise to the Axial family **A**3. The fourth branch point, denoted C23, is a reverse period-doubling bifurcation that connects **V**3 to the Circular family **C**2, whose orbits are planar, and encompass

both primaries.

Depending on the value of μ, it is either the second or the third branch point along the Vertical family **V**3 that gives rise to the Backflip orbits. This branch point is denoted V32, regardless of its relative position along **V**3. Specifically, for μ less than the critical value μ_{12}, where $\mu_{12} \approx 0.399$, the Backflip bifurcation occurs after the branch point that we refer to as "V45", whereas for μ greater than μ_{12}, the Backflip bifurcation occurs before branch point V45. The latter case can be seen in the bifurcation diagram for $\mu = 0.45$, in Fig. 5.25. At the branch point V45, the Vertical family **V**3 meets the Vertical families **V**4/**V**5 that connect to the libration points V4 and V5.

All four branch points along **V**3 are present for all values of μ, as can be seen in Fig. 5.6, which displays the loci **V**31, **V**32, and **V**45, and in Fig. 5.7, which shows the loci of reverse period-doubling bifurcations, including **C**23, as well as **V**45.

Of particular interest is the intersection of the loci **V**45 and **V**32 at the critical value μ_{12}, where $\mu_{12} \approx 0.399$, as seen in Fig. 5.6 and Fig. 5.8. These intersections are not artifacts of the representation: the two loci actually intersect, giving rise to a higher codimension singular point, at which the bifurcation orbits V45 and V32 coincide. Numerically, the singularity at μ_{12} also corresponds to a singular point of the extended system used to track these loci (see Chapter 3).

Not surprisingly, the singularity at μ_{12} gives rise to additional complexity in the global solution structure. In fact, additional loci of branch points emanate from the singularity, namely, **V**42/**V**52 and **X**45, as shown in Fig. 5.8. As can be seen in Fig. 5.8, the new branch points exist for μ greater than μ_{12}.

5.1.7 Branch points along the Vertical family V4/V5

The families **V**4 and **V**5, that originate at the libration points L4 and L5, respectively, connect to each other, and to the Vertical family **V**3, at the branch point V45; see, for example, Fig. 5.13. Along **V**4/V5 there are at least three branch points, but the precise number depends on the value of μ.

For μ less than μ_{12}, where $\mu_{12} \approx 0.399$, there are three branch points along **V**4/V5, away from the libration points, namely, V41, V51, and the above-mentioned branch

point V45; see, for example, Fig. 5.13. These three branch points exist for all values of μ, as seen in Fig. 5.9, which shows the locus **V**41 (the locus **V**51 coincides with the locus **V**41 in the figure), and in Fig. 5.6-5.8, which show the locus **V**45. The family that bifurcates from **V**4 at V41 is called **W**4. It connects to the symmetry partner of V41, namely, V51, on **V**5.

For μ greater than μ_{12}, there is another branch point along the Vertical family **V**4, namely V42, and its symmetry partner V52 along **V**5. The locus **V**42, which coincides with the locus **V**52, corresponds to one of the additional curves that emanate from the singularity at μ_{12} in Fig. 5.8.

The family that bifurcates from V42 is called **X**4. It connects to its symmetry partner, **X**5 from V52, namely, at the branch point X45. The locus **X**45 corresponds to another additional curve that emanates from the singularity at μ_{12} in Fig. 5.8. Representative orbits along **X**4 can be seen in Fig. 5.37, for the case $\mu = 0.45$.

5.1.8 Branch points along the Halo family H1

For each value of μ there are three families of Halo orbits, namely the families that bifurcate from the first branch point on the Lyapunov families **L**1, **L**2, and **L**3. These branch points are denoted L11, L21, and L31, respectively, and the corresponding bifurcating Halo families are denoted **H**1, **H**2, and **H**3. For each μ the families **H**2 and **H**3 end in collision orbits.

The family **H**1 connects to a family of "circular" orbits **C**2, whose orbits encompass both primaries. This bifurcation, which is *not* a reverse period-doubling, is denoted C21; see, for example, Fig. 5.13. The locus **C**21 is shown in Fig. 5.11. Evidently the branch point C21 is present for all values of μ.

Between the starting point L11 and the end point C21, the Halo family **H**1 possesses another branch point, denoted H11, where **H**1 connects to the family **W**4/**W**5. The locus **H**11, shown in Fig. 5.10, indicates that the branch point H11 exists for all μ.

5.1.9 Branch points along the Backflip family B3

The Backflip families **B**1, **B**2, and **B**3 bifurcate from the Vertical families **V**1, **V**2, and **V**3 at the branch points V12, V22, and V32, respectively. These families exist for all values of μ, as can be seen in Figs. 5.4-5.6, which contain the loci **V**12, **V**22, and **V**32. The families **B**1 and **B**2 end in collision orbits, as is indicated in each of the bifurcation diagrams in Figs. 5.13-5.25. Orbits along **B**1 and **B**2 for the case of the Earth-Moon system can be seen in Fig. 4.18 and Fig. 4.19, respectively. A detailed description of the complicated, but smooth, transitions along the family **B**1 for the case of the Earth-Moon system is given in [31].

For small values of μ, the Backflip family **B**3 connects to a planar family, called **D**1, at the branch point D11. This branch point can be seen, for example, in Fig. 5.13, along with a second branch point along **D**1, namely, D12, from which a family called **E**1 bifurcates.

The locus **D**11, shown in Fig. 5.12, contains a fold at the critical value μ_7, where $\mu_7 \approx 0.104$. As μ increases past the critical value μ_7, the branch points D11 and D12 approach and annihilate each other.

We infer that the Backflip family **B**3 connects to the planar family **D**1, when μ is less than μ_7. An example is the Earth-Moon system in Fig. 4.2, for which representative **B**3 orbits are shown in Fig. 4.20, and representative orbits along the separate family **E**1 in Fig. 4.25.

However, when μ is greater than μ_7 then the families **B**3 and **E**1 have merged into one family (which is still called **B**3). This case can be observed in the bifurcation diagrams in Figs. 5.20-5.25, in each of which μ is greater than μ_7. Representative orbits along **B**3 for this case are shown in Fig. 5.31, for $\mu = 0.45$.

5.1.10 Discussion

For μ less than the critical value μ_2, where $\mu_2 = 1/2 - \sqrt{23/108} \approx 0.0385$ (see Table 5.1 and Fig. 4.1), each triangular point is a *center* $\times$ *center* $\times$ *center* of Eq. (2.51). There are two frequencies for the planar motion, ω_s and ω_l, where $\omega_s^2 = (1 + \sqrt{D})/2$ and $\omega_l^2 = (1 - \sqrt{D})/2$, with $D = 1 - 27\mu(1 - \mu)$. There is also one frequency $\omega_z = 1$ for

the vertical motion. The corresponding periods T (where $T = 2\pi/\omega$) are shown in Fig. 4.1.

The Lyapunov Center Theorem shows that for each μ less than μ_2 there exists a family of planar periodic orbits, associated with ω_s, called the Short-Period orbits [81]. These Short-Period orbits can be viewed as perturbed elliptic Keplerian orbits. As $\mu \to 0$, $\omega_s \to 1$ and $\omega_l \to 0$. As μ increases from 0, ω_s decreases and ω_l increases until at $\mu = \mu_2$, $\omega_s = \sqrt{2} = \omega_l$.

For each integer $k \geq 1$ there is a mass fraction $\mu = \mu^R(k)$ where $\omega_s/\omega_l = k$, so that a resonance occurs. Here $\mu^R(1) = \mu_2$ and $\mu^R(k) \to 0$ as $k \to \infty$. For $\mu \notin \{\mu_k^r\}_{k=1}^{\infty}$, the Lyapunov Center Theorem shows that each triangular point has a second planar family $\mathbf{L}i$, $i = 4, 5$ of periodic orbits, associated with ω_l, called the Long-Period family. For $\mu = \mu^R(k)$, the Lyapunov Center Theorem does not apply for the long-period orbits and a more detailed analysis is required [62, 64].

Deprit and Henrard have mapped out an intricate web of interconnections between the Short- and Long-Period families [27, 62, 64]. In particular they describe the bifurcation where a Long-Period orbit coincides with a Short-Period orbit traced out p times, for some integer p determined by the ratio of the short- to long-period frequencies at L4. For example, for the Sun-Jupiter CR3BP, where $\mu = 0.00953875$, $\omega_s/\omega_l \approx 12.14$ and $p = 13$.

As $\mu \to \mu_2$, the Short- and Long-Period orbits coalesce into a single family, where the period approaches $2\pi\sqrt{2}$. For each $\mu > \mu_2$, each triangular libration point is an unstable *spiral point* $\times$ *spiral point* $\times$ *center*. However, one can continue from $\mu = \mu_2$ for $\mu > \mu_2$ to obtain a family of orbits with period $2\pi\sqrt{2}$ [27].

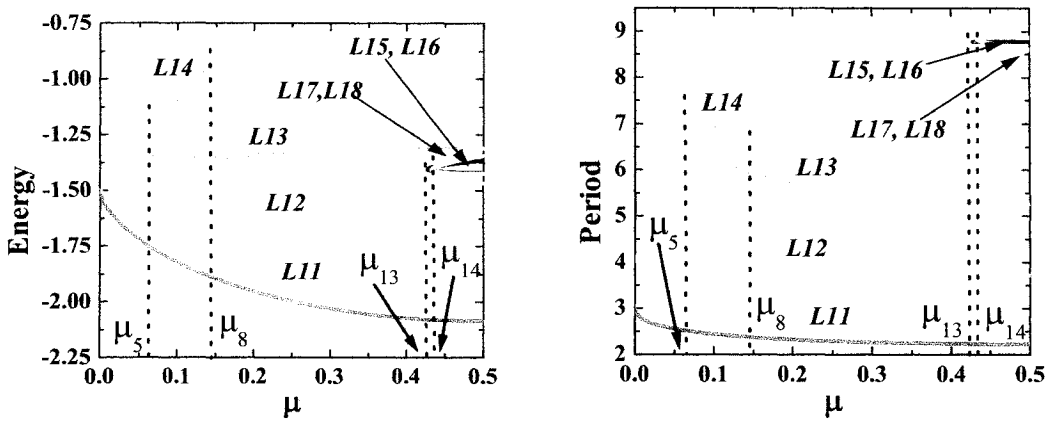

Figure 5.1: Loci of branch points on the planar Lyapunov family **L1**.

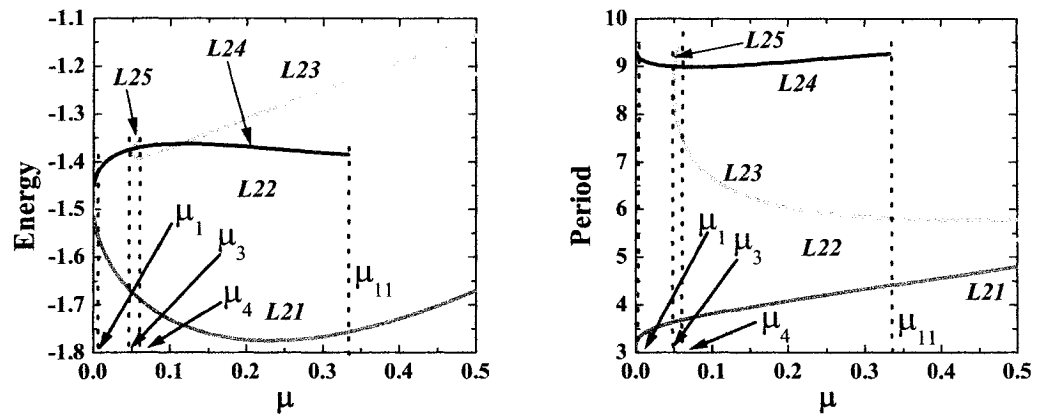

Figure 5.2: Loci of branch points on the planar Lyapunov family **L2**.

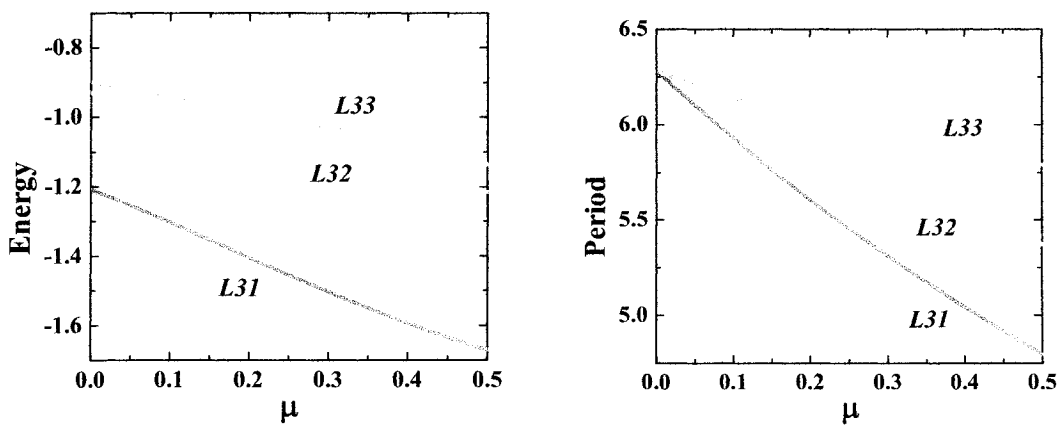

Figure 5.3: Loci of branch points on the planar Lyapunov family **L3**

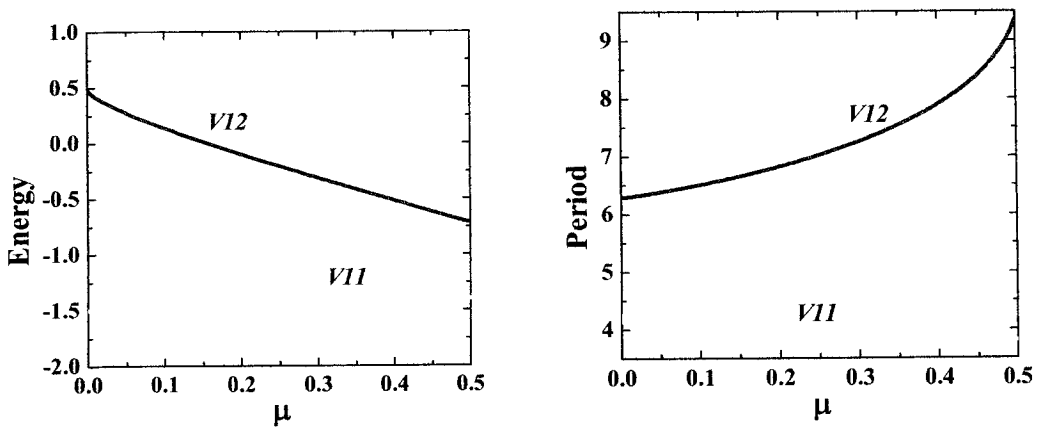

Figure 5.4: Loci of branch points along the Vertical family **V1**.

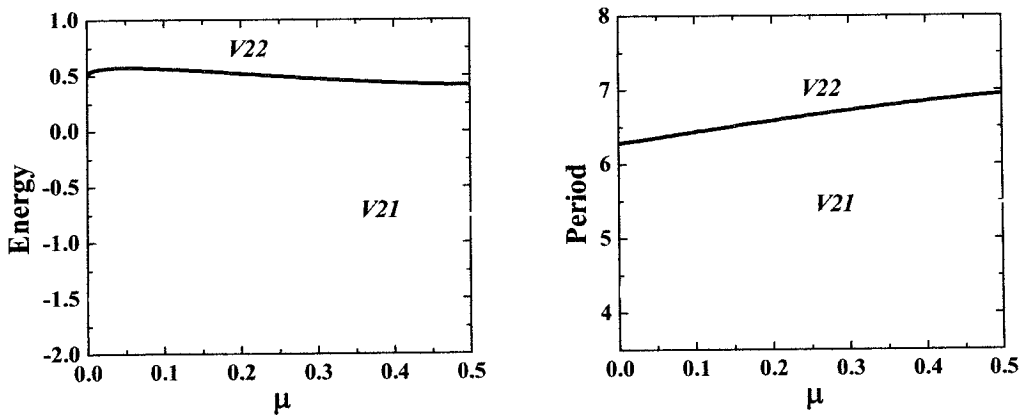

Figure 5.5: Loci of branch points along the Vertical family **V2**.

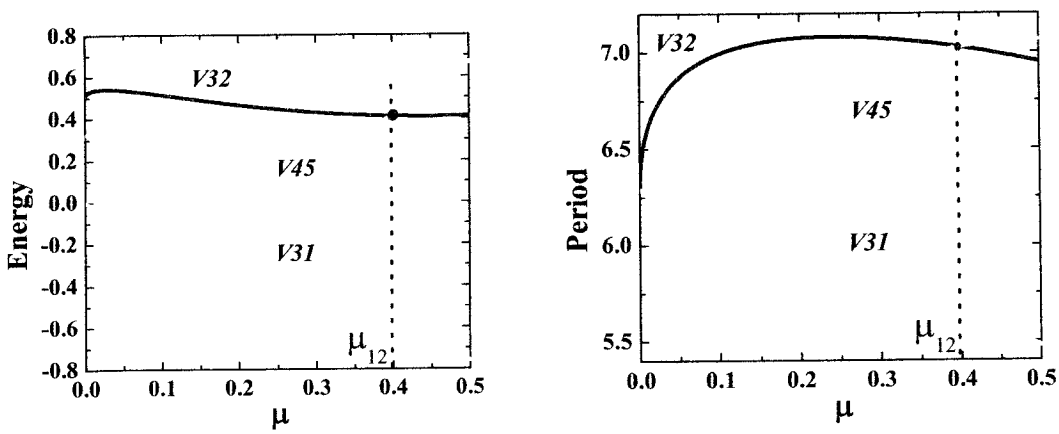

Figure 5.6: Loci of branch points along the Vertical family **V3**.

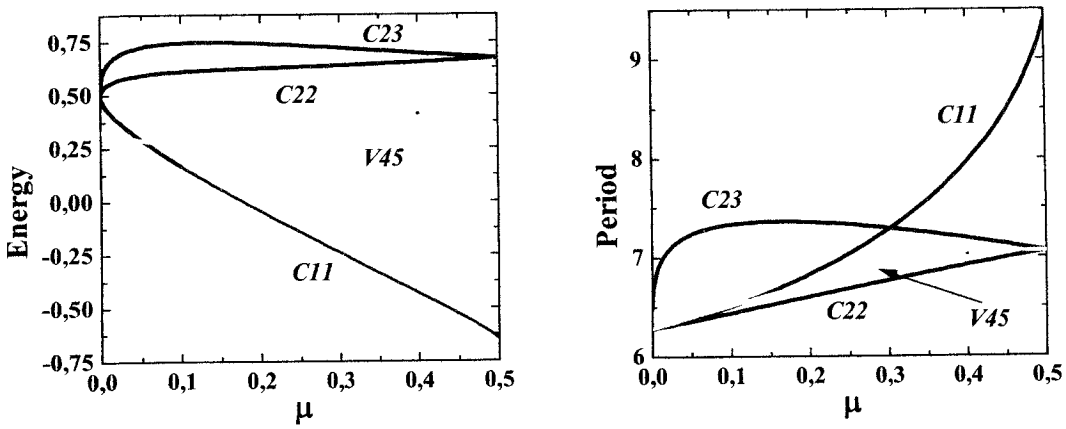

Figure 5.7: Loci of reverse period-doubling bifurcations that connect the Vertical families to circular, planar orbits. At the branch point C11 the Vertical family **V1** connects to the circular, planar family **C1**, whose orbits encompass the larger primary. At the branch points C22 and C23 the Vertical families **V2** and **V3** connect to the circular, planar family **C2**, whose orbits encompass both primaries. The panels also show the locus **V45**.

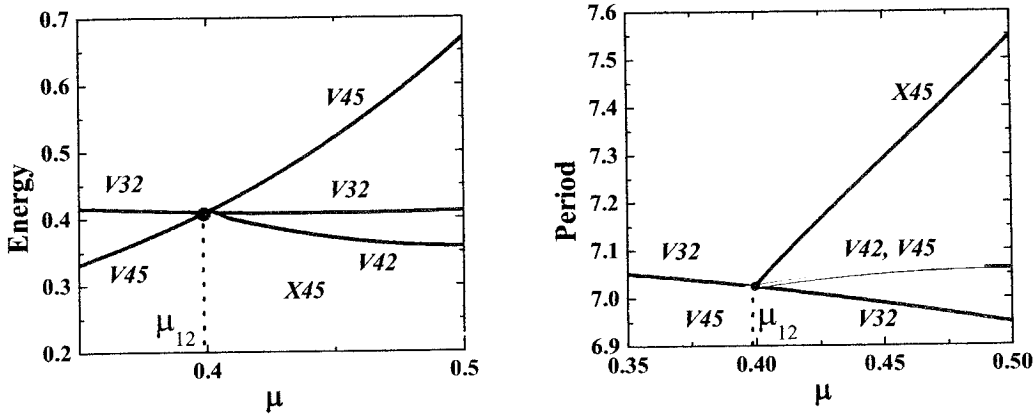

Figure 5.8: Additional loci along the Vertical orbits emanate from the singularity at $\mu \approx 0.39933$.

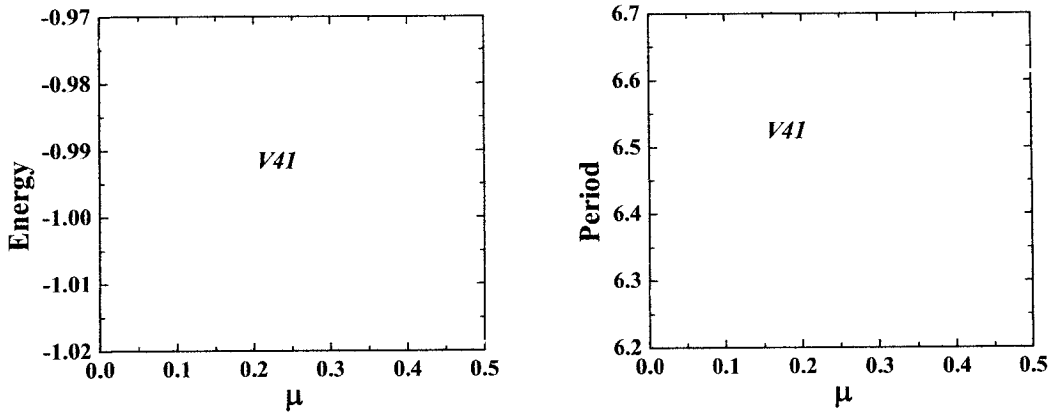

Figure 5.9: The locus **V**41 of branch points V41, where the Vertical family **V**4 connects to the family **W**4.

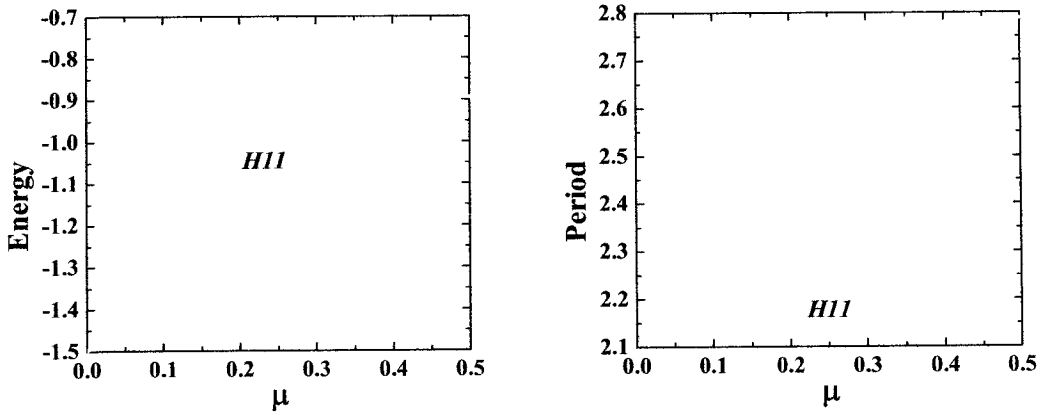

Figure 5.10: The locus **H**11 of branch points H11, where the Halo family **H**1 connects to the family **W**4/**W**5.

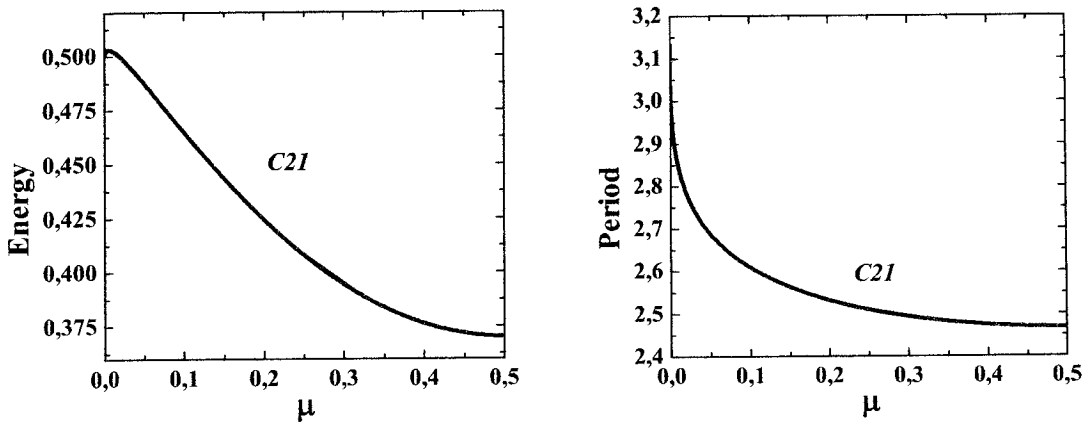

Figure 5.11: The locus **C**21 of branch points C21, where the Halo family **H**1 connects to the family of circular, planar orbits **C**2.

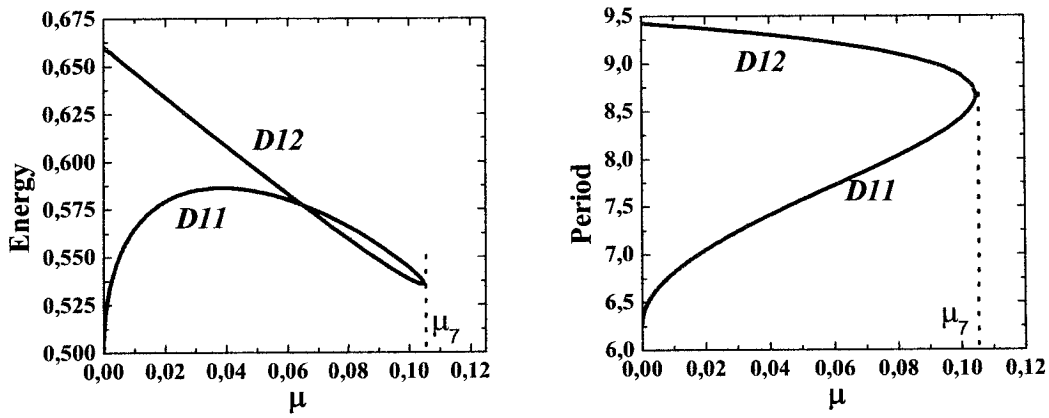

Figure 5.12: Loci **D11** and **D12** of branch points D11 and D12, where the **B3**- and **E1**-families connect to the planar family **D1**.

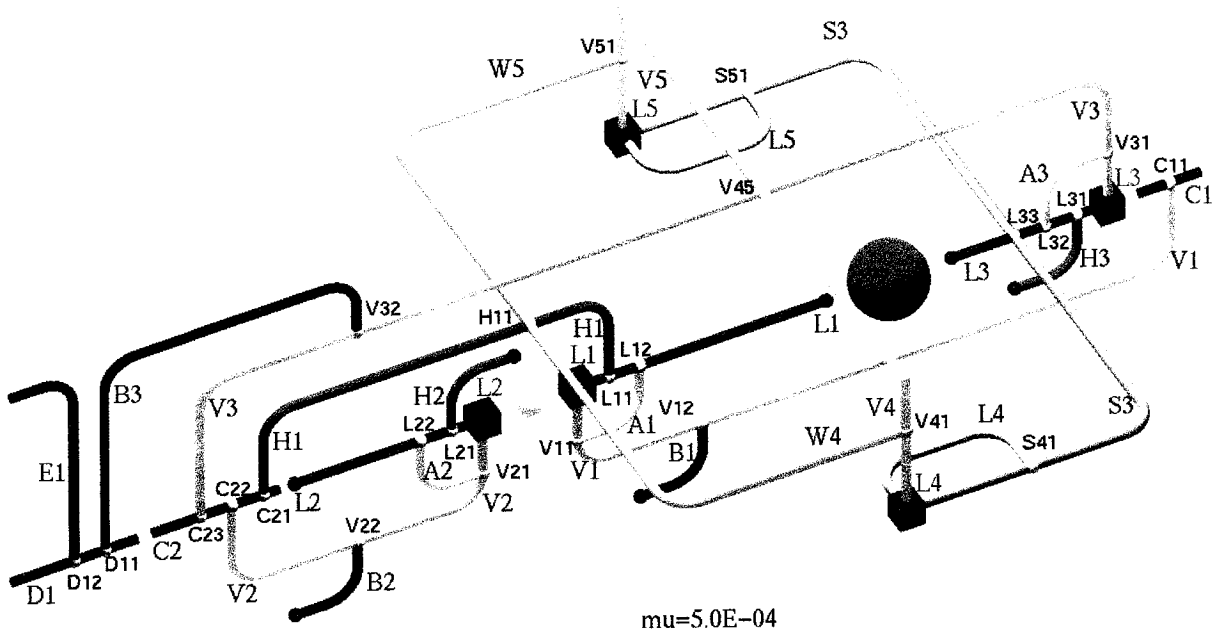

Figure 5.13: Bifurcation diagram for $\mu = 5.0 \cdot 10^{-4}$.

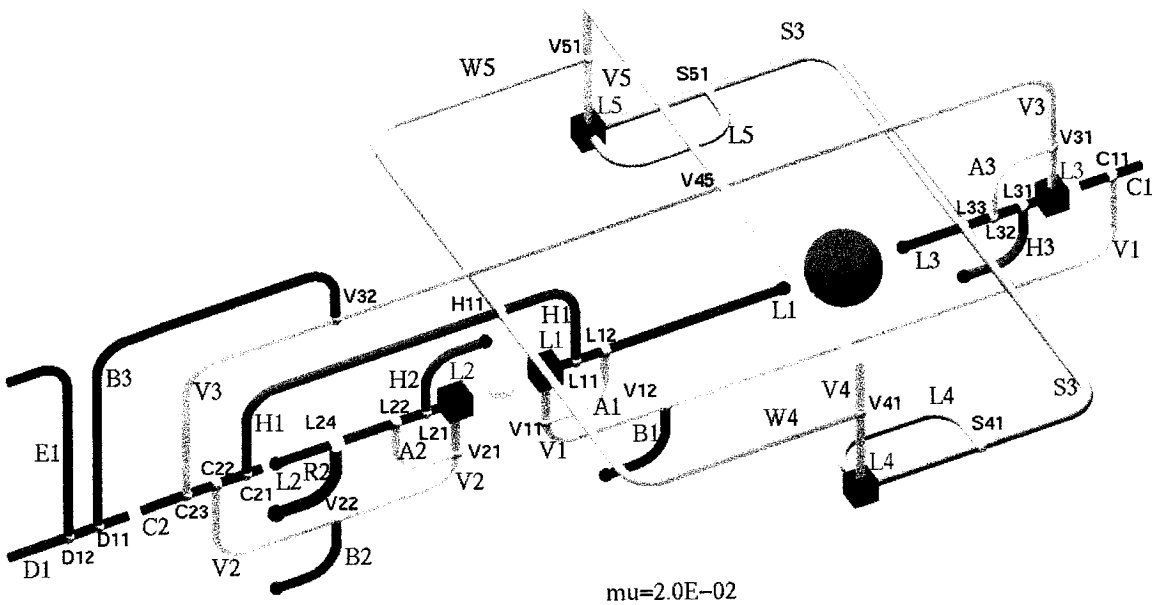

Figure 5.14: Bifurcation diagram for $\mu = 0.02$. Compared to the preceding diagram (Fig. 5.13), there is the new family **R2** (shown in bright red color).

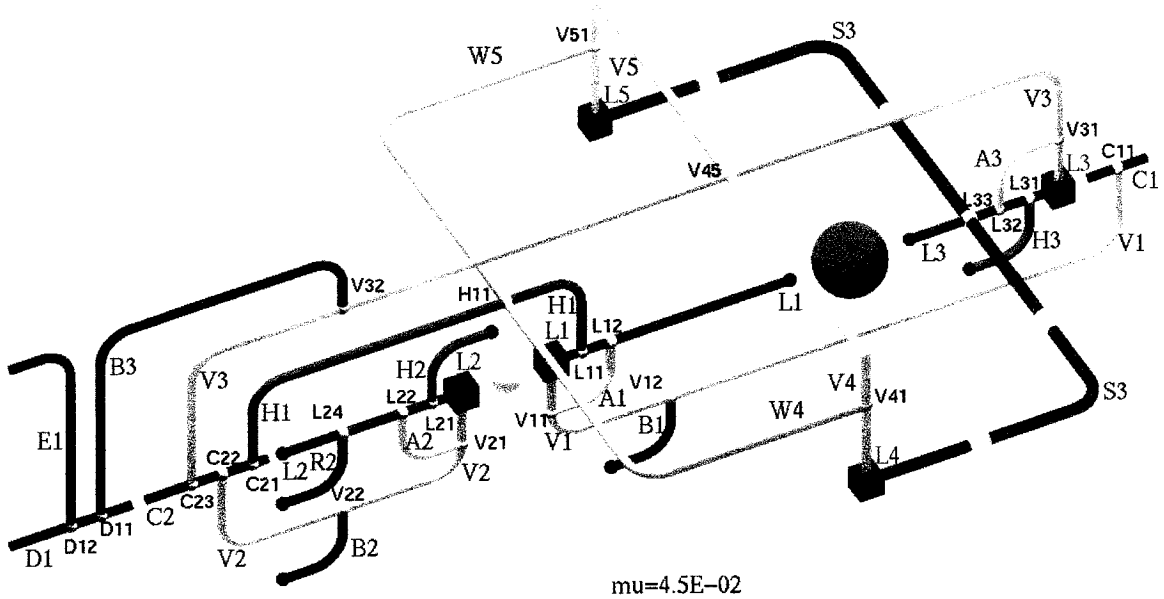

Figure 5.15: Bifurcation diagram for $\mu = 0.045$.

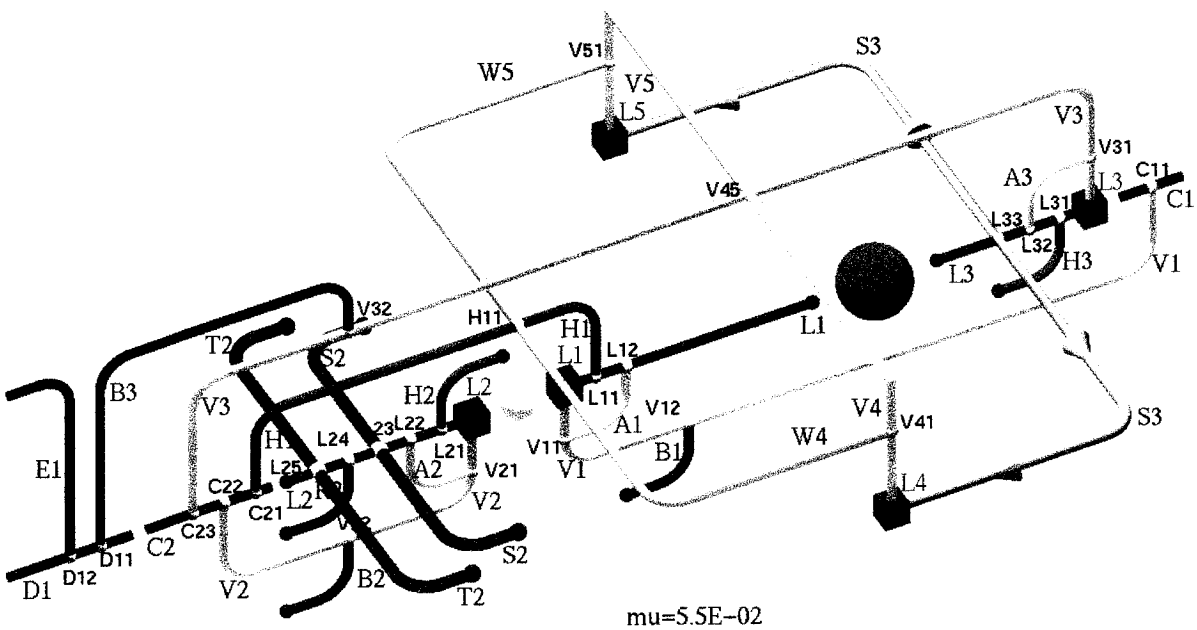

Figure 5.16: Bifurcation diagram for $\mu = 0.055$.

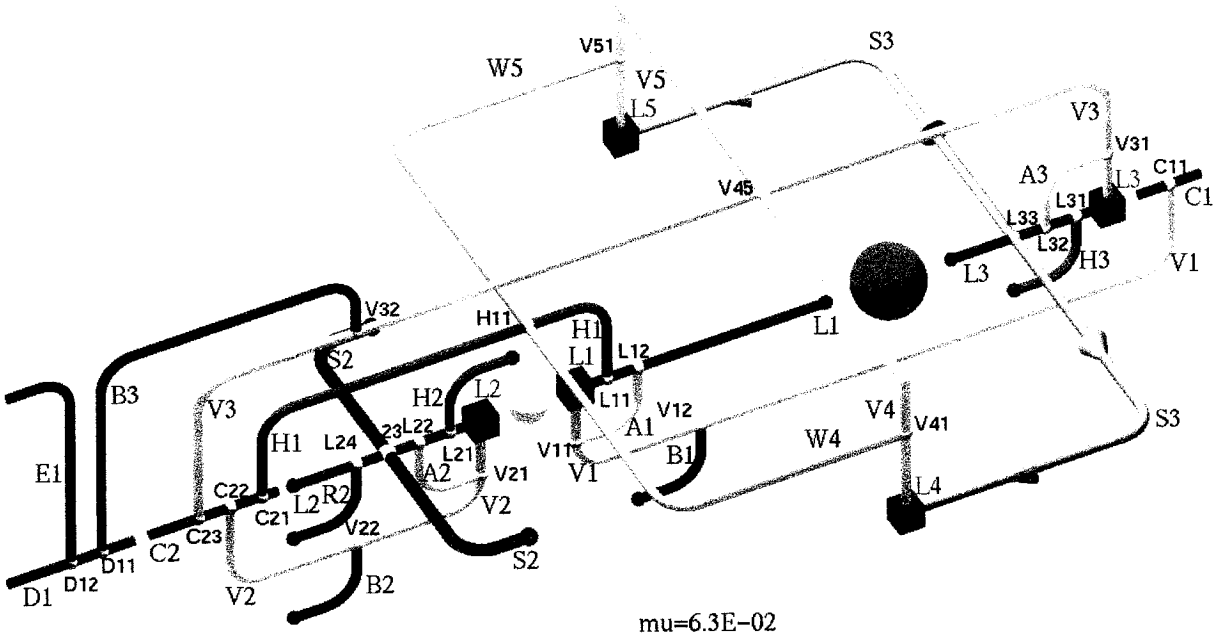

Figure 5.17: Bifurcation diagram for $\mu = 0.063$.

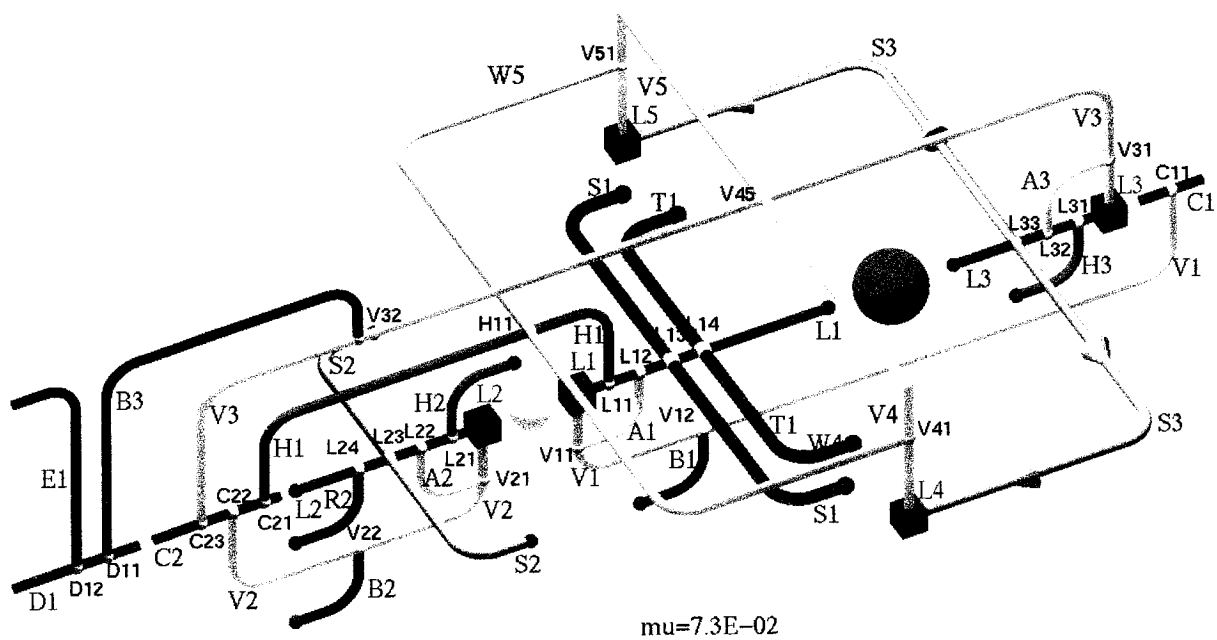

Figure 5.18: Bifurcation diagram for $\mu = 0.073$.

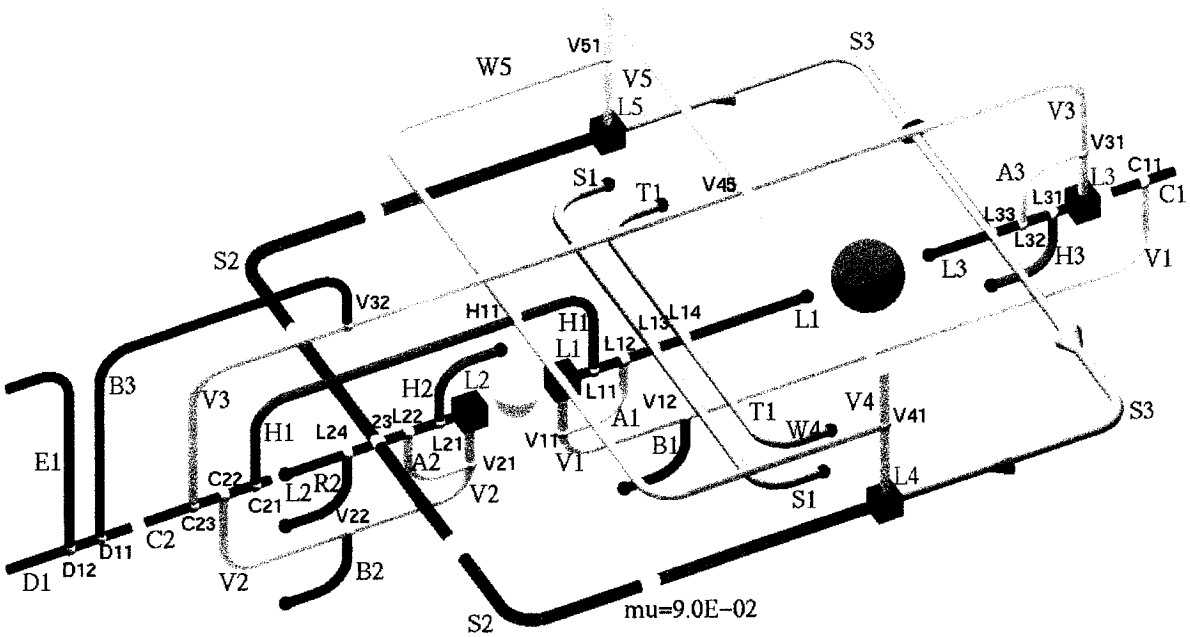

Figure 5.19: Bifurcation diagram for $\mu = 0.09$.

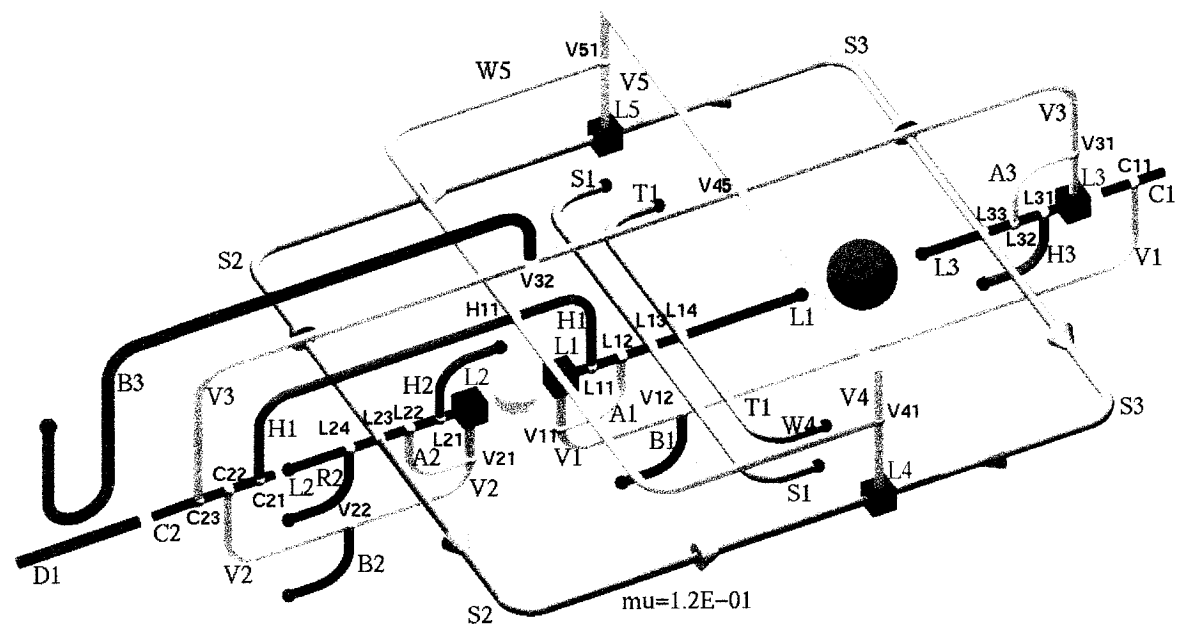

Figure 5.20: Bifurcation diagram for $\mu = 0.12$.

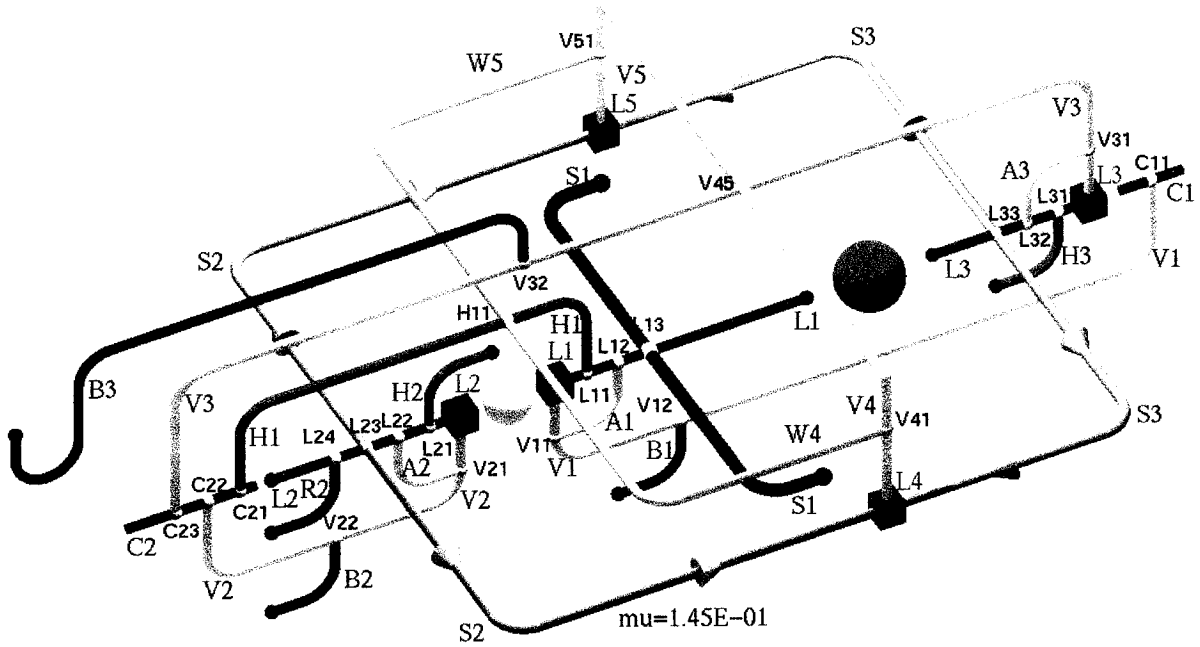

Figure 5.21: Bifurcation diagram for $\mu = 0.145$.

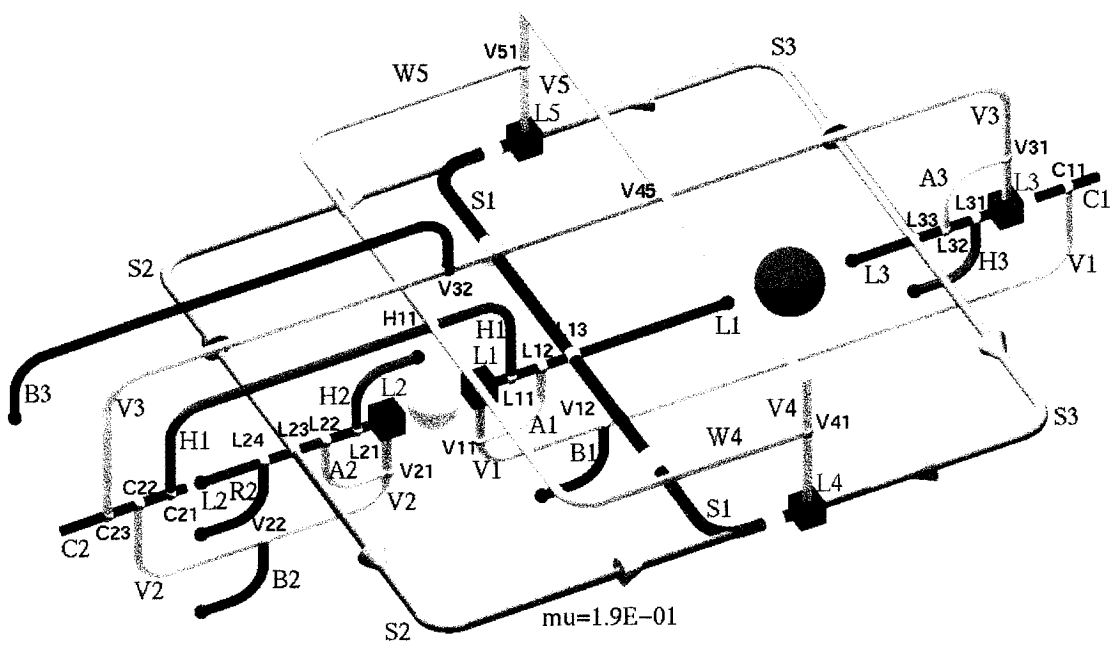

Figure 5.22: Bifurcation diagram for $\mu = 0.19$.

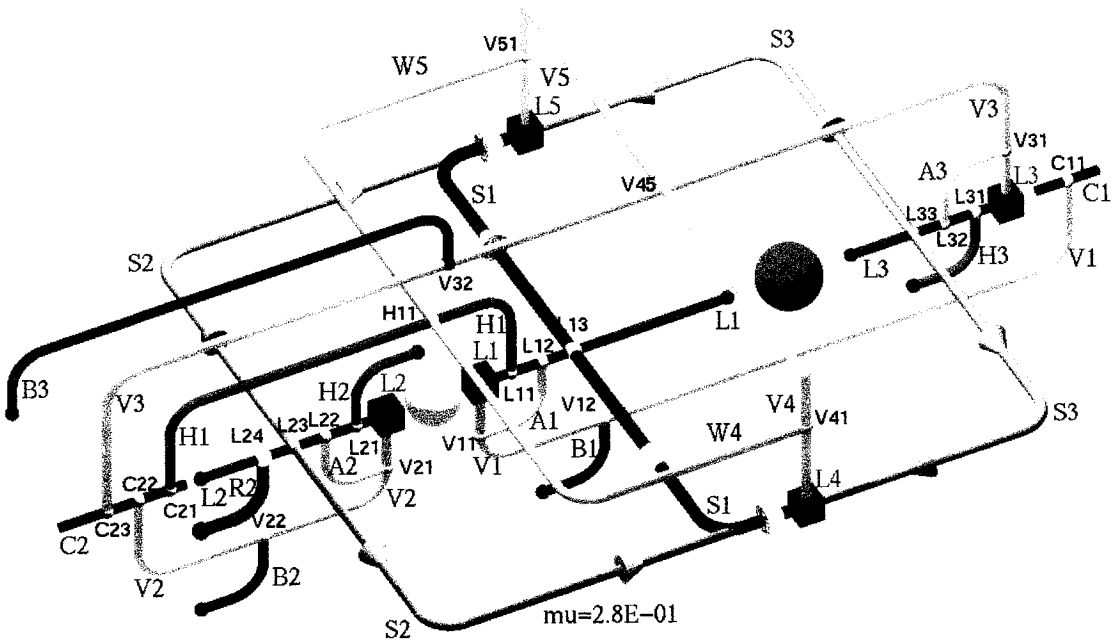

Figure 5.23: Bifurcation diagram for $\mu = 0.28$.

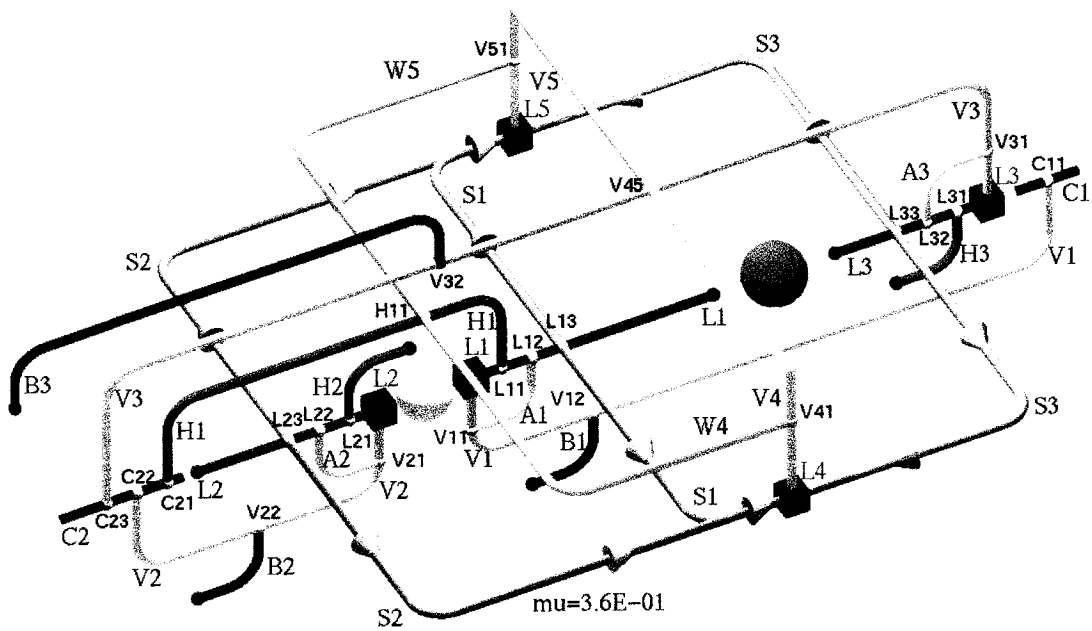

Figure 5.24: Bifurcation diagram for $\mu = 0.36$.

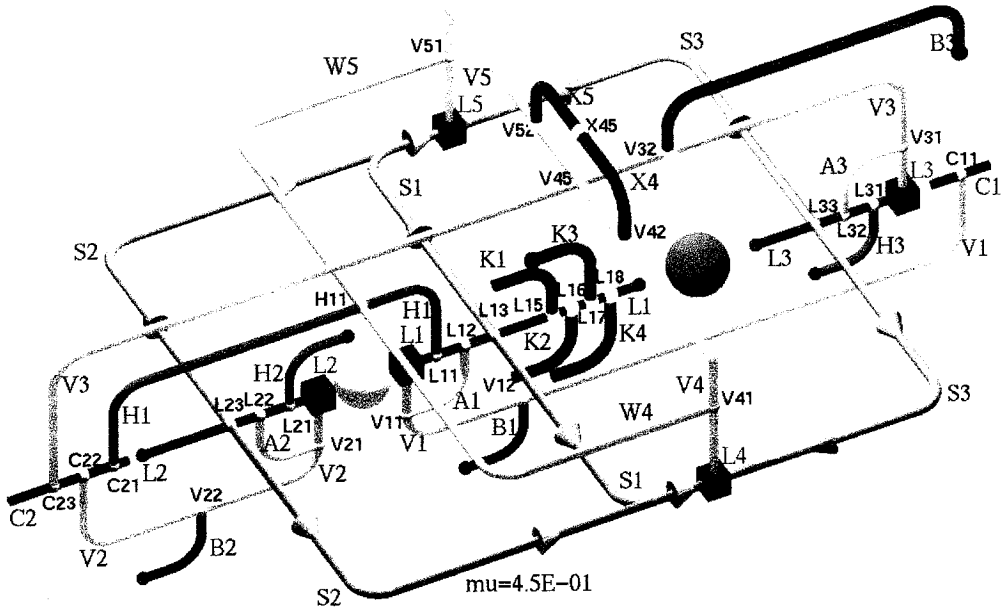

Figure 5.25: Bifurcation diagram for $\mu = 0.45$. Compared to the preceding diagram (Fig. 5.24), there is the new family $\mathbf{X4}/\mathbf{X5}$, the branch point V32 is now to the right of the branch point V45, and there are the new **K**-families that bifurcate from **L1**.

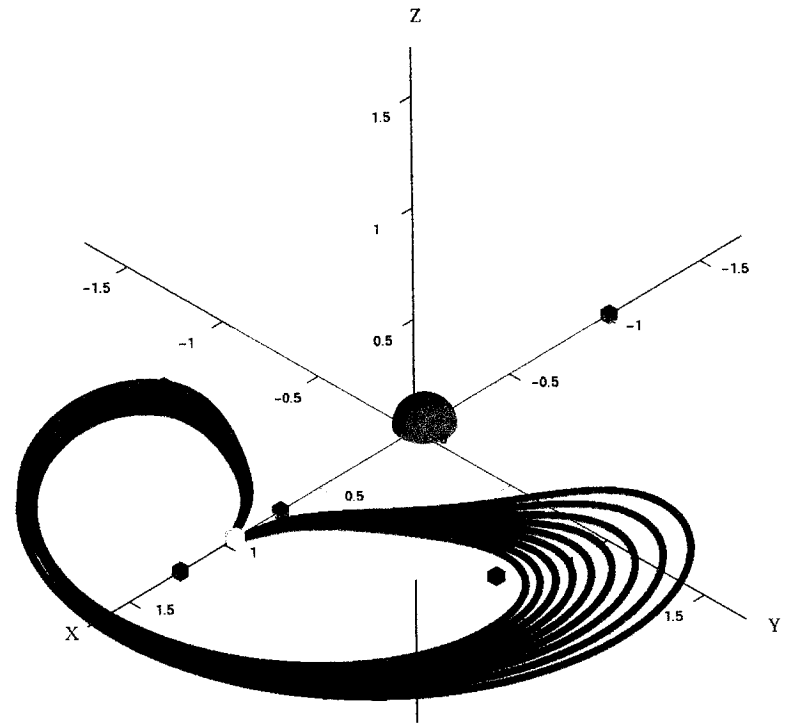

Figure 5.26: The orbit family **S2** for $\mu = 0.055$.

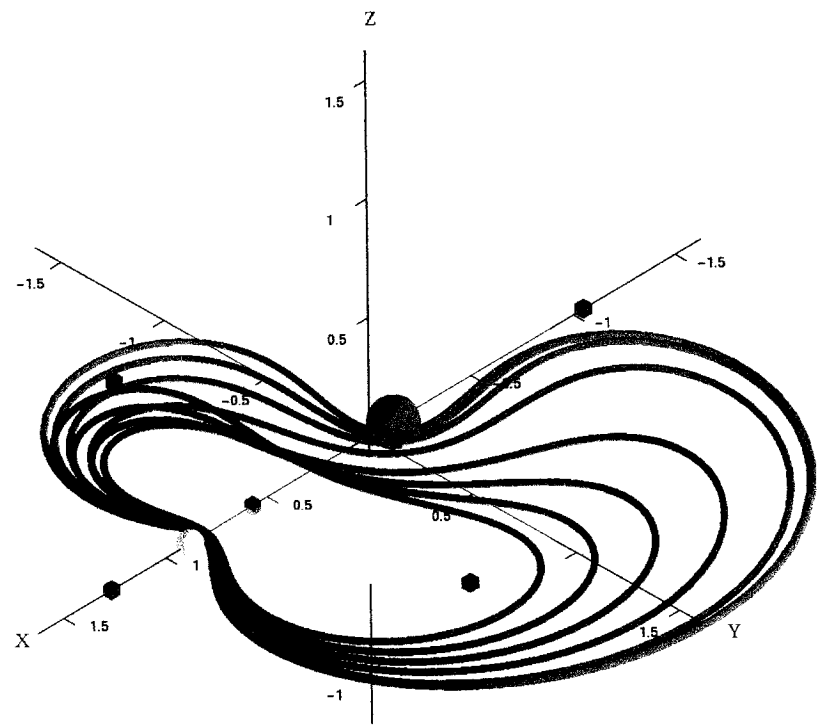

Figure 5.27: The orbit family **S1** for $\mu = 0.12$.

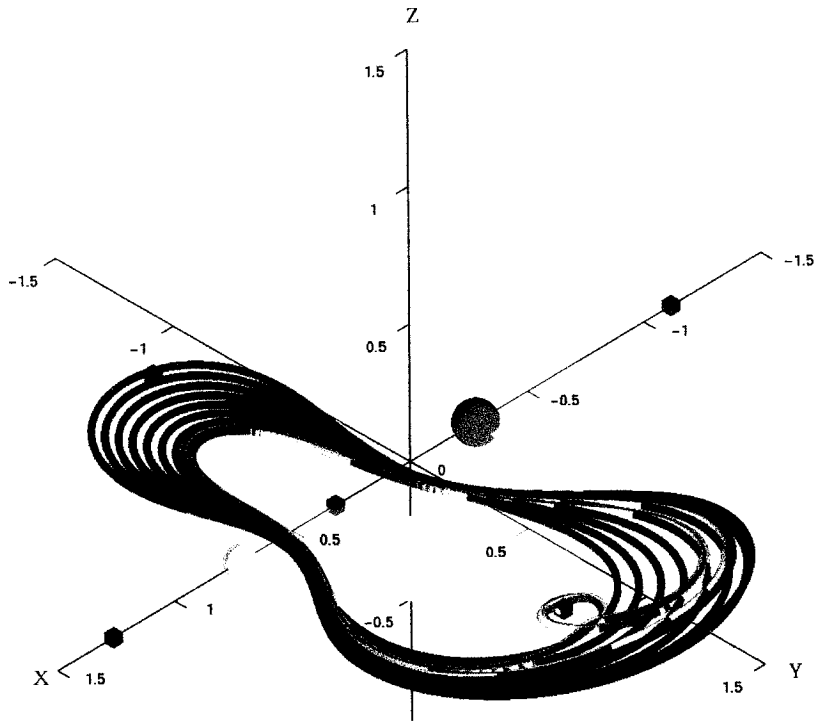

Figure 5.28: The orbit family **S1** for $\mu = 0.28$.

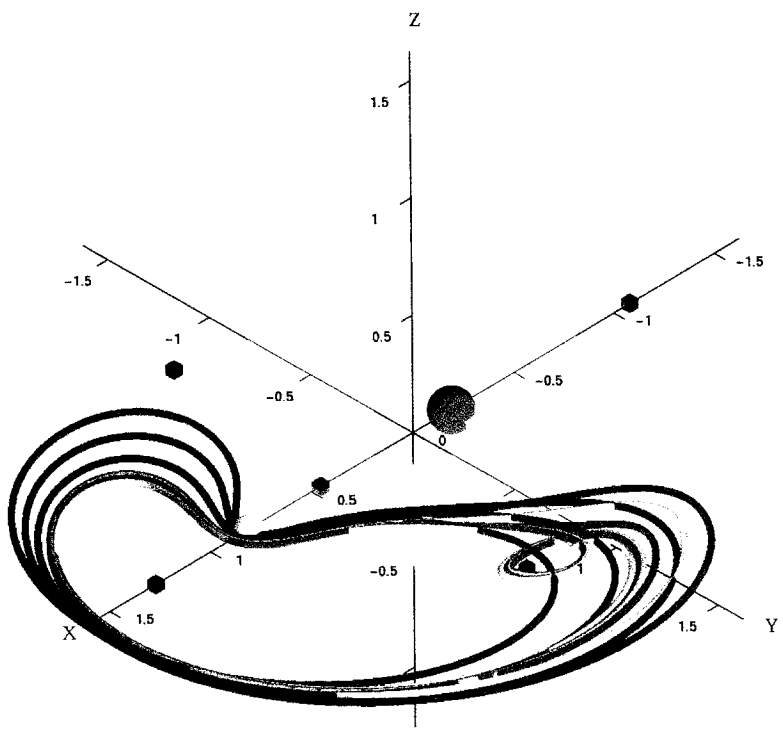

Figure 5.29: The orbit family **S2** for $\mu = 0.19$.

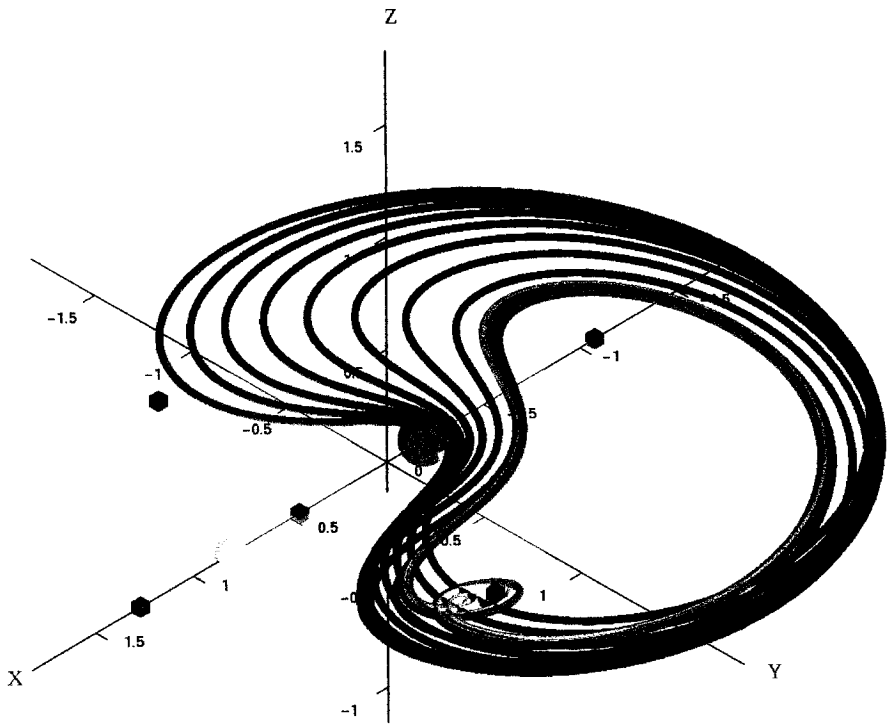

Figure 5.30: The orbit family **S3** for $\mu = 0.19$.

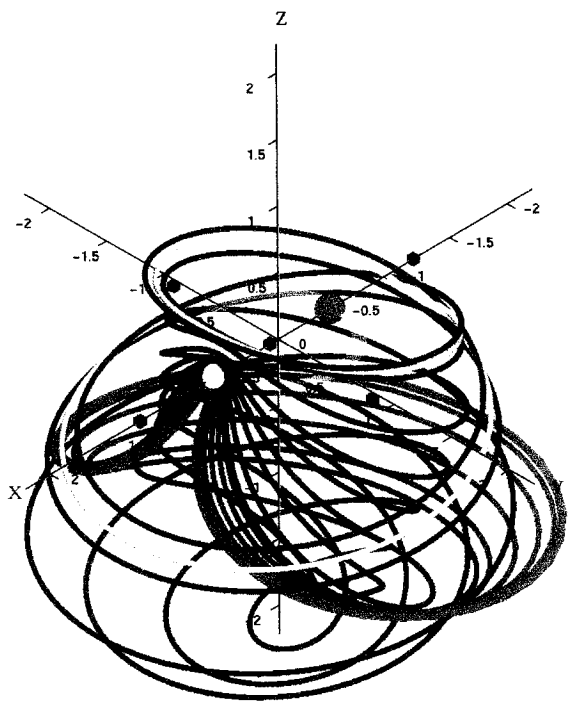

Figure 5.31: The orbit family **B3** for $\mu = 0.45$.

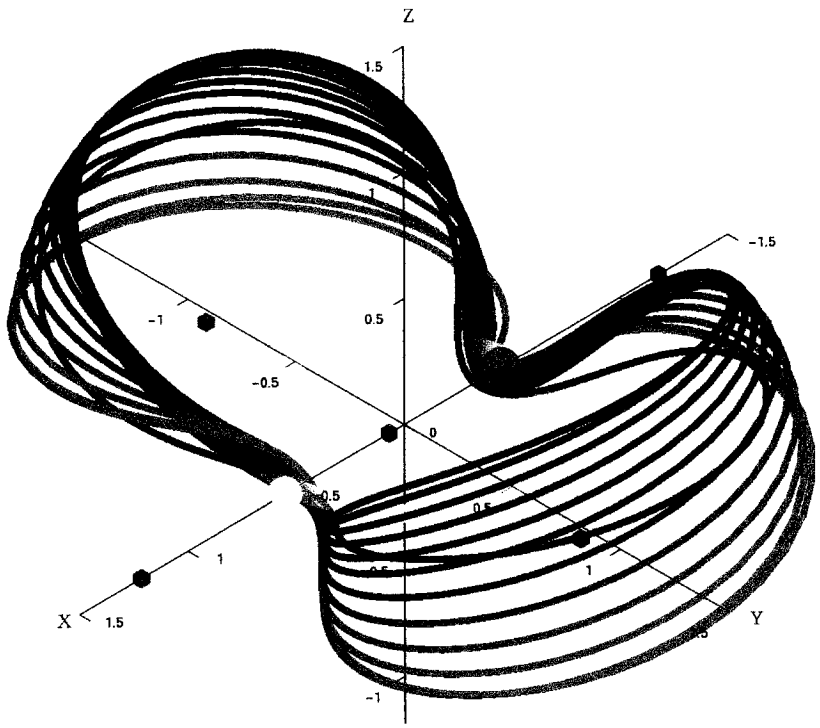

Figure 5.32: The orbit family **K1** for $\mu = 0.45$.

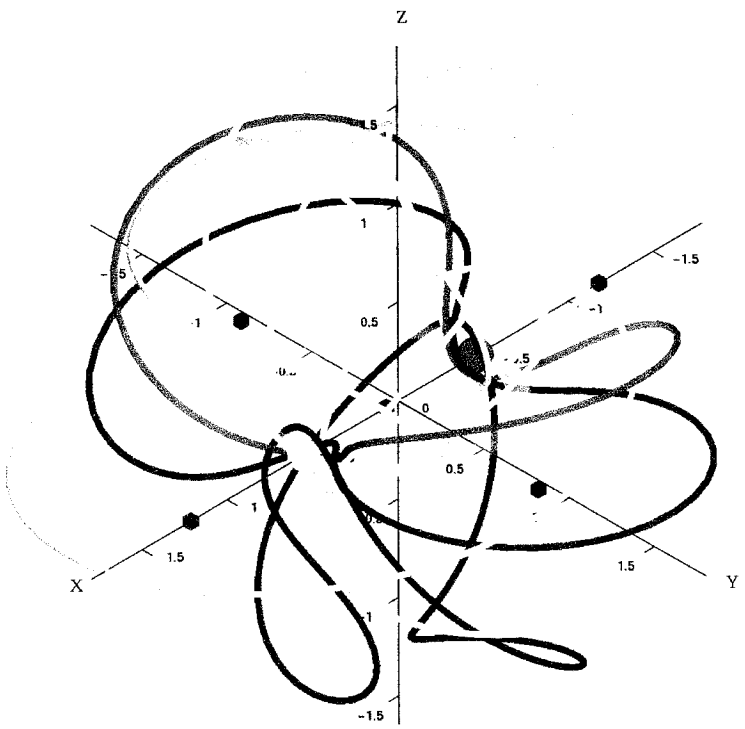

Figure 5.33: The first part of the orbit family **K2** for $\mu = 0.45$ (this family is divided into two parts only for clear representation of its orbits).

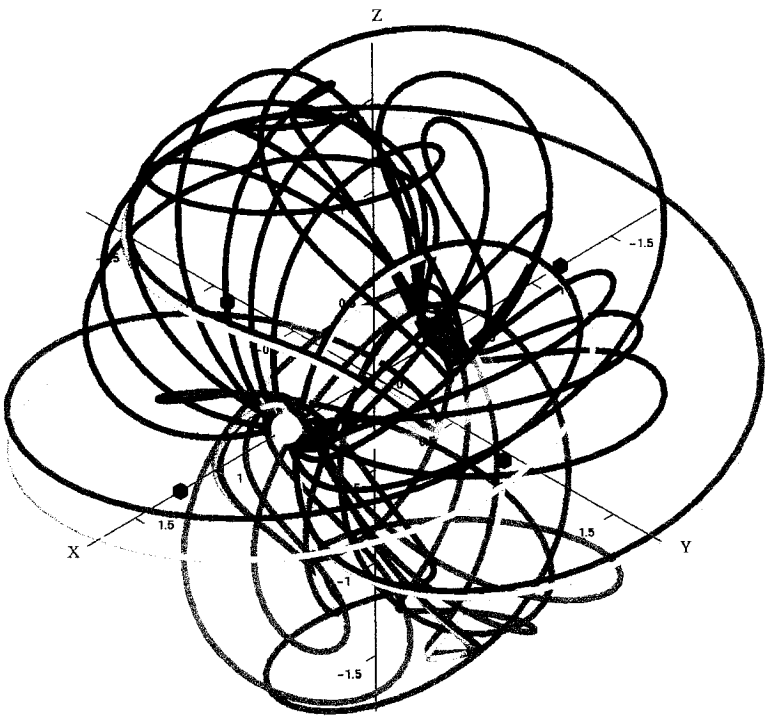

Figure 5.34: Continuation of the orbit family **K2** for $\mu = 0.45$.

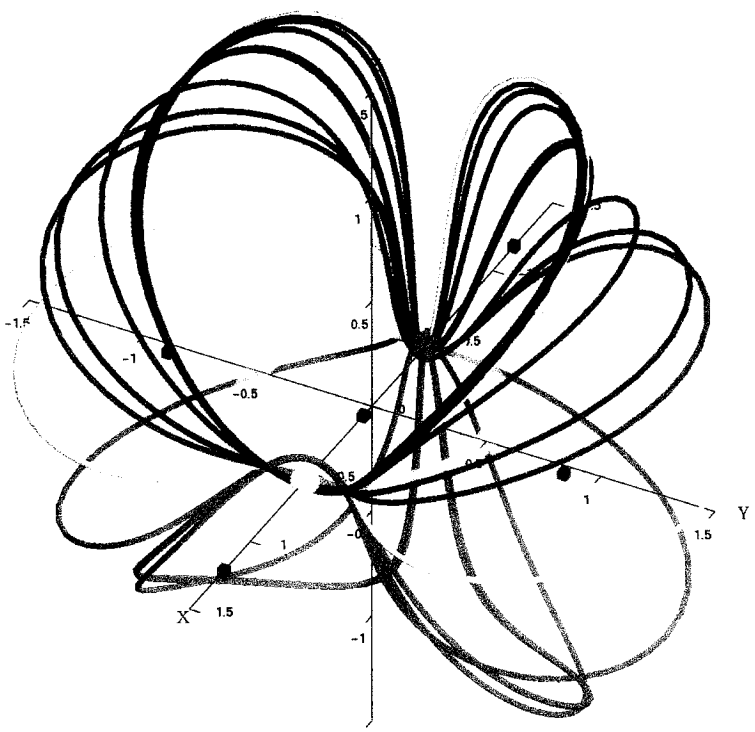

Figure 5.35: The orbit family **K3** for $\mu = 0.45$.

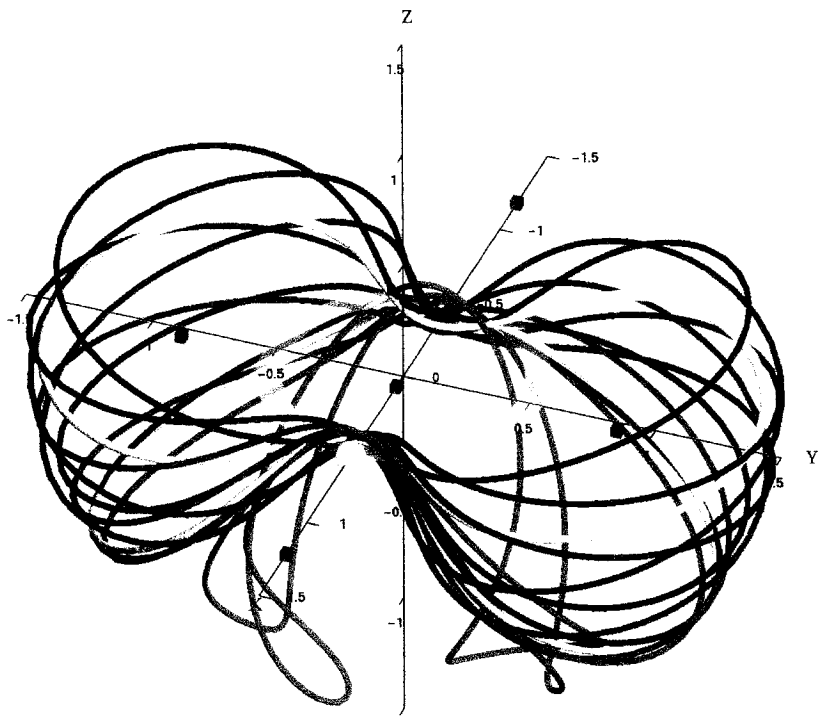

Figure 5.36: The orbit family **K**4 for $\mu = 0.45$.

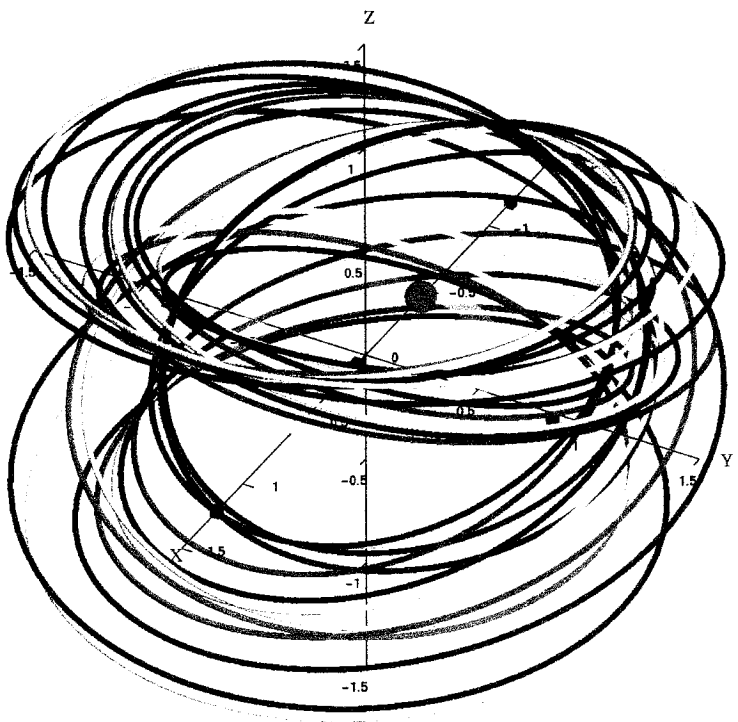

Figure 5.37: The orbit family **X**4 for $\mu = 0.45$.

5.2 Loci of Homoclinic Orbits

In the preceding section we have shown how certain branch points along families of periodic solutions depend on the mass-ratio parameter μ. In particular, much information on periodic solution families, as μ is varied, can be deduced from the computed loci of branch points. The same holds for loci of the homoclinic orbits, which is the subject of the current section.

A homoclinic (or doubly asymptotic) orbit is a trajectory that asymptotically approaches the same equilibrium point (or periodic orbit) both as $t \to +\infty$ and $t \to -\infty$. A heteroclinic orbit is a trajectory that asymptotically approaches one equilibrium point (or periodic orbit) as $t \to +\infty$ and another equilbrium (or periodic orbit) as $t \to -\infty$. In this section we only consider orbits that are homoclinic to an equilibrium.

For an equilibrium point or periodic orbit to have a homoclinic orbit, its stable and unstable manifolds must intersect. Under certain conditions, an orbit homoclinic to an equilibrium is the limit of a sequence of periodic orbits; (See [58], Theorem 6.1.1, and [109].)

The study of homoclinic orbits, and their bifurcations, constitutes a significant area of research. The existence of certain types of homoclinic orbits is known to have important consequences for the global behavior of a dynamical system. It is possible, for example, that the existence of a particular type of homoclinic orbit implies the existence of infinitely many other homoclinic orbits "nearby" in phase space. Indeed, the subject of homoclinic orbits and homoclinic bifurcations is of great complexity. In this respect, the CR3BP is no exception: it gives rise to many homoclinic orbits and homoclinic bifurcations. For example, [26] list homoclinic orbits for L1, L2 and L3 for numerous values of μ. [63] shows that for the Sun-Jupiter CR3BP, where $\mu = 0.00953875$, an orbit homoclinic to L3 does not exists, although the stable and unstable manifolds come close to intersecting. This disproves a conjecture by Brown. However, [63] does demonstrate that there are orbits homoclinic to some periodic orbits about L3 in that system.

In the thesis we restrict our attention to orbits that are homoclinic to L4 or L5, and

that terminate families of periodic solutions already encountered in previous sections. Specifically, we consider the homoclinic orbits that, for certain ranges of μ-values, terminate the planar families **S**1, **S**2, and **S**3. These homoclinic orbits are denoted **S**1∞, **S**2∞, and **S**3∞, respectively. We compute loci of homoclinic orbits for these families, using a basic, but simple numerical algorithm, that is briefly recalled in Chapter 3.

Results are shown in Fig. 5.38, where the maximum of the y-component of homoclinic orbits is plotted versus μ. The left panel includes the locus **S**1∞ of homoclinic orbits that terminate **S**1. The right panel in Fig. 5.38 includes the loci of homoclinic orbits **S**2∞ and **S**3∞, that terminate **S**2 and **S**3, respectively, even though there is only one curve in the diagram, as explained in Sec. 5.2.3 below.

We note that AUTO incorporates algorithms, collectively known as HOMCONT [16], for the detection and subsequent continuation of several types of homoclinic bifurcations. In principle, these algorithms are directly applicable to the CR3BP, given the use of an unfolding parameter, as already done in an essential way in the thesis. Such a study, while of great interest, is, however, beyond the scope of our current work.

5.2.1 Homoclinic orbits that terminate the family S1

The planar family **S**1 bifurcates from the branch point L13 along the planar Lyapunov family **L**1. As already discussed in Sec. 5.1.1, the branch point L13 exists for all μ greater than the critical value μ_5, where $\mu_5 \approx 0.066$, as seen in Fig. 5.1, which contains the locus **L**13.

There are, in fact, two parts to the family **S**1, due to the reflection symmetry across the $x-z$-plane, as schematically shown in the bifurcation diagrams, *e.g.*, in Fig. 5.18. Both parts of the family **S**1 initially terminate in collision orbits, as indicated by red spheres in Figs. 5.18-5.21. However, when μ is greater than the critical value μ_9, where $\mu_9 \approx 0.147$, then each of the two parts of the family **S**1 terminates in a homoclinic orbit. One of these orbits is homoclinic to the libration point L4, while the other is homoclinic to L5. These homoclinic orbits are both denoted **S**1∞, and their locus **S**1∞ is shown in the left panel of Fig. 5.38. Evidently the homoclinic orbits

S1∞ exist for all μ between the critical value μ_9 and $\mu = 1/2$. In Figs. 5.22-5.25 the homoclinic endings of **S1** are explicitly indicated: the family is shown to connect to L4 (and to L5), but arrows along the family are used to indicate that the approach is in a homoclinic sense.

5.2.2 Homoclinic orbits that terminate the family S2

The planar family **S2** bifurcates from the branch point L23 along the planar Lyapunov family **L2**. As already discussed in Sec. 5.1.2, the branch point L23 exists for all μ greater than the critical value μ_3, where $\mu_3 \approx 0.049$, as seen in Fig. 5.2, which contains the locus **L23**.

As is the case for the family **S1**, both symmetric parts of the family **S2** initially terminate in collision orbits, as indicated by red spheres in Figs. 5.16-5.18. However, when μ is greater than the critical value μ_6, where $\mu_6 \approx 0.080$, then each of the two symmetric parts of the family **S2** terminates in a homoclinic orbit, one homoclinic to L4, and the other to L5. These homoclinic orbits are both denoted **S2**∞, and their locus **S2**∞ is shown in the right panel of Fig. 5.38. Evidently the homoclinic orbits **S2**∞ exist for all μ between the critical value μ_6 and $\mu = 1/2$. In Figs. 5.19-5.25 the homoclinic endings are indicated by arrows along the family **S2**.

5.2.3 Homoclinic orbits that terminate the family S3

The planar family **S3** bifurcates from the branch point L33 along the planar Lyapunov family **L3**; for an example see Fig. 5.13. As already discussed in Sec. 5.1.3, the branch point L33 exists for all values of μ, as can be seen in Fig. 5.3, which contains the locus **L33**.

The two symmetric parts of the family **S3** initially connect to the libration points L4 and L5, by virtue of the Lyapunov Center Theorem, as indicated in Fig. 5.13 and in Fig. 5.14. Indeed, in these figures the family **S3** corresponds to the so-called Short-Period family already discussed in Sec. 4.1.

However, when μ is greater than the critical value μ_2 then each of the two symmetric parts of the family **S3** terminates in a homoclinic orbit, one homoclinic to L4, and

the other to L5. These homoclinic orbits are both denoted **S3∞**. Note that the critical value μ_2, where $\mu_2 \approx 0.0385$, is the same as the critical value of the Hamiltonian Hopf point mentioned in Sec. 4.1.

The locus **S3∞** of the homoclinic orbits **S3∞** corresponds to only part of the curve shown in the right panel of Fig. 5.38. In fact, one observes the co-existence of up to three homoclinic orbits for a certain range of μ-values, namely, between the critical value μ_6 and $\mu = 1/2$ (and beyond). The diagram has been drawn for the μ-interval $[0, 1]$, rather than for $[0, 1/2]$, in order to show that the loci of these co-existing homoclinic orbits correspond to a single curve.

We infer that the homoclinic orbit **S3∞** that terminates **S3** no longer exists when μ is less than the critical value μ_2. Examination of the computed homoclinic orbits along the locus **S3∞** shows that these homoclinic orbits shrink to a point, namely, the libration point L4 (or L5), as μ decreases towards the critical value μ_2.

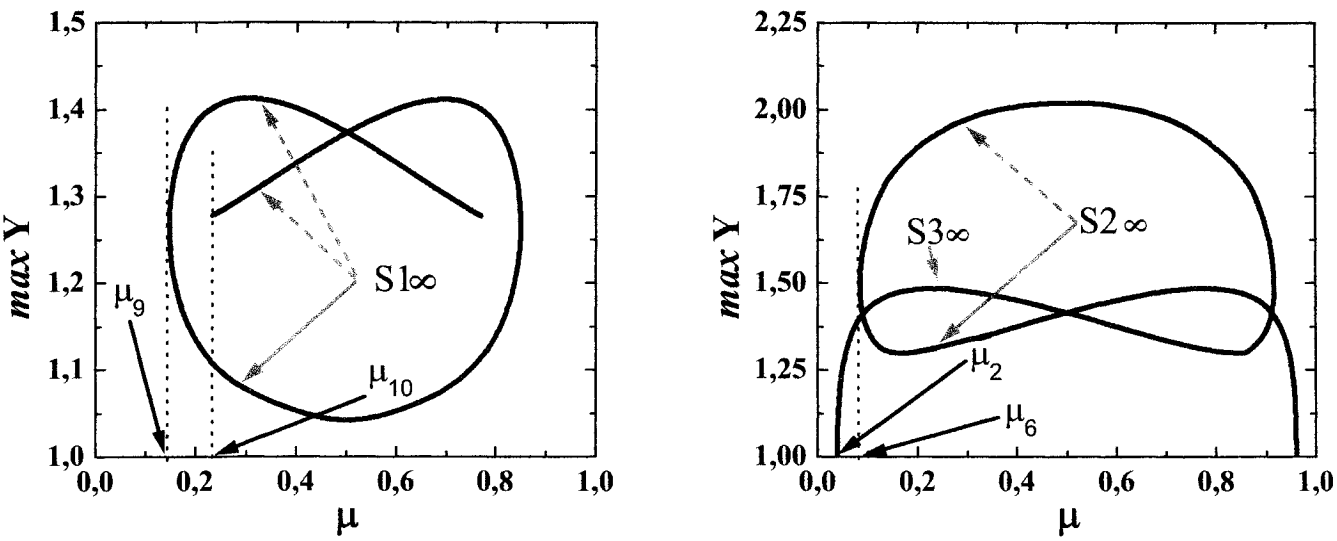

Figure 5.38: Loci of homoclinic orbits that terminate the families **S1**, **S2**, and **S3**. The vertical axis is the maximum of the y-component along the orbit. The points of self-intersection of the curves are artifacts of the representation.

5.3 The Case $\mu = 1/2$

The particular case $\mu = 1/2$ possesses symmetries that are not present for other values of μ. In this case, the primaries are located symmetrically across the $y-z$-plane at $(\pm 1/2, 0, 0)$, the L1 libration point is located at the origin, the triangular libration points are on the y-axis, and the equations of motion (2.51) are invariant under the transformation $x \to -x, t \to -t$.

In the planar CR3BP, the case $\mu = 1/2$ is called the Copenhagen problem. See [107] for an extensive discussion of periodic orbits in the Copenhagen problem. [23] and [91, 90] described a number of orbits homoclinic to L4 for this problem.

In the general case of the Elliptic Restricted 3-Body Problem, the model of particle motion strictly along the z-axis is called the Sitnikov problem [79, 76]. . The general Sitnikov problem was the inspiration for some fundamental analysis of chaotic system [82, 30]. In the CR3BP, this model is called the Macmillan problem. In contrast to the general Sitnikov problem, the Macmillan problem has solutions in closed form with elliptic integrals. The bifurcations from the Vertical family for the case $\mu = 1/2$ were also studied by [10].

There are some important structural changes in the bifurcation diagram for $\mu = 1/2$, compared to the diagrams for μ less than $1/2$, as presented in Fig. 4.2 and Figs. 5.13-5.25. One of these changes concerns the branch points C22, C23, and V45, which can be seen, for example, in Fig. 5.25. For the case where $\mu = 1/2$, these branch points coincide, as explained in Sec. 5.3.1 below.

Another important change in the bifurcation diagram for $\mu = 1/2$ is that the family of Vertical orbits $\mathbf{V}1$ no longer connects directly to the planar Circular family $\mathbf{C}1$, as explained in Sec. 5.3.2. Related to this change, the Vertical family $\mathbf{V}1$ then contains additional branch points that lead to a plethora of families not previously encountered in this thesis. Many of these new families also exist when μ is less than $1/2$, but there they cannot be reached via the routes considered earlier in this thesis (for fixed μ). A more complete study of these new families, including their persistence for μ less than $1/2$, would be an interesting topic, which is, however, beyond the scope of this thesis.

5.3.1 The branch points C22, C23, and V45

The bifurcation diagrams in Figs. 5.13-5.25 are only schematic; the actual location of branch points along the various solution families depends on the value of μ. In this context, the branch point V45 "slides down" the curve **V3** towards the point C23, as μ increases towards the value 1/2. When $\mu = 1/2$, the two orbits represented by C23 and V45 are identical, and hence both are planar. Moreover, as μ approaches the value 1/2, the branch point C22 also approaches C23 (and hence V45). Indeed, Fig. 5.7 shows that the loci **C22**, **C23**, and **V45**, coincide at $\mu = 1/2$. This meeting point corresponds to a single, planar branching orbit. This orbit is a member of the planar family **C2**, and the families **V2**, **V3**, **V4** (and **V5**), bifurcate from it via a period-doubling bifurcation. The branching orbit has two multipliers equal to 1, two multipliers equal to -1, and another complex pair on the unit circle. (When approached along **V2**, **V3**, **V4**, or **V5**, the branch point can be called a "reverse" period-doubling bifurcation, as was done earlier.)

5.3.2 The Vertical family V1

Another significant feature that distinguishes the bifurcation diagram for $\mu = 1/2$ from the diagrams for μ less than 1/2, concerns the nature of the Vertical family **V1** that bifurcates from the libration point L1. When $\mu = 1/2$, orbits from the family **V1** are perfectly vertical, *i.e.*, each orbit has the property that $x = y = 0$, while its z-component oscillates periodically. The amplitude of this oscillation increases, as one moves along the family **V1** away from the libration point L1. Consequently, it is impossible for the family **V1** to connect at its other end to a planar family, as is the case when μ is less than 1/2, where **V1** connects to the planar family **C1** at the reverse period-doubling bifurcation point C11. (See, for example, Fig. 5.25). Furthermore, when $\mu = 1/2$ there is a sequence of branch points along the family **V1**. The families that bifurcate at these branch points connect at their other end to planar orbits.

A representation of **V1** for the case $\mu = 1/2$ is given in the left panel of Fig. 5.39. The portion of **V1** shown there contains five branch points, whose bifurcating families are also shown. The sequence of branch points along **V1** continues beyond the diagram

limits.

The family that bifurcates from the first branch point V11 along **V**1 is in fact, the Axial family **A**1, which connects to the planar Lyapunov family **L**1 at the branch point L12.

Now consider the second branch point along **V**1, for the case $\mu = 1/2$, in the left panel of Fig. 5.39. This branch point is the key to understanding why the Vertical family **V**1 no longer connects directly to the planar family **C**1, as it does for μ less than 1/2; for example, in Fig. 5.25. Comparing the left panel in Fig. 5.39, for $\mu = 1/2$, to the right panel, for $\mu = 0.499$, one notices that the second branch point perturbs when μ becomes unequal to 1/2. When $\mu = 1/2$, one must switch branches at the second branch point, in order to reach the planar orbit C11 at the end of the bifurcating family, while for $\mu = 0.499$ there is a smooth path along **V**1 to C11. Recall that the orbit C11 belongs to the planar family **C**1, and that C11 corresponds to a reverse period-doubling bifurcation, whose orbit encompasses one of the primaries.

Note that the second bifurcating family from **V**1, as shown in the left panel of Fig. 5.39, consists of two symmetric parts. As described above, the left part connects to the planar family **C**1 at the reverse period-doubling bifurcation C11. The orbit C11 encompasses one of the primaries. The part on the right connects to the symmetry partner of the orbit C11, *i.e.*, the reflection of C11 with respect to $x = 0$. The orbit of the symmetry partner of C11 encompasses the other primary.

Comparing the left and right panel in Fig. 5.39, we also see that of the five branch points along **V**1 that appear in the left panel, only the second and the third perturb, while the other three branch points persist. However, more perturbed bifurcations occur outside the scope of the Fig. 5.39.

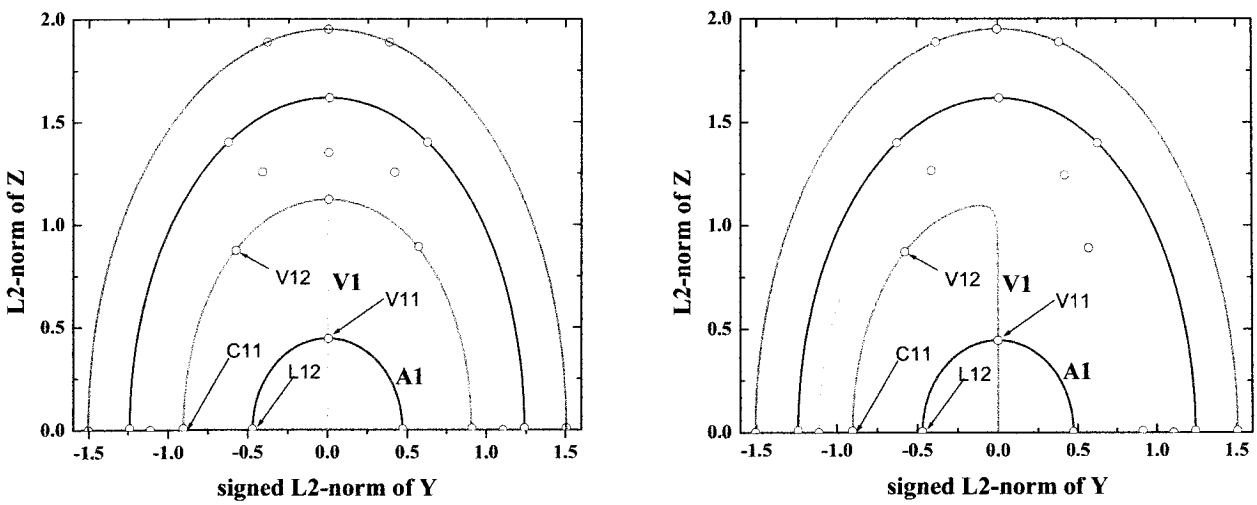

Figure 5.39: Left: The family **V1** for the case $\mu = 1/2$, showing its first five branch points, with the corresponding bifurcating families. All bifurcating families connect at their other end to families of planar orbits. Right: A bifurcation diagram for $\mu = 0.499$, that shows how the bifurcations along **V1** in the left panel are perturbed.

Chapter 6

The Data Visualization and Animation Software DR Orbits

6.1 Introduction

Graphical representation of complicated scientific data can be essential for their better understanding. Thus, visualization of scientific data is an important area of computer science. There is scientific software, like Mathcad, Matlab, Maple, Mathematica, *etc.*, containing special parts for data visualization using 2D and 3D graphics; and special programs, like Origin, for scientific data visualization only. However, for specific complicated problems, such as the CR3BP, we have to develop special graphic tools because of the specificity and complexity of the data. A good graphical representation of CR3BP data permits us to see details of an arrangement of orbits of the family in three-dimensional space, two-dimensional projections, time dependencies, *etc.* As one of the best tools for ODE bifurcation analysis, AUTO, has a built-in graphics tool, but it is not suitable for the CR3BP. Recently, a new tool, r3blaut04 [117], was created for AUTO; however, it is a more universal tool than a tool for the CR3BP. Thus, we have developed a new tool especially for the CR3BP.

6.2 Objectives

The new tool, called DR Orbits, focuses on the following objectives:

1. *Usability.* The graphical user interface of DR Orbits provide an easy-to-learn, easy-to-use, user-friendly environment.

2. *Generality.* DR Orbits can be used for different graphical representation of CR3BP data: three-dimensional graphics in real space and in the space of velocities; two-dimensional projections of all possible three-dimensional pictures; representation of time dependencies of coordinates and velocities; representation of the primaries and the libration points.

3. *Animation.* Animation of the solutions of the CR3BP is very useful for spacecraft mission design: from any orbit in the rotating frame of reference we can proceed to a real orbit of a spacecraft in the inertial frame of reference.

6.3 Development, environment and architecture

The AUTO2000 source code is written in C, and it is mainly used under Unix/Linux [42]. However, DR Orbits was designed as a multiplatform tool for Unix/Linux and MS Windows operating systems. Thus, OpenGL and GLUT [57, 56, 114, 3, 2, 54] were selected to create three-dimensional interactive graphics, and C was chosen as a programming language for better compatibility with AUTO. Additionally, for better GUI, the GLUI [95] library and the language C++ were used.

6.4 User requirement specification

6.4.1 User requirements

- Installation of the program.

  OS MS Windows: A user installs the program and all necessary data files and libraries from CD ROM using the Windows Setup Wizard. The orbit data base is copied and unpacked from a self-extracted file, using simple actions in the MS Windows operating system.

  OS Unix/Linux: There is a version of DR Orbits for these systems without GUI. This version is used with AUTO for immediate graphical representation of

AUTO solutions of the CR3BP. A user needs to install all the necessary libraries for OpenGL support separately.

Below we describe only the Windows version of DR Orbits, which has been developed more completely than the Linux version.

- Starting the program.

  A user starts the program using the abilities of the Windows(/Unix/Linux) operating system(s).

  A user should be able to read data from the data base.

- Selecting the data to be drawn.

  After the program is started, it draws the **L1** orbit family for $\mu = 0.0005$.

  A user may select any μ value from a list and any orbit family for this μ value for graphical representation.

- Selecting the type of diagram.

  A user can choose different types of diagrams and dependencies (3D and 2D) for the representation.

- Selecting options and settings.

  The GUI provides different options (general features of the diagram representation) and settings (colors and lines) for the diagram.

- Manipulations.

  A user can translate, rotate, and scale the diagram for better viewing.

- Representing tube graphics.

  A user can draw a 3D-diagram using tube graphics for better viewing.

- designing satellite mission.

  A user can choose one orbit from a represented family for animated representation of the satellite mission in the inertial frame of reference.

- Stopping the program.

  A user can stop the program at any time.

6.4.2 Non-functional requirements

Hardware

CPU: Pentium III 800 or higher;

Memory: 256 Megabytes or higher;

HDD: 2 Megabytes hard drive space available for the software installation.

Software

Operating system: MS Windows XP;

Applications: No other applications are needed.

6.5 System design and implementation

6.5.1 System architecture

Figure 6.1 depicts the system components: GUI, the basic user interface, data manipulation component, data base, and graphical object.

The GUI component is responsible for querying the data base, where all data are stored using arrays. All data in the data object are parsed from the data base files.

6.5.2 User interface design and implementation

Basic user interface design

The basic user interface (BUI) for DR Orbits was designed using the GLUT library. GLUT functions support interaction with the OpenGL program using the keyboard, mouse and pop-up menu. Because the GLUT library is platform-independent (there are variants of GLUT for MS Windows and UNIX/Linux), the BUI of DR Orbits is also platform-independent. This BUI provides all control functions necessary for the program. The BUI is described in detail in Appendix 1, Sections A.6.2 - A.6.3, A.6.17 - A.6.19. However, the BUI does not satisfy modern requirements for user interface design, and that is why the GUI, which satisfies the above-mentioned requirements better, was added to the BUI.

Graphic user interface design

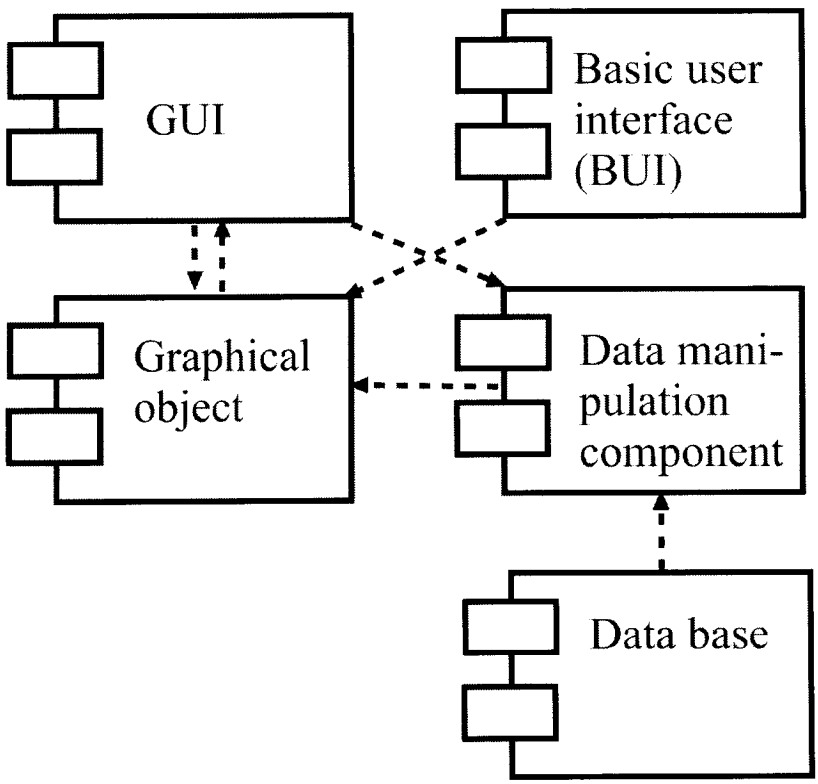

Figure 6.1: System components

The GUI was designed to satisfy all user requirements for graphics representation, control, and manipulation. All GUI objects are grouped in a separate window. For the user's convenience, GUI objects are placed in small groups in separate panels. The functions of each GUI object can be described as follows:

- The mu value listbox allows a user to select from the existing list the value of the mass ratio μ of the CR3BP. This selection defines all orbit families which exists and can be drawn for this μ value. By default, the first family (**A1**) from the list of orbit families is shown.
- The Family listbox allows choosing the orbit family from the list corresponding to the chosen μ value.
- The Graph Type listbox allows a user to choose a 3D- or 2D-type of diagram and

different types of dependencies to be drawn, namely:

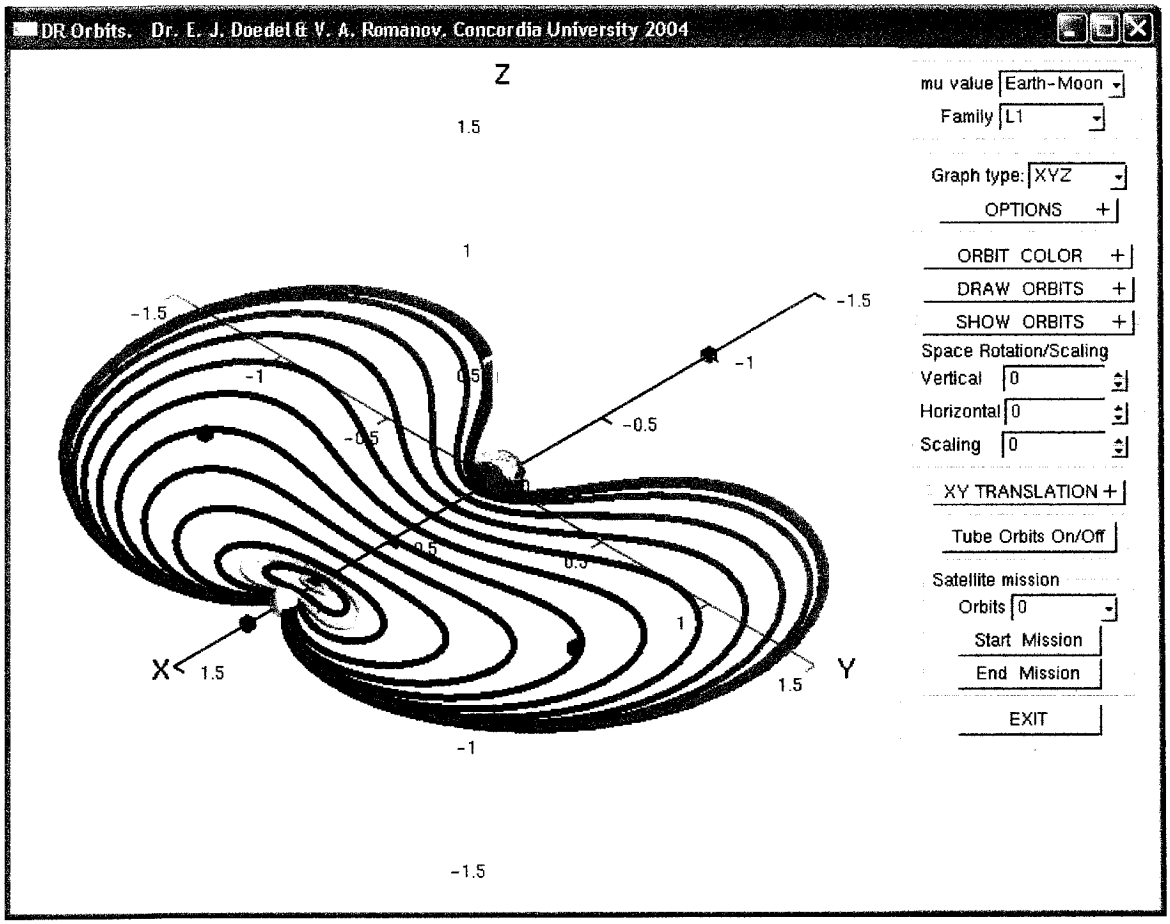

Figure 6.2: GUI component design

3D diagram of the orbit family, coordinates of the libration points, primaries, and the orbit plane of the second primary ;

3D diagram representing velocities for the orbit family in the space of velocities;

a group of 2D diagrams representing 2D projections of the 3D diagrams;

a group of 2D diagrams representing time dependencies of the coordinates or the velocities of the orbits.

- The OPTIONS rollout (see below) allows a user to chose general options for diagrams, such as background color, axis colors and axis label font, and to switch

on/off the drawing of the primaries and the libration points. This control item allows viewing of the stability of each orbit of an orbit family as well.

- The ORBIT COLOR rollout permits a user to choose a color scheme for all orbits of the family and an individual color for each bifurcation orbit.
- The DRAW ORBITS rollout permits a user to draw all orbits or each second, third, or fourth orbit of the family using different line thickness (from 1 to 5 pixels).
- The SHOW ORBITS rollout allows a user to draw one orbit or any group of consecutive orbits.
- The Space rotating/scaling panel and the XY TRANSLATION rollout permit a user to do spatial transformations with the diagram.
- The Tube Orbits On/Off button allows to draw orbits using tube (pipe line) graphics.
- The Satellite mission panel permits a user to see the satellite mission for the chosen orbits in the inertial frame of reference. The mission is shown in a separate window.
- The EXIT button stops the program.

Graphic user interface implementation

For the implementation of the GUI, many control objects from the GLUI library have been used. To improve the interface of the OpenGL program, the GLUI library [95] was created based on GLUT library. The GLUI library uses call-back functions [95], which provide corresponding actions for each control elements. The GLUI library contains many standard GUI control objects, which can be used easily for the GUI design: buttons, listboxes, checkboxes, radio buttons, panels, spinners, *etc.* This library also contains specific control objects such as rollouts, and rotation and translation control elements.

A *rollout* is a collapsible panel used to group together related control objects. A collapsed rollout looks like a button with the a plus sign on it, while an expanded

rollout looks as a panel showing all its control objects [95]. A rollout can be expanded/collapsed at any time by mouse click.

The translation control Translation XY allows a user to manipulate X and Y coordinates in 3D diagrams by clicking on on-screen arrows.

Collapsed elements of the GUI of DR Orbits are described below:

- The OPTIONS rollout contains 10 radio buttons which permit to switch on/off corresponding options.
- The ORBIT COLOR rollout contains the listbox Color and the secondary Bif. Orbits Colot rollout which contains the BifOrb spinner and the BifCol list.
- The DRAW ORBITS spinner contains two spinners: Step and Line.
- The SHOW ORBITS spinner contains two spinners, One orbit and Orbit range, and the All orbits button.
- The XY TRANSLATION spinner contains the Translation XY translation control element of the GLUI library.

6.6 Data manipulation component design

The AUTO solutions are stored in a specific internal file format [42]. The data manipulation component of DR Orbits extracts from the AUTO files only the data which are necessary for graphical representation of one orbit family, *i.e.*, coordinates and velocities for each point of the orbit, the period of each orbit, the type of orbits (bifurcation orbit or not), and the stability index (number of Floquet multipliers on the unit circle). This component also prepares data for graphical representation: it calculates the number of orbits of the family, the number of bifurcation orbits; it normalizes the data, calculates the coordinates of the libration points and primaries, *etc.* Additionally, the data manipulation component provides cubic spline interpolation for the spacecraft mission. As a result, the data manipulation component creates the data object in the operating memory that contains all data needed for the graphic representation of the orbit family.

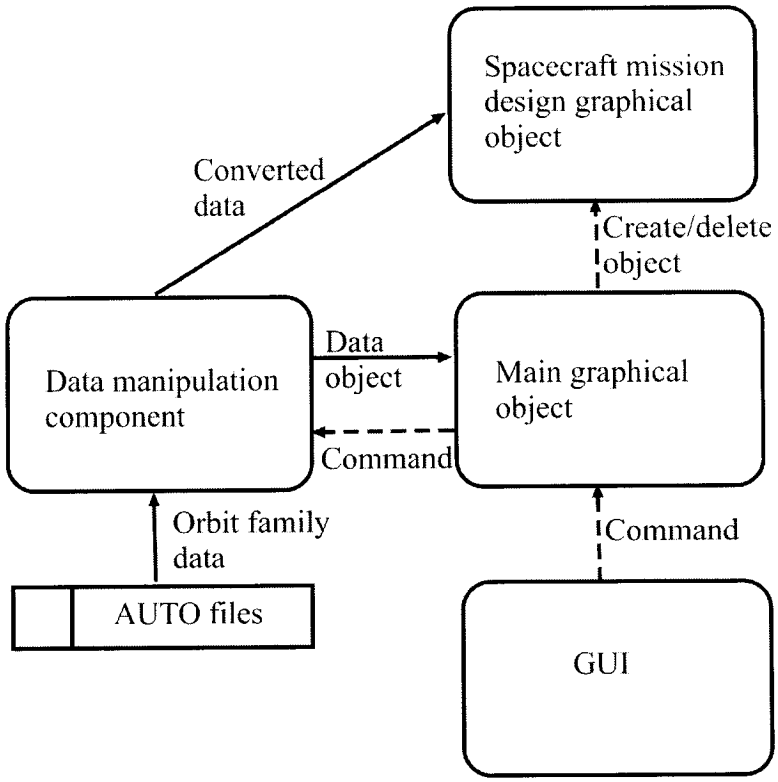

Figure 6.3: DR Orbits data flow diagram.

6.7 Running and testing

The test cases for DR Orbits are geared to examine the functionality of all the software components. In order to maximize stability of the program, we have elaborated test cases which follow the normal operation of DR Orbits. Some test cases were created to check exceptions. (We omit giving a detailed description of the test cases.)

6.7.1 Data manipulation component testing

To test this component, we draw all possible three-dimensional diagrams of all the orbit families for all μ values that are represented in the data base of DR Orbits. Since the data object contains all necessary data for diagram drawing, this test case is exhaustive for the testing of this component.

The test cases for exception testing include corrupted data base files. For the most

corrupted files DR Orbits may crash.

6.7.2 BUI testing

The BUI test cases were created to check the function keys and other keys and key combinations; mouse buttons and mouse motion; and the pop-up menu provided by GLUT library. These test cases were executed randomly for some orbit families and for some μ values.

6.7.3 GUI testing

The GUI test cases were created to check all the abilities of the GUI objects (rollouts, buttons, list, radio buttons, spinners, etc.) and some of its combinations. These test cases were executed randomly for some orbit families and for some μ values.

Some coordination problems between the BUI and the GUI were found : operations of space transformations (moving, rotation, scaling) are fixed differently for BUI and GUI, so for this case, mixing the two interfaces can give problems, which will be fixed in the next version of DR Orbits.

6.7.4 Mission design (animation) testing

These test cases were performed for almost all types of orbit families for the Earth-Moon system, and for all orbits families for other μ values different from the Earth-Moon case. We chose the first, the last, and the middle orbit of each family to check the mission. Some missions were tested for more than two periods.

6.8 Results

6.8.1 Creating diagrams of orbit families

First, an orbit family can be drawn in three-dimensional space as trajectories of the infinitesimal body of the CR3BP. These trajectories can be drawn as curves (lines) or tubes (pipe lines). Use of lines is the simplest and the fastest way to show the solution, but pipelines present a more realistic three-dimensional picture. However,

the tube diagram requires more computational and graphical resources of a computer and more CPU time (from one to four minutes). Examples of three-dimensional diagrams for some orbit families are shown in Figs. 6.4-6.5.

Second, the velocities of the infinitesimal body can be drawn in the three-dimensional velocity space. All attributes of the previous diagrams can be used for this case as well. Examples of three-dimensional velocity diagrams for some orbit families are shown in Fig. 6.6.

Third, any two-dimensional projection on a coordinate plane can be drawn for any three-dimensional diagram. Examples of such projections are shown in Figs. 6.7-6.8.

Fourth, the time dependence of any coordinate or velocity can be drawn. For this case, the period of each orbit is normalized to 1. Examples of such diagrams are shown in Fig. 6.9.

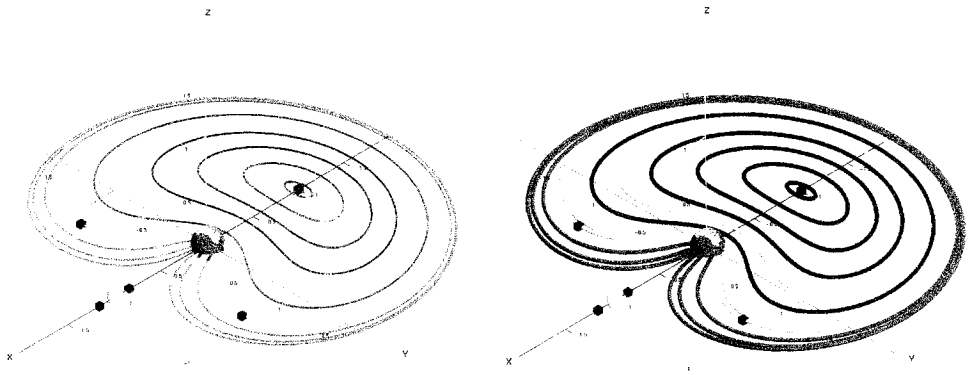

Figure 6.4: Examples of three-dimensional line diagrams of the planar orbit orbit family **L3** for the Earth-Moon system (***left***) and the diagram of the same orbit family using tubes (***right***).

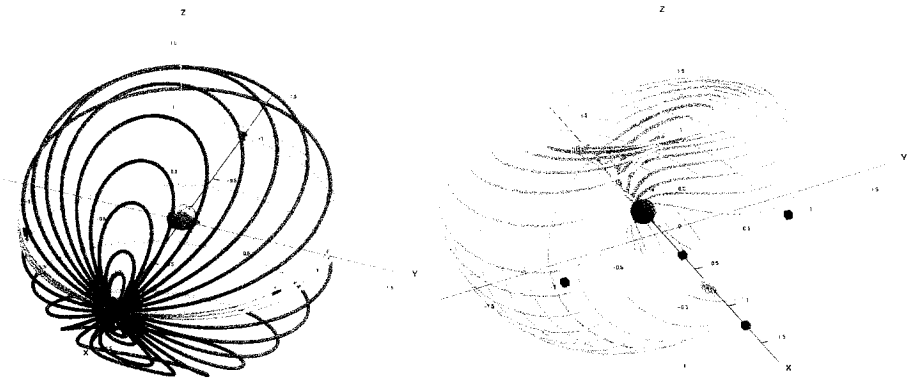

Figure 6.5: Examples of three-dimensional diagrams using tubes: the orbit family **V2** for the Earth-Moon system (***left***), and the orbit family **A3** for $\mu = 0.28$ (***right***).

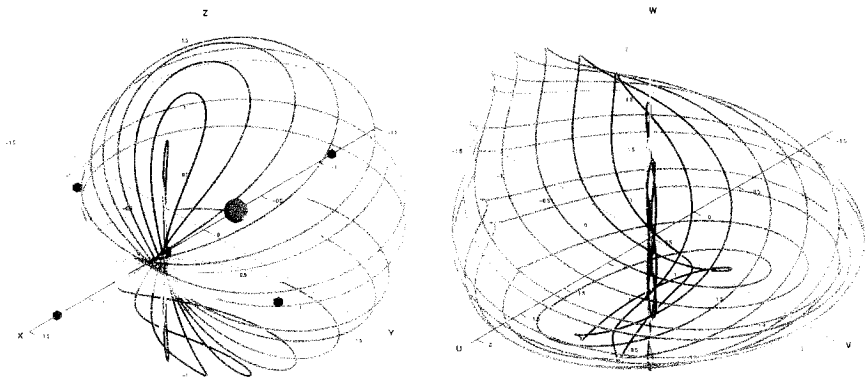

Figure 6.6: The vertical orbit family **V1** for $\mu = 0.28$ (***left***), and the diagram of the same family in the three-dimensional velocity space (***right***).

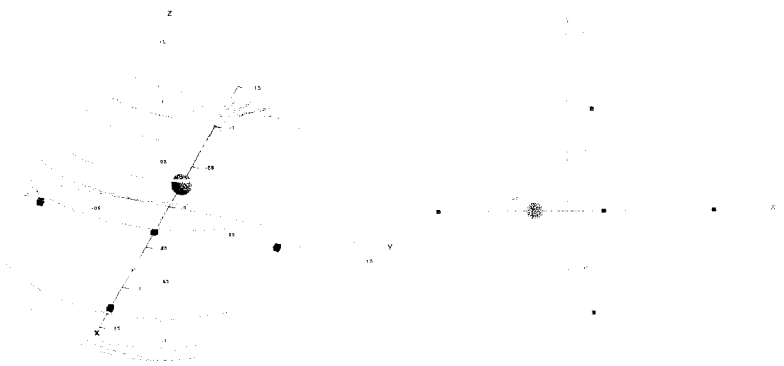

Figure 6.7: The vertical orbit family **V3** for $\mu = 0.28$ (***left***), and the two-dimensional projection of the same family on the $XY-$plane (***right***).

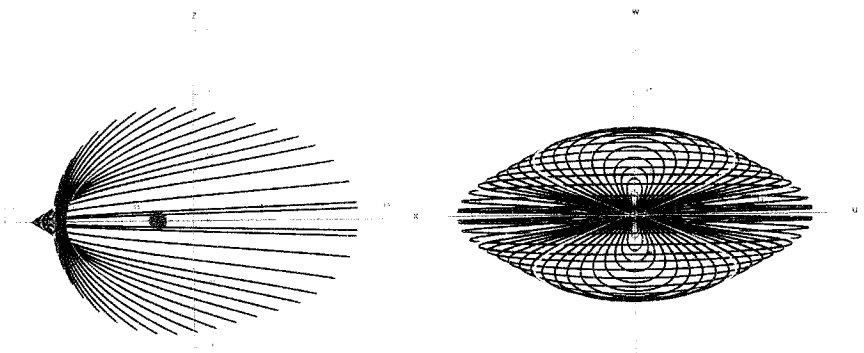

Figure 6.8: Projections of the three-dimensional diagram of Fig. 6.7: the projection on the $XZ-$coordinate plane (***left***), and the projection on the $UW-$coordinate plane of the velocity space (***right***)

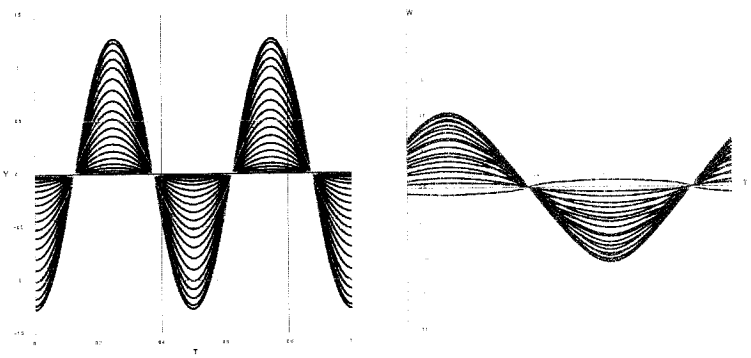

Figure 6.9: Examples of time dependencies: coordinate $X(t)$ (***left***), and velocity W(t) (***right***) of the vertical orbit family **V3** for $\mu = 0.28$

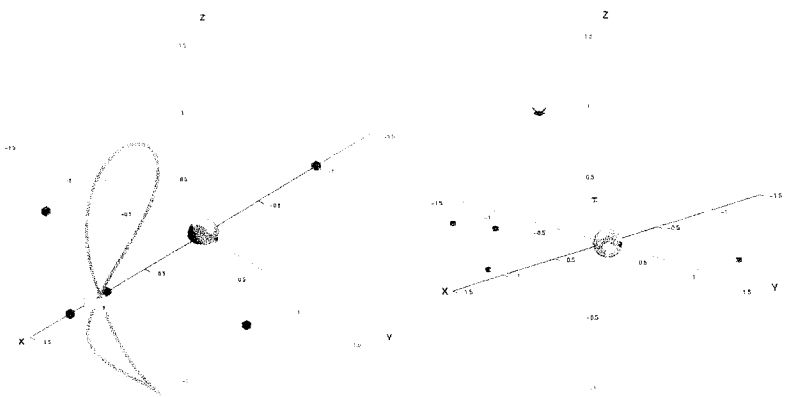

Figure 6.10: A vertical orbit of the orbit family **V1** for the Earth-Moon system (in the rotating frame of reference) (***left***), and the trajectory of a satellite (red UFO) for time $t < T$, moving along this orbit in the inertial frame of reference (***right***). (T is a period of the orbit in the rotating frame of reference.)

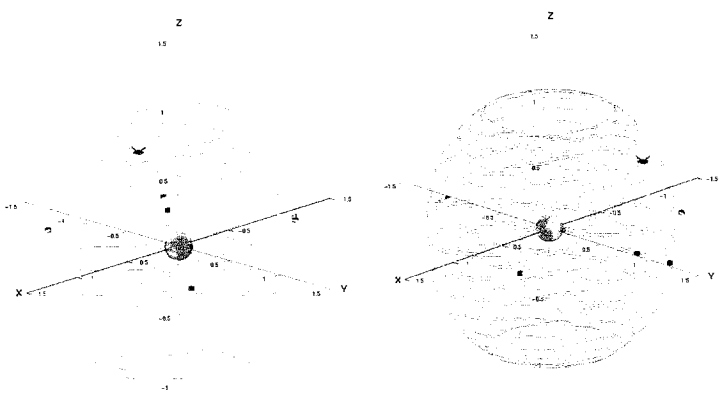

Figure 6.11: The trajectory of a satellite for time $t > 2T$, moving along the orbit from Fig. 6.10 in the inertial frame of reference (***left***), and the same trajectory for the time $t \gg T$(***right***).

6.8.2 Creating an animated satellite mission

Any orbit of an orbit family can be chosen for satellite mission design in the inertial frame of reference with the origin at the barycenter of the primaries. This mission is shown as an animation. Frames of such animations are shown in Figs. 6.10-6.12.

6.8.3 Stability of the orbit family

DR Orbits can show the stability properties of each orbit in an orbit family. As mentioned above, the stability index is the number of Floquet multipliers on the unit

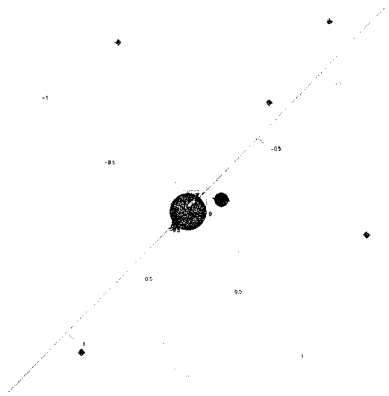

Figure 6.12: The planar trajectory of a satellite moving along an orbit of the orbit family C2 in the inertial frame of reference.

circle: if this number is six, the orbit is (linearly) stable, if the number is less than six, the orbit is unstable. If the option STABILITY ON is selected then the color of each orbit shows its stability property (Table 6.1). Examples of two diagrams showing the stability properties of orbits are presented in Fig 6.13.

Table 6.1: Number of Floquet multipliers and orbit colors for the stability diagram.

Number of Floquet multipliers on the unit circle	Color of an orbit
6	red
5	magenta
4	cyan
≤ 3	blue

6.8.4 Orbit representation

We can use different color schemes for the representation of an orbit family. A different color can be chosen for each bifurcation orbit. We can represent not only the whole family, but also any number of consecutive orbits or any individual orbit in the picture. For orbits drawn with lines we can choose the line thickness (from 1 to 5 pixels). To see details of the diagram we can change the background color, the color of axes, the

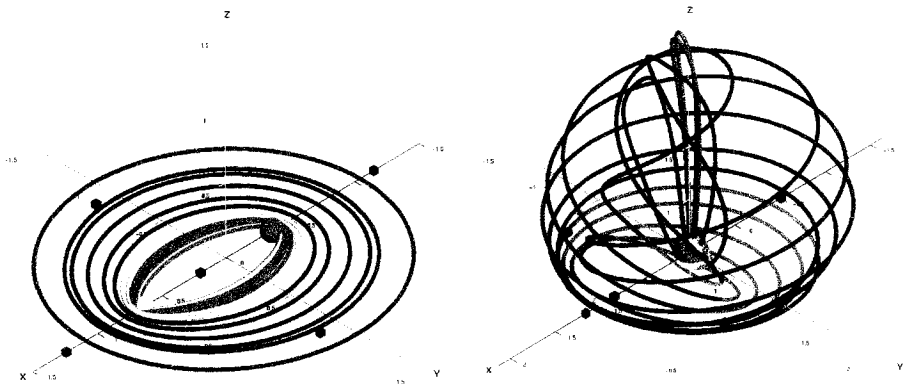

Figure 6.13: Example of two diagrams showing stability of orbits: The orbit family **C2** for $\mu = 0.36$ (***left***), and the orbit family B2 for the Earth-Moon system (***right***).

size of the font of the axes labels, and the images of the primaries and the libration points as well.

6.8.5 Space transformations

The diagram can be rotated over any angle around vertical and horizontal axes, and can be enlarged up to 50 times or shrunk up to 10 times compared to its normal size. (Moreover, the BUI has wider limits for these manipulations.) The diagram can be translated in the window plane, so that its center can be in the corner of the window.

Chapter 7

Conclusions and Future Development

7.1 Conclusions

We have investigated the structure of periodic orbit families of the Circular Restricted 3-Body Problem for all values of the mass ratio μ $(0 \leq \mu \leq 0.5)$. We started from the orbit families which emanate from the libration points, and via their bifurcation orbits we investigated the secondary families, as well as some tertiary families. "Critical" μ values define the appearance or disappearance of families. The structure of these solution families has been represented in bifurcation diagrams.

7.2 Future development

The investigation of the CR3BP can be continued and generalized into several directions:

1. Investigation of stable and unstable manifolds of dynamical systems:

Unstable fixed points ("steady states" or "stationary solutions") have an "unstable manifold" (and, typically, a "stable manifold") associated with them. These "invariant" manifolds are important for studying the dynamics of a system. For example, the Genesis mission was designed to follow such a manifold, which allows the spacecraft to travel from one place to another at "zero" fuel cost [77]. Numerical con-

tinuation methods based on boundary value continuation techniques [74] have been used to study the global structure of invariant manifolds of dynamical systems. The results of such research for the circular restricted three-body problem may be useful for future space mission design.

2. Relativistic effects in the restricted three-body problem:

Relativistic effects in a post-Newtonian approximation of the CR3BP are essential for some chaotic orbits [111]. These effects can be used as a possible test of general relativity [111]. Numerical continuation methods permit to build the full solution structure of the relativistic periodic orbits associated with the libration points. Some of these orbits may be more suitable then others for a novel test of general relativity [84], because of accumulation of small relativistic effects during cumulative periods of motion.

3. Elemental periodic orbits associated with the libration points of a rotating gravitating ellipsoid:

It is known that there are five libration (stationary) points for the rotating gravitating ellipsoid. At the present time, stability of these libration points was investigated partially for the case of an ellipsoid which is asymptotically close to a sphere. Using numerical continuation methods, it is possible not only to investigate stability of the libration points, but also the elemental periodic orbits (i.e. orbits associated with the libration points), and some secondary bifurcating orbits for any form of the rotating gravitational ellipsoid [41]. Results of such research could be useful for the investigation of the three-dimensional motion of stars, stellar aggregations and black holes in elliptical galaxies, the process of dark matter accumulation, star formation in elliptical galaxies and around them, and for the evolution of galaxies in general [52].

Bibliography

[1] E. L. Allgower and K. Georg. Numerical path following. In *Handbook of Numerical Analysis*. Vol. 5, North Holland Publishing, 1996.

[2] E. Angel. *OpenGL: A Primer*. Addison-Wesley, 2002.

[3] E. Angel. *Interactive Computer Graphics. A Top-down Approach with OpenGL*. Addison-Wesley, 2003.

[4] V.I Arnold. *Ordinary Differential Equations. (in Russian)*. Regular and Chaotic Dynamics, Izhevsk, 2000.

[5] V.I. Arnold, V.V. Kozlov, and A.I. Neistadt. *Mathematical Aspects of Classical and Celestial Mechanics (in Russian)*. VINITI, Moscow, 1985.

[6] U. M. Ascher, J. Christiansen, and R. D. Russell. Collocation software for boundary value ODEs. *ACM Trans. Math. Software*, 7:209–222, 1981.

[7] U. M. Ascher, R. M. M. Mattheij, and R. D. Russell. *Numerical Solution of Boundary Value Problems for Ordinary Differential Equations*. SIAM, 1995.

[8] U. M. Ascher and L. R. Petzold. *Computer Methods for ODEs and DAEs*. SIAM, 1998.

[9] U. M. Ascher and R. J. Spiteri. Collocation software for boundary value differential-algebraic equations. *SIAM J. Sci. Comput.*, 15:938–952, 1995.

[10] E. Belbruno, J. Llibre, and M. Ollé. On the families of periodic orbits which bifurcate from the circular Sitnikov motions. *Cel. Mech. Dyn. Astron.*, 60:99–129, 1994.

[11] W.-J. Beyn, A. Champneys, E. J. Doedel, W. Govaerts, B. Sandstede, and Yu. A. Kuznetov. Numerical continuation and computation of normal forms. In B. Fiedler, editor, *Handbook of Dynamical Systems*, volume 2, pages 149–219. Elsevier Science, 2001.

[12] P.H. Borcherders. The restricted gravitational three-body problem trajectories associated with Lagrange fixed points. *European J. of Physics*, 17:63–70, 1996.

[13] J. V. Breakwell and J. V. Brown. The "Halo" family of 3-dimensional periodic orbits in the Earth-Moon restricted 3-body problem. *Celestial Mechanics*, 20:389–404, 1979.

[14] A.D. Bruno. *The Restricted 3 Body Problem: Plane Periodic Orbits.* de Gruyter, Berlin-New York, 1994.

[15] Harvard University Center for Astrophysics. Unusual minor planets. Available via http://cfa-www.harvard.edu/iau/lists/Unusual.html, 2003.

[16] A. Champneys and Yu. A. Kuznetsov. Numerical detection and continuation of codimension-two homoclinic bifurcations. *Int. J. Bifurcation and Chaos*, 4:795–822, 1994.

[17] K.-C. Chen. On Chenciner-Montgomery's orbit in the three-body problem. *Discrete and Continuous Dynamic Systems*, 7:85–90, 2001.

[18] A. Chenciner, J. Gerver, R. Montgomery, and C. Simó. Simple choreographic motions of n bodies: A preliminary study. Technical report, 2001. Departament de Matemàtica i Anàlisi, Universitat de Barcelona.

[19] A. Chenciner and R Montgomery. A remarkable periodic solution of the three body problem in the case of equal masses. *Annals of Mathematics*, 152:881–901, 2000.

[20] A. C. Clarke. Stationary orbits. *J. British Astronomical Association*, pages 232–237, December 1947. Reprinted in *Ascent to Orbit: A Scientific Autobiography*, A.C. Clarke, Wiley, 1984.

[21] A.C. Clarke. Extraterrestial relays. *Wireless World*, pages 305–308, 1945.

[22] J.W. Cornelisse, H.F.R. Schöyer, and K.F. Wakker. *Rocket Propulsion and Spaceflight Dynamics.* Pitman, London, 1979.

[23] J.M.A. Danby. Orbits in the Copenhagen problem asymptotic at L_4 and their genealogy. *Astron. J.*, 72(2):198–201, 1967.

[24] C. de Boor and B. Swartz. Collocation at Gaussian points. *SIAM J. Numer. Anal.*, 10:582–606, 1973.

[25] A. Deprit and B. Deprit. Stability of the triangular Lagrangian points. *Astronomical Journal*, 72:173–, 1967.

[26] A. Deprit and J. Henrard. Symmetric doubly asymptotic orbits in the restricted three-body problem. *Astron. J.*, 70(4):271–274, 1965.

[27] A. Deprit and J. Henrard. A manifold of periodic orbits. In Z. Kopal, editor, *Advances in Astronomy and Astrophysics*, pages 1–124. Academic Press, 1968.

[28] A. Deprit and J. Henrard. Construction of orbits asymptotic to a periodic orbit. *Astron. J.*, 74:308–316, 1969.

[29] A. Deprit and D. Palmore. Analytical continuation and first-order stability of the short-period orbits in the Sun-Jupiter system. *Astronomical Journal*, 71:94–98, 1966.

[30] F. Diacu and P. Holmes. *Celestial Encounters.* Princeton, 1996.

[31] D.J. Dichmann, E.J. Doedel, and R.C. Paffenroth. The computation of periodic solutions of the 3-body problem using the numerical continuation software AUTO. In G. Gomez, M.W. Lo, and J. J. Masdemont, editors, *Libration Point Orbits and Applications*, pages 489–528. World Scientific, 2003.

[32] E. J. Doedel. AUTO, a program for the automatic bifurcation analysis of autonomous systems. *Congr. Numer.*, 30:265–384, 1981.

[33] E. J. Doedel. Nonlinear numerics. *Int. J. Bifurcation and Chaos*, 7(9):2127–2143, 1997.

[34] E. J. Doedel, A. R. Champneys, T. F. Fairgrieve, Yu. A. Kuznetsov, B. Sandstede, and X. J. Wang. AUTO97: Continuation and bifurcation software for ordinary differential equations. Available via http://cmvl.cs.concordia.ca, 1997.

[35] E. J. Doedel, W. Govaerts, and Yu. A. Kuznetsov. Computation of periodic solution bifurcations in ODEs using bordered systems. *SIAM J. Numer. Anal.*, 41:401–435, 2003.

[36] E. J. Doedel, W. Govaerts, Yu. A. Kuznetsov, and A Dhooge. Numerical continuation of branch points of equlibria and periodic orbits. *Int. J. Bifurcation and Chaos. Special issue commemorating the 100th anniversary of the birth of John von Neumann*, 15(3), 2005 (to appear).

[37] E. J. Doedel, A. D. Jepson, and H. B. Keller. Numerical methods for Hopf bifurcation and continuation of periodic solution paths. In R. Glowinski and J. L. Lions, editors, *Computing Methods in Applied Sciences and Engineering VI*, pages 127–136. North Holland, Amsterdam, 1984.

[38] E. J. Doedel, H. B. Keller, and J. P. Kernévez. Numerical analysis and control of bifurcation problems: I. *Int. J. Bifurcation and Chaos*, 1:493–520, 1991.

[39] E. J. Doedel, H. B. Keller, and J. P. Kernévez. Numerical analysis and control of bifurcation problems: II. *Int. J. Bifurcation and Chaos*, 1:745–772, 1991.

[40] E. J. Doedel, R. C. Paffenroth, H. B. Keller, D. J. Dichmann, J. Galán-Vioque, and A. Vanderbauwhede. Continuation of periodic solutions in conservative systems with application to the 3-body problem. *Int. J. Bifurcation and Chaos*, 13(6):1353–1381, 2003.

[41] E. J. Doedel, V. A. Romanov, R. C. Paffenroth, H. B. Keller, D. J. Dichmann, J. Galán, and A. Vanderbauwhede. Elemental periodic orbits associated with the libration points in the circular restricted 3-body problem. *(in preparation)*, 2005.

[42] E.J. Doedel, R.C. Paffenroth, A.R. Champneys, T.F. Fairgrieve, Yu.A. Kuznetsov, B.E. Oldeman, B. Sandstede, and X. Wang. *AUTO 2000: Continuation and Bifurcation Software for Ordinary Differential Equations (with HomCont).* http://www.ama.caltech.edu/ ~redrod/auto2000/distribution/, 2002.

[43] G.E. Duboshin. *Celestial Mechanics. Principal Problems and Methods (in Russian).* Nauka, Moscow, 1975.

[44] D. W. Dunham and C. E. Roberts. Stationkeeping techniques for libration-point satellites. *J. Astronautical Sciences*, 49(1):127–144, 2001.

[45] T. F. Fairgrieve and A. D. Jepson. O. K. Floquet multipliers. *SIAM J. Numer. Anal.*, 28(5):1446–1462, 1991.

[46] R. Farquhar. *The Control and Use of Libration-Point Satellites.* PhD thesis, Department of Aeronautics and Astronautics, Stanford University, 1968.

[47] R. W. Farquhar. The flight of ISEE-3/ICE: origins, mission history and a legacy. *J. Astronautical Sciences*, 49(1):23–73, 2001.

[48] R. W. Farquhar and D. W. Dunham. Use of libration points for space observatories. In *Observatories in Earth Orbit and Beyond*, pages 391–395. Kluwer Academic Publishers, 1990.

[49] R. W. Farquhar and D. W. Dunham. Libration point missions, 1978-2002. In *Libration Points Orbits and Applications*, pages 45–73. World Scientific, 2003.

[50] R. W. Farquhar and A. K. Kamel. Quasi-periodic orbits about the translunar libration point. *Celestial Mechanics*, 7:458–473, 1973.

[51] D. Folta and K. Richon. Libration orbit mission design at L2: A MAP and NGST perspective. In *AIAA/AAS Astrodynamics Specialist Conference*, 1998. AIAA 98-4469.

[52] S.A. Gasanov and L.G. Lukyanov. The libration points for the motion of a star inside an elliptical galaxy. *Astronomy Reports*, 78:851–857, 2002.

[53] F.T. Geyling and H.R. Westerman. *Introduction to Orbital Mechanics.* Addison-Wesley, 1971.

[54] G. Glaeser and H. Stachel. *Open Geometry: OpenGL + Advanced Geometry.* Addison-Wesley, 1999.

[55] G. Gómez, J. Llibre, R. Martínez, and C. Simó. *Dynamics and Mission Design Near Libration Points, Vol. II: Fundamentals: The Case of Triangular Libration Points*, volume 3. World Scientific, 2001.

[56] P. Grogono. *Advanced Computer Graphics. Lecture notes.* Concordia University, http://www.cs.concordia.ca/ ~comp676/6761notes.pdf, 2003.

[57] P. Grogono. *Getting Started with OpenGL. Supplementary Course Notes for COMP 471 and COMP 6761.* Concordia University, http://www.cs.concordia.ca/ ~comp676/gldoc.pdf, 2003.

[58] J. Guckenheimer and P. Holmes. *Nonlinear Oscillations, Dynamical Systems and Bifurcations of Vector Fields.* Springer-Verlag, 1983.

[59] G.A. Gurzadyan. *Space Dynamics. Second Edition of Theory on Interplanetary Flights.* Taylor & Francis, 2002.

[60] M. Henderson. Multiple parameter continuation: Computing implicitly defined k-manifolds. *Int. J. Bifurcation and Chaos*, 12(3):451–476, 2002.

[61] M. Hénon. *Generating Families in the Restricted Three-Body Problem. Lecture Notes in Physics. V 1,2.* Springer, 1997.

[62] J. Henrard. Concerning the genealogy of long period families at L_4. *Astronomy and Astrophysics*, 5:45–52, 1970.

[63] J. Henrard. On Brown's conjecture. *Celestial Mechanics*, 31:115–122, 1983.

[64] J. Henrard. The web of periodic orbits at L_4. *Cel. Mech. Dyn. Astron.*, 83:291–302, 2002.

[65] K. C. Howell. Families of orbits in the vicinity of the collinear libration points. *J. Astronautical Sciences*, 49(1):107–125, 2001.

[66] K. C. Howell and E. T. Campbell. Three-dimensional periodic solutions that bifurcate from halo families in the circular restricted three-body problem. *Spacecraft Mechanics AAS*, pages 1–20, 1999.

[67] A. D. Jepson. *Numerical Hopf Bifurcation.* PhD thesis, Applied Mathematics, California Institute of Technology, 1981.

[68] O. Junge, J. Levenhagen, A. Seifried, and M. Delnitz. Identification of halo orbits for energy efficient formation flying. In *Int. Symp. Formation Flying, Toulouse*, pages 1–8, 2002.

[69] P.G. Kazantzis. Families of periodic orbits in the restricted three-body problem: Sun-Jupiter case. *Astrophysics and Space Science*, 61:357–367, 1979.

[70] P.G. Kazantzis. Families of three-dimensional periodic orbits in the restricted three-body problem: Sun-Jupiter case. *Astrophysics and Space Science*, 61:477–486, 1979.

[71] H. B. Keller. Numerical solution of bifurcation and nonlinear eigenvalue problems. In P. H. Rabinowitz, editor, *Applications of Bifurcation Theory*, pages 359–384. Academic Press, 1977.

[72] W. S. Koon, M. W. Lo, J. E. Marsden, and S. D Ross. The Genesis trajectory and heteroclinic connections. In *AAS/AIAA Astrodynamics Specialist Conference*, 1999. AAS 99-451.

[73] W. S. Koon, M. W. Lo, J. E. Marsden, and S. D. Ross. Heteroclinic connections between periodic orbits and resonance transitions in celestial mechanics. *Chaos*, 10:427–469, 2000.

[74] B. Krauskopf, H. M. Osinga, E. J. Doedel, M. E. Henderson, J. Guckenheimer, A. Vladimirsky, M. Dellnitz, and O. Junge. A survey of methods for computing (un)stable manifolds of vector fields. *Int. J. Bifurcation and Chaos. Special issue commemorating the 100th anniversary of the birth of John von Neumann*, 15(3), 2005 (to appear).

[75] Yu.A. Kuznetsov. *Bifurcation Theory. Second edition.* Springer-Verlag, 1995.

[76] J. Libre, K. R. Meyer, and Solar J. Bridges between the generalized Sitnikov family and the Lyapunov family of periodic orbits. *Journal of Differential Equations*, 154:140–156, 1999.

[77] M. W. Lo, B. Williams, W. Bollman, D. Han, Y. Hahn, J. Bell, E. Hirst, R. Corwin, P. Hong, K. Howell, B. Barden, and R. Wilson. Genesis mission design. *J. Astronautical Sciences*, 49(1):169–184, 2001.

[78] K. Lust. Improved numerical Floquet multipliers. *Int. J. Bifurcation and Chaos*, 11(9):2389–2410, 2001.

[79] C. Marchal. *The Three-Body Problem.* Elsevier, 1990.

[80] A.P. Markeev. *Libration Points in Celestial Mechanics and Space Dynamics (in Russian).* Nauka, Moscow, 1978.

[81] K.R. Meyer. *Periodic Solutions of the N-body Problem.* Springer, 1999. Lecture Notes in Mathematics, volume 1719.

[82] J. Moser. *Stable and Unstable Motions in Dynamical Systems.* Princeton, 1973.

[83] F. J. Muñoz-Almaraz, E. Freire, J. Galán, E. J. Doedel, and A. Vanderbauwhede. Continuation of periodic orbits in conservative and Hamiltonian systems. *Physica D*, 181(1-2):1–38, 2003.

[84] NASA. *Press-release: Gravity Probe B Enters Science Phase, Ready to Test Einstein's Theory. Status report*, volume 04-228. 2004.

[85] D. Nesvorný and L. Dones. How long-lived are the hypothetical Trojan populations of Saturn, Uranus and Neptune. *Icarus*, 160:271–288, 2002.

[86] L.A. Pars. *A Treatise on Analytical Dynamics.* Heinemann, London, 1965.

[87] E. Perdios. Doubly asymptotic orbits at the unstable equilibrium in the elliptic restricted problem. In V.V. Markellos and Y. Kozay, editors, *Dynamical Trapping and Evolution of the Solar System*, pages 339–350. Reidel Publishing Co., 1983.

[88] E. Perdios. Non-symmetric doubly-asymptotic orbits at the outer collinear equilibrium point l3. *Astrophysics and Space Science*, 199:185–189, 1993.

[89] E. Perdios, C.G. Zagouras, and O. Ragos. Three-dimensional bifurcations of periodic solutions around the triangular equlibrium points of the restricted three-body problem. *Celestial mechanics and Dynamical Astronomy*, 51:349–362, 1991.

[90] E.A. Perdios. Asymptotic orbits and terminations of families in the Copenhagen problem. *Astrophysics and Space Science*, 240:141–152, 1996.

[91] E.A. Perdios. Asymptotic orbits and terminations of families in the Copenhagen problem. ii. *Astrophysics and Space Science*, 254:61–66, 1997.

[92] H. Poincaré. *Les Méthodes Nouvelles de la Mécanique Céleste.* Dover Publications, New York, 1957.

[93] H. Poincaré. *Selected works. In three volumes. V. 1. New Methods of Celestial Mechanics. (in Russian).* Nauka, Moscow, 1971.

[94] H. Pollard. *Celestial Mechanics.* The Mathematical Assoc. of America, 1976.

[95] P. Rademacher. *GLUI. A GLUT-based User Interface Library.* http://www.cs.unc.edu/ ~rademach/glui/, 1999.

[96] W. C. Rheinboldt. *Numerical Analysis of Parametrized Nonlinear Equations.* Wiley-Interscience, 1986. University of Arkansas Lecture Notes in the Mathematical Sciences.

[97] D. L. Richardson. Halo orbit formulation for the ISEE-3 mission. *J. Guidance and Control*, 3:543–548, 1980.

[98] J. Rodriguez-Canabal and M. Hechler. Orbital aspects of the SOHO mission design. In *Orbital Mechanics and Mission Design*, pages 347–356, 1989. AAS 89-171.

[99] A.E. Roy. *The Foundations of Astrodynamics.* The Macmillan Co., 1967.

[100] A.E. Roy. *Orbital Motion.* John Wiley & Sons, New York, 1988.

[101] R. D. Russell and J. Christiansen. Adaptive mesh selection strategies for solving boundary value problems. *SIAM J. Numer. Anal.*, 15:59–80, 1978.

[102] H. Schaub and J.L. Junkins. *Analytical Mechanics of Space Systems.* American Inst. of Aeronautic and Astronautic, Inc., 2003.

[103] R. Seydel. *From Equilibrium to Chaos. Practical Bifurcation and Stability Analysis. Second edition.* Springer-Verlag, 1995.

[104] C. Simó. New families of solutions in n-body problems. In *European Congress of Mathematics, Vol. 1 (Barcelona, 2000)*, volume 201 of *Prog. Math.*, pages 101–115. Birkhäuser, Basel, 2001.

[105] C. Simó. Periodic orbits of the planar n-body problem with equal masses and all bodies on the same path. Technical report, 2001. Departament de Matemàtica i Anàlisi, Universitat de Barcelona.

[106] C. Simó. Dynamical properties of the figure eight solution of the three-body problem. *Contemporary Mathematics*, 292:209–228, 2002.

[107] V. Szebehely. *Theory of Orbits: The Restricted Problem of Three Bodies.* Academic Press, 1967.

[108] G.V Uphoff. The art and science of lunar gravity assist. *Orbital Mechanics and Mission Design*, 69:333–336, 1989.

[109] A. Vanderbauwhede and B. Fiedler. Homoclinic period blow-up in reversible and conservative systems. *Z. Angew. Math. Phys.*, 43:292–318, 1992.

[110] F.P.J. von Rimrott. *Introductory Orbit Dynamics.* Friedr.Vieweg & Sohn, Braunschweig/Wiesbaden, 1989.

[111] L.F. Wanex. Chaotic amplification in the relativistic restricted three-body problem. *Z. Naturforsch.*, 58a:13–22, 2003.

[112] E.T. Whittaker. *A Treatise on the Analytical Dynamics of Particles and Rigid Bodies with an Inroduction to the Problem of Three Bodies. Fourth edition.* Dover Publications, New York, 1944.

[113] W.E. Wisel. *Spaceflight Dynamics.* McGraw-Hill Book Co., 1989.

[114] M. Woo, J. Neider, Davis T., and D. Shreiner. *OpenGL Programming Guide.* Addison-Wesley, 1999.

[115] C.G. Zagouras and P.G. Kazantzis. Three-dimensional oscillations generating from plane periodic ones around collinear lagrangian points. *Astrophysics and Space Science*, 61:389–409, 1979.

[116] C.G. Zagouras, E. Perdios, and O. Ragos. New kind of asymptotic periodic orbits in the restricted three-body problem. *Astrophysics and Space Science*, 240:273–293, 1996.

[117] Chenghai Zhang. *Computation and Visualization of Periodic Orbits in the Circular Restricted Three-Body Problem.* M. Comp. Sci. Thesis, Department of Computer Science, Concordia University, 2004.

Appendices

Appendix A

DR Orbits User's Manual

A.1 Product name

The name of this program is DR Orbits, a graphical tool for the visualization of the orbit families of the *Circular Restricted 3-Body Problem* calculated with AUTO.

A.2 Document overview

This document covers the installation and usage of DR Orbits. It also provides some information for troubleshooting. This **User's Manual** includes the following information:

1. Hardware and software requirements for running DR Orbits.
2. Brief description of the data used by DR Orbits.
3. Installation guide.
4. Description of the user interface with examples of using DR Orbits.

A.3 Hardware and software requirements

1. Computer Pentium III 500 GHz or higher;
2. 128 KB of operating memory (256 KB are preferable);
3. 2 GB of free hard disk space;
4. Windows XP Pro operating system.

The present version of DR Orbits was not compiled and tested for Windows 98, Windows 2000, or Windows Me, but it should work under these operating systems without essential limitations.

A *Unix/Linux version* of DR Orbits will be developed in the near future.

A.4 Data used by DR Orbits

The program shows periodic orbits of the Circular Restricted 3-Body Problem calculated with AUTO.

REFERENCES:

1. E. Doedel, R. C. Paffenroth, H. B. Keller, D. J. Dichmann, J. Galán-Vioque, A. Vanderbauwhede, *Calculation of periodic solutions of conservative system with application to the 3-body problem*, Int.Journ.of Bifurcation and Chaos, **13** (2003) 1353-1381.

2. E. J. Doedel, V. A. Romanov, D. J. Dichmann, R. C. Paffenroth, H. B. Keller, J. Galán-Vioque, A. Vanderbauwhede, *Elemental Periodic Orbits Associated with the Libration Points in the Circular Restricted 3-Body Problem(in preparation)*.

DR Orbits shows all elemental periodic orbits associated with the libration points in the Circular Restricted 3-Body Problem for the critical values of the mass ratio μ [2] listed in Table A.3).

Table A.1: The representative values of the mass ratio μ

μ	μ
0.0005	0.120
0.01215 (Earth-Moon)	0.145
0.045	0.190
0.055	0.280
0.063	0.360
0.073	0.450
0.090	

For these μ values DR Orbits can show the orbit families (if they exist for the selected μ) listed in Table A.2. The choice of above-mentioned values, and a detailed descriptions of all orbit families can be found in the papers [1, 2] and references therein.

A.5 Installation guide

0. If you have a previous version of DR Orbits on your computer, it is strongly recommended to delete it using Start → Control Panel → Add or Remove Program → Dr Orbits. If you install the new version of DR Orbits in the same directory then you need not to delete the shortcut from the desktop and the subdirectory MU.

1. Insert the CD with DR Orbits into CD-ROM driver and open it in "My Computer" window. The CD contains this manual in the file Manual.pdf. Read it carefully before installation.

2. For installation, start the program Setup.exe from the CD. You will see the Setup Wizard window (Fig.A.1).

Table A.2: Elemental periodic orbit families

The planar Lyapunov families: **L1**, **L2**, **L3**
The Vertical families: **V1**, **V2**, **V3**, **V4_V5**
The Short-period Lyapunov families: **S4**, **S5**
The Long-period Lyapunov Families: **L4**, **L5**
The Axial families: **A1**, **A2**, **A3**
The Backflip families: **B1**, **B2**, **B3**
The planar "Circular" families: **C1**, **C2**
The planar D-family: **D1**
The E-family: **E1**
The T-family: **T1**, **T2**
The S-family: **S1**, **S2**
The Halo families: **H1**, **H2**, **H3**
The K-families: **K1**, **K2**, **K3**, **K4**
The R-family: **R2**
The Long-periodic planar families: **S1l**, **S2l**, **S3l**
The W-family: **W4_W5**
The X-family: **X**

Click the button **Next** to go to the next window, where you can change the installation folder (Fig.A.2). Make necessary changes and/or click the button **Next** here and the installation program will start the installation. The program will copy all files on your computer in approximately one minute. When the installation is finished, press the **Close** button to quit the installation program.

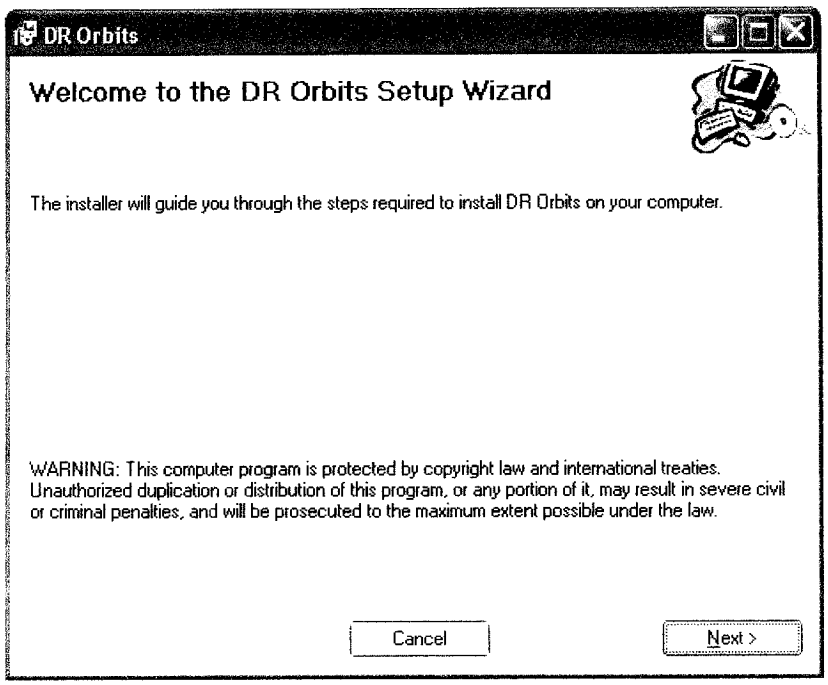

Figure A.1: Setup Wizard: Step 1

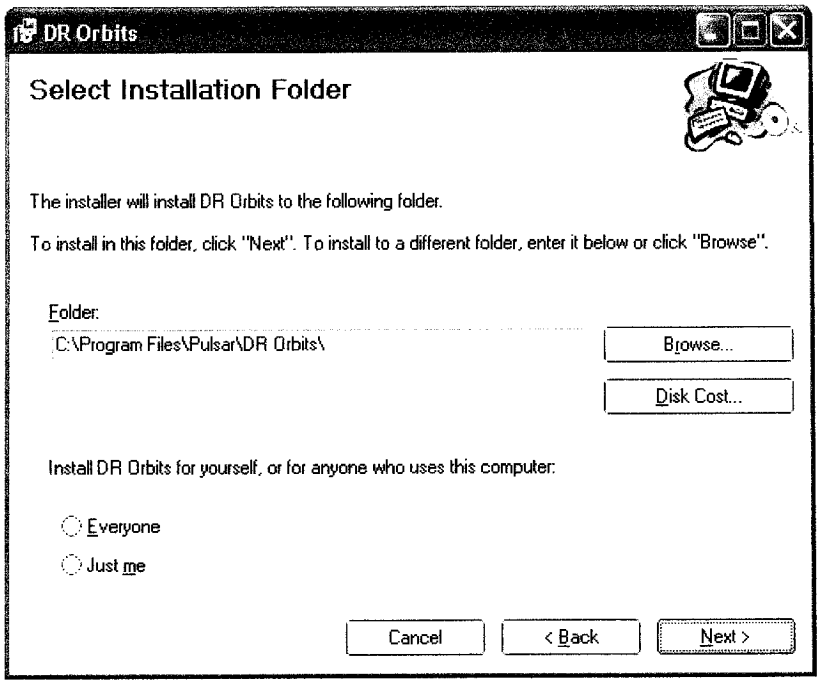

Figure A.2: Setup Wizard: Step 2

3. Create a shortcut on the desktop to the program Orbits_**.exe which will be in the directory where you have installed the program. (Two *'s in the name of the file are digits which show the version of the program you are using.)

4. Start the program.

REMOVING of DR Orbits. To remove the program from your computer, delete manually the folder MU from the directory where you installed the program. To delete the program use Start - Control Panel - Add or Remove Programs. Find the program DR Orbits and remove it. Also delete the shortcut from your desktop.

A.6 Quick start

A.6.1 Starting and stopping DR Orbits

Double-click on the program shortcut to start DR Orbits.

One can exit DR Orbits by closing the main window of the program or by clicking the **EXIT** button of the user interface window (see below).

A.6.2 Description of the DR Orbits windows

After starting DR Orbits, you will see two windows jointly in the main program window (Fig. A.3).

The white-background window on the left (we refer to it below as the diagram window) contains a three-dimensional diagram of the orbits with the two primaries

(blue and yellow spheres representing the Earth and the Moon), the coordinate axes of the rotating barycentric coordinate frame, a semi-transparent disk showing the orbit plane of the second primary orbit, and small colored cubes showing the libration points.

The gray window on the right (we refer to it below as the GUI window) contains a graphic user interface with lists, spinners, rollouts, checkboxes, and buttons.

Despite the fact that these two windows are jointed in one window of the MS Windows operating system, you have to choose one of them as the current window.

A.6.3 Using the keyboard and the mouse for operating control

There are some additional options which allow to see an orbit family. Use the **arrow keys** or **left mouse button** drag-and-drop in the left window for rotation of the diagram and **Insert/Delete** keys for scaling. Before doing this, make sure that the diagram window is the current window. To switch the current window click on it anywhere using the left mouse button. Use the **PgUp** key to show the orbits one by one. This option is useful for the choice of an orbit for the satellite mission (see below). Use the **Home** key to see a range of consecutive orbits: choose the first orbit using **PgUp**, and after that add any number of consecutive orbits by pressing the **Home** key . The **End** key restores the full diagram. By default, all orbits are drawn in a red-blue color gradient scheme: the first orbit is pure red, the last one is pure blue. If there is only one orbit in the diagram, it is always blue. Bifurcation orbits are green by default.

A.6.4 Graphical user interface

All features of the GUI (lists, spinners, rollouts, checkboxes, and buttons) (Fig. A.4, left) can be used for control of the diagram, and for changing the options and settings.

A.6.5 Choosing a μ value

Use the mu value pop-up list for the choosing the desired μ value for which you wish to see an orbit family (Fig. A.4, middle).

A.6.6 Choosing the orbit family

For each μ value there are several orbit families. Only one of these can be chosen for graphical representation. Use the Family pop-up list to choose the orbit family that you want to see (Fig. A.4, right).

By default, when the program is started, the Lyapunov orbit family **L**1 for the smallest μ value $\mu = 5.0 \cdot 10^{-4}$ is shown. After changing the μ value, the program will draw the Axial orbit family **A**1 for the new μ value.

NOTE. After changing the μ value or the orbit family, some options and settings of the program are restored to their default values.

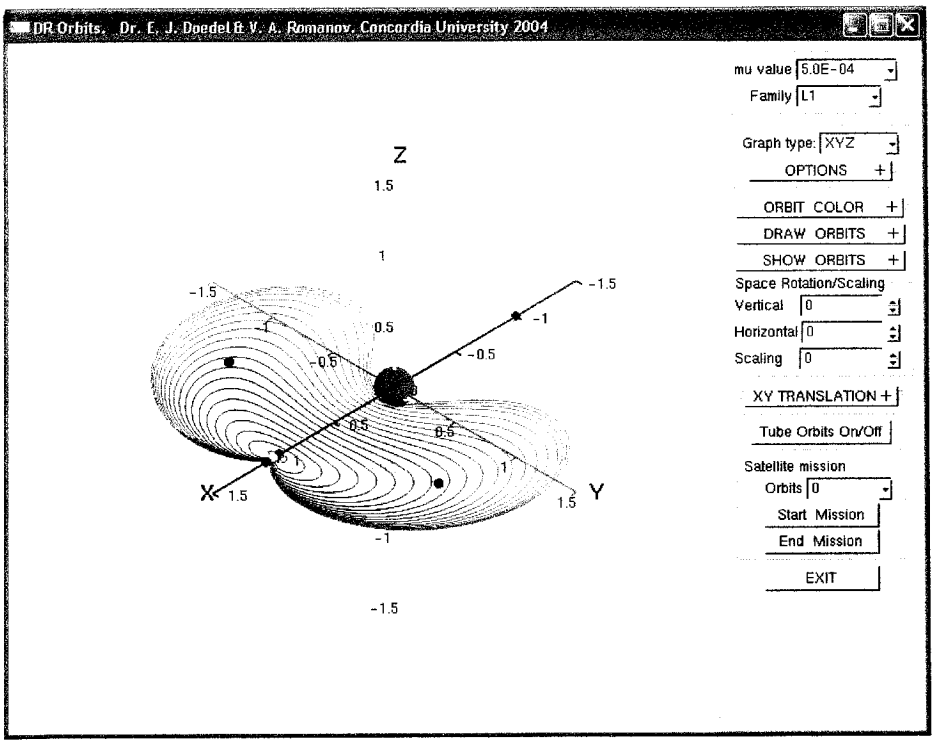

Figure A.3: The main window of the DR Orbits program.

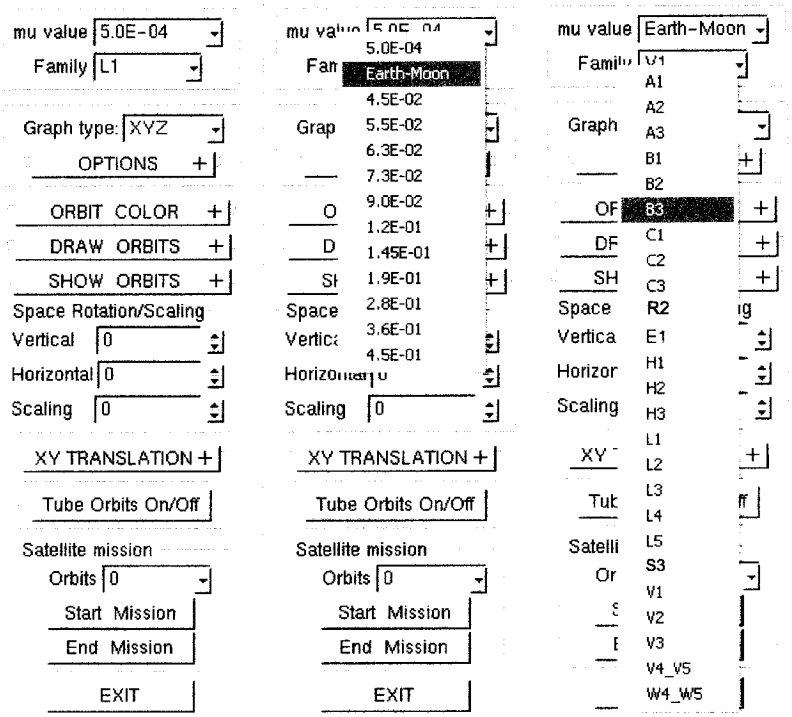

Figure A.4: The main user interface. I. *Left.* The general view. *Middle.* The list mu value for choosing of μ value. *Right.* List Family for selecting the orbit family for the chosen μ value.

A.6.7 Choosing the type of a diagram

Use the Graph type list for choosing the diagram type to be shown in the diagram window (Fig. A.8, left). The choices are

1. XYZ (by default) draws the three-dimensional diagram of the orbit family in 3D coordinate space.
2. UVW draws the three-dimensional velocity diagram for the corresponding orbit family in three-dimensional velocity space.
3. XY / XZ / YZ draws a two-dimensional projection of the coordinates of the orbit family.
4. X(t) / Y(t) / Z(t) draws the time-dependence of the corresponding coordinate for one normalized period for the orbit family.
5. UV / UW / VW draws a two-dimensional projection of the velocities of the orbit family.
6. U(t) / V(t) / W(t) draws the time-dependence of the velocity for one normalized period for the orbit family.

A.6.8 Options

The program options are chosen with the OPTIONS rollout. As an interface object, a rollout can be defined as a rolling/unrolling panel, which contains other interface objects (lists, spinners, checkboxes, buttons, etc.). If you click on a rolled rollout, it is unrolled and you can see and use its objects. A click on the unrolled rollout rolls it back. (The visible interface objects placed under the rollout are moved down when rollout is unrolled.) The OPTIONS rollout contains the following checkboxes (Fig. A.8, middle-left):

1. Black Background - if this option is checked, the background of the diagram is black. (The black or white color of the axes changes automatically if the Axes Color OFF option is checked.)
2. Stability ON - if this option is checked, the color of each orbit in the diagram is chosen according to the stability of the orbit: the "most unstable" orbits are blue, stable orbits are red, with four degrees of instability.
3. Large font - switch the size of the diagram labels.
4. Axes Labels OFF - if this option is checked, the axes labels are invisible.
5. Axes Color OFF - if this option is checked, the axes color is black for a white background and white for a black background.
6. Moon Orbit OFF, Lagrange P's OFF, Moon OFF, and Earth OFF - these options control the plotting of the Moon orbit (gray disk), the libration points, and the primaries (the Earth and the Moon) in the diagram.

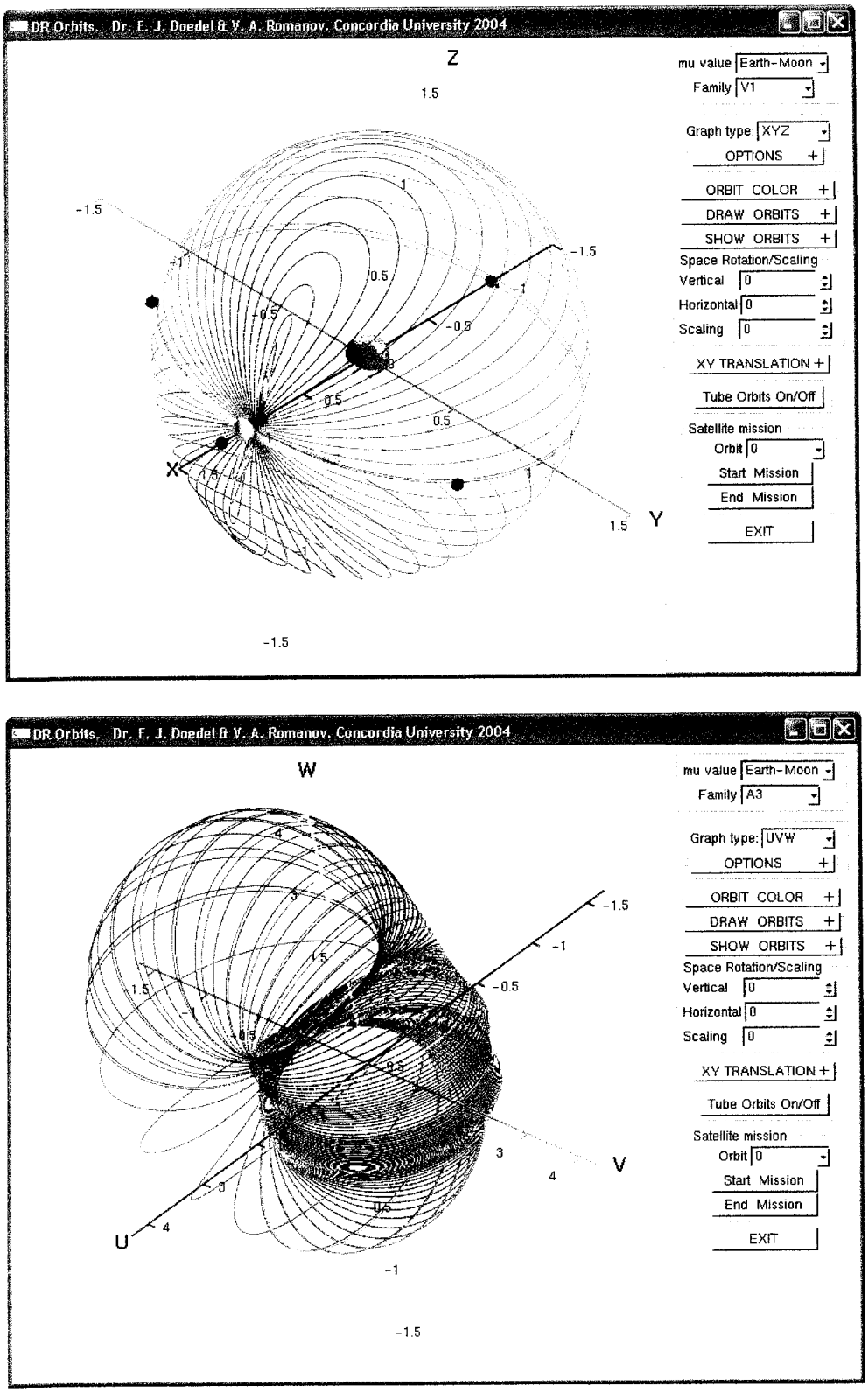

Figure A.5: An **V1** orbit family (scaled and rotated) of the Earth-Moon system in three-dimensional coordinate space (***top***), and the **A3** orbit family in three-dimensional velocities space (***bottom***).

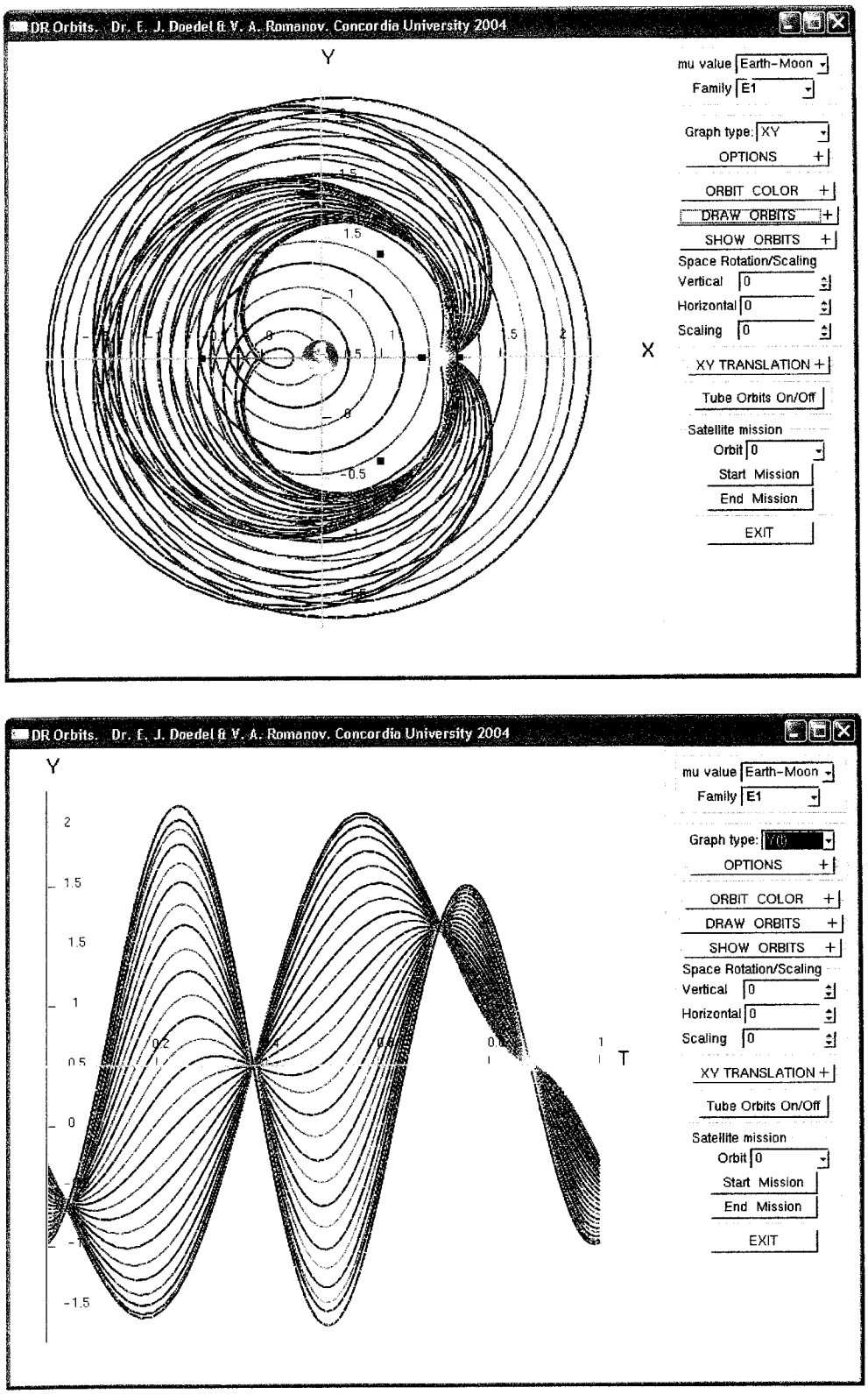

Figure A.6: The projection of the **E1** orbit family of the Earth-Moon system on the XY-plane (***top***), and the time dependence of the X-coordinate of this family (***bottom***).

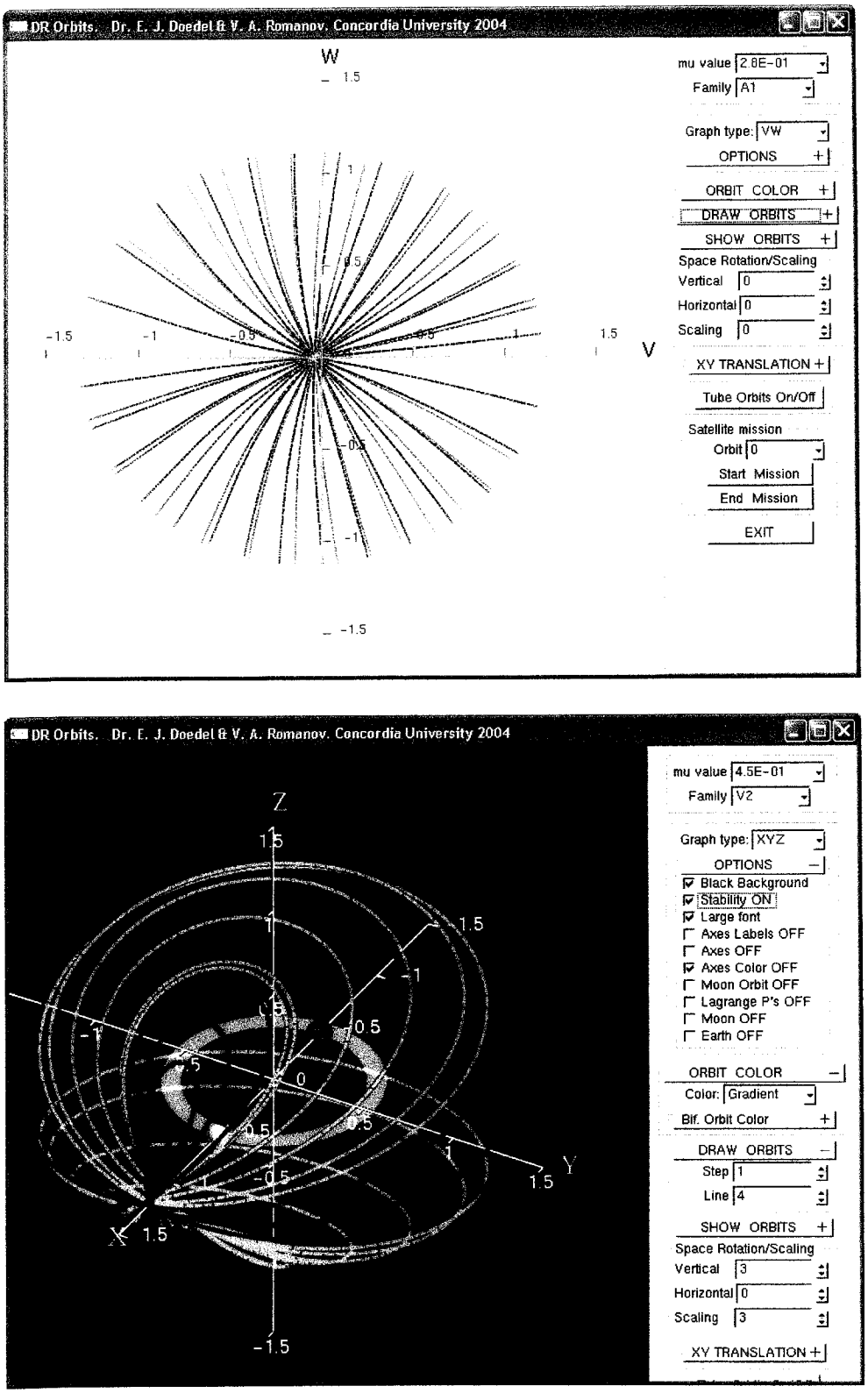

Figure A.7: The projection of the **A1** orbit family for $\mu = 0.28$ on the VW-plane of three-dimensional velocity space (***top***), and a demonstration of different options(***bottom***).

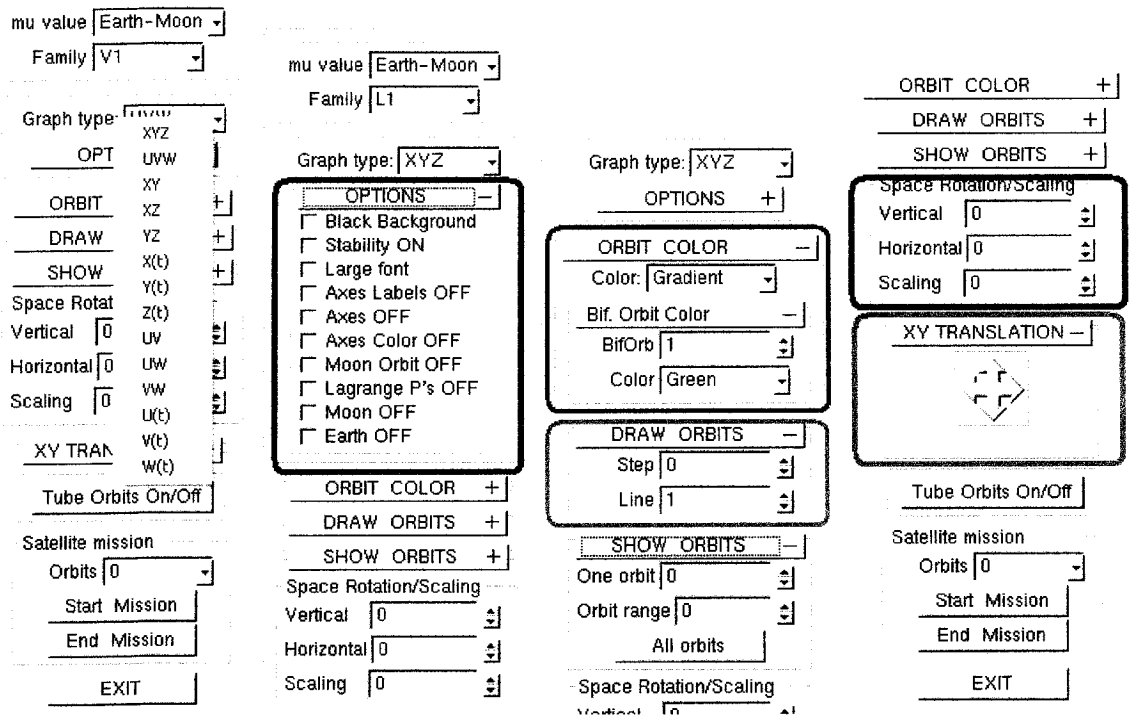

Figure A.8: The main user interface. II.

Left.

The list of the diagram types.

Middle-left.

Red rectangle: The OPTIONS expanded rollout (expandable/collapsible panel) with checkboxes switching graphical options.

Middle-right.

Red rectangle: The ORBIT COLOR expanded nested rollout containing the Color list for choosing the color of orbits on the diagram, and another Bif. Orbit Color expanded rollout which contains two items: the BifOrb spinner for choosing the number of bifurcation orbits; and the BifCol list for choosing the color of the chosen bifurcation orbit.

Blue rectangle: The DRAW ORBITS rollout contains two spinners: Step for the choice of the drawing orbits, and Line for the choice of the thickness of the lines of the diagram.

Green rectangle: The SHOW ORBITS rollout contains two spinners and one button: the One Orbit spinner for choosing one orbit which only must be plotted, the Orbit range spinner chooses the range of the orbit to plot, the All orbits button plots all orbits of the chosen family.

Right.

The Space Rotation/Scaling panel containing spinners: Vertical for rotation around vertical axis, Horizontal for rotation around horizontal axis, and Scaling for scaling of the diagram.

*Blue rectangle:*The XY TRANSLATION rollout contains translation control arrows.

Green rectangle: The Satellite Mission panel contains the Orbits list for for choosing the orbit for the satellite mission and two buttons: Start Mission and End Mission.

NOTE: Color rectangles are used only in this figure to emphasize the parts of the user interface in this picture.

A.6.9 Choosing the orbit color

By default, the orbit family is plotted using different colors: the first orbit of the family is pure red, the last one is pure blue, and the intermediate orbits are plotted using a smooth transition from red to blue. Bifurcation orbits are green by default. The ORBIT COLOR rollout (Fig. A.8, middle-right) contains the Color list, with which you can choose other colors for the orbit family.

The ORBIT COLOR rollout also contains another rollout, namely, Bif. Orbit Color which contains the BifOrb spinner, and the BifCol list. You can choose some bifurcation orbits numerated from 1 to n_{max} using the BifOrb spinner and then you can choose the color of this orbit from the BifCol list. Thus, each bifurcation orbit can be drawn in a different color. If an orbit family has no bifurcation orbit, the value of the BifOrb spinner is 0.

A.6.10 Step size and thickness of lines

By default, all the orbits of the family are plotted using the line with minimal thickness: one pixel. The DRAW ORBITS rollout (Fig. A.8, middle-right) contains the spinners: Step and Line. You can use the first of them to draw every second, third, or fourth orbit only. The spinner Line can change the thickness of the line from one to five pixels.

A.6.11 Choosing an orbit or group of orbits for graphical representation

By default, the whole orbit family is presented in the diagram. The SHOW ORBITS rollout (Fig. A.8, middle-right) contains two One orbit and Orbit range spinners, and one All orbits button. You can use the One orbit spinner to go through all the orbits: only the orbit which number is in the spinner will be shown in the diagram. The Orbit range spinner adds to a diagram a few orbits from the orbit chosen in the One orbit spinner, so you can see any group of consecutive orbits in the diagram. The All orbits button restores the default picture.

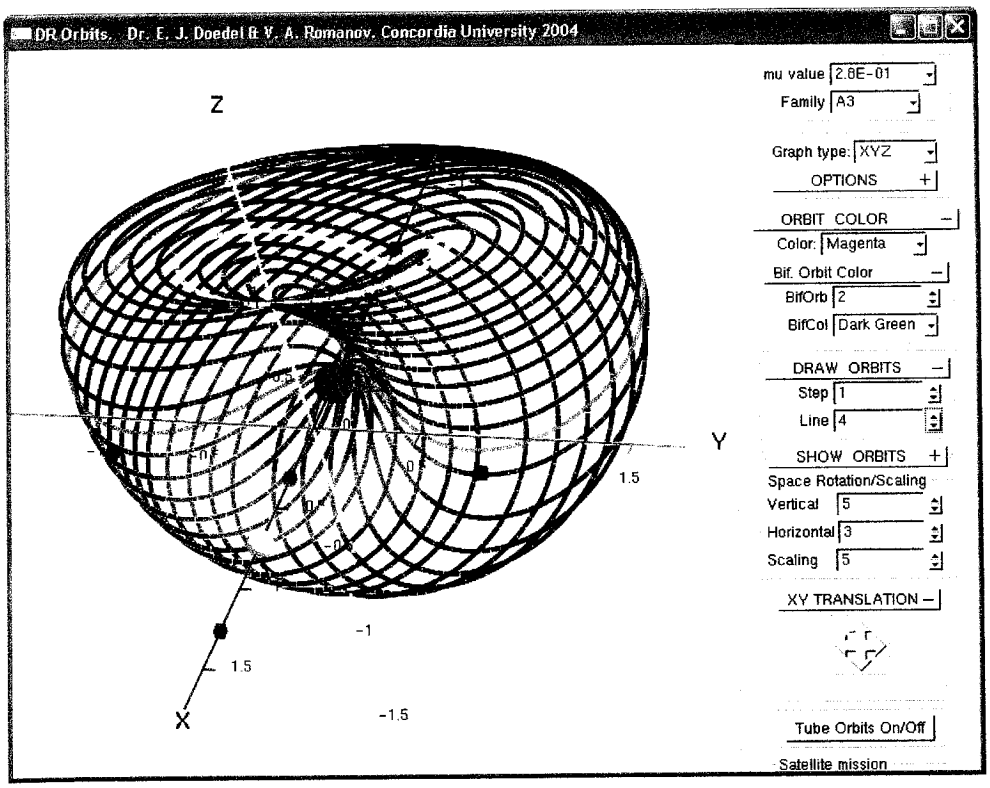

Figure A.9: Different settings for the picture of **A3** orbit family for $\mu = 0.28$.

A.6.12 Rotation and scaling

The panel Space Rotation/Scaling (Fig. A.8, right) contains three spinners: Vertical for vertical rotation of the diagram, Horizontal for horizontal rotation, and Scaling for the scaling of the picture. Step of rotation is 5^o, step of scaling is 10% for increasing and 5% for decreasing of the default picture size. All this operations could be performed using mouse and keyboard as well (See A.6.3).

A.6.13 Translation of the diagram

The XY TRANSLATION spinner (Fig. A.8, right) contains special control interface for moving of the diagram in the plane of the window. You can drag-and-drop inside of the small square with *the double-arrowed cross* and the diagram will be moved in the window plane (XY-plane).

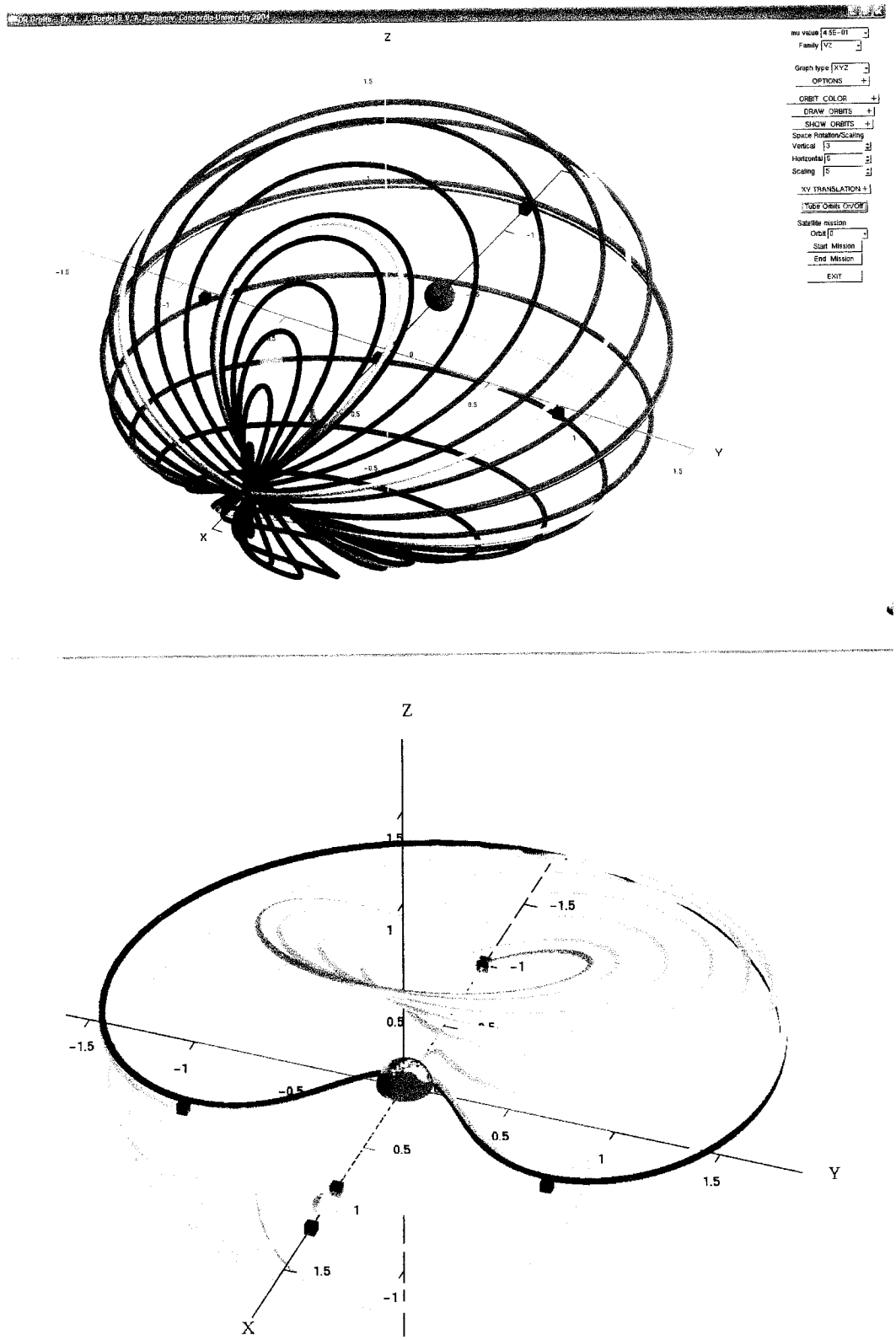

Figure A.10: Tube graphics of the **V2** orbit family for $\mu = 0.45$ (***top***), and an example of three-dimensional tube graphics saved with Paint as PNG file (***bottom***).

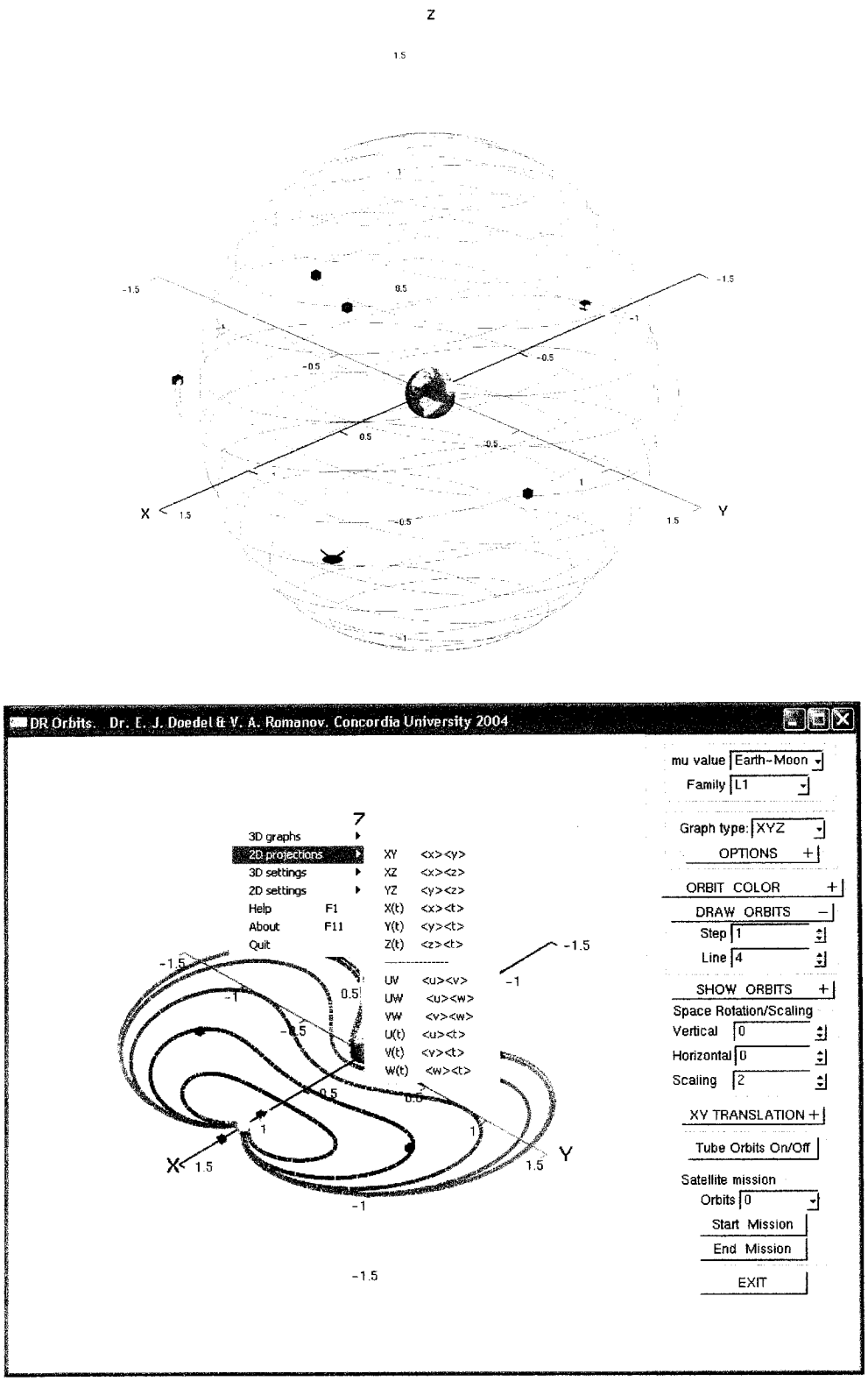

Figure A.11: an example of a satellite mission in the inertial frame of reference(***top***), and the pop-up menu (***bottom***).

A.6.14 Tube graphics

If you press the Tube Orbits On/Off button (Fig. A.8, right), the program redraws the diagram using three-dimensional tubes instead of lines. This operation requires significant processor resources and can take in one or two minutes for some complicated orbits . Thus, this final representation is best done after choosing the orbits and options. When the operation is performed, it is better to avoid any interaction with the computer, because any redrawing of the screen starts the tube operation from the beginning.

This option does not work for two-dimensional pictures.

Sometimes the program can crash during this operation. In this case, one needs to release the computer resources (close programs and processes) and start DR Orbits again.

A.6.15 Satellite missions

You can see the orbital motion of the satellite in the inertial frame of references (Fig. A.8, right). The orbit can be chosen from the list Orbits (the value from this list should coincide with the value of the spinner One orbit). This orbit will immediately be plotted in the diagram. If you press the Start Mission button, the new window will open. In this window you will see the rotating Earth, Moon, and libration points, and a moving satellite that describes the orbit in the inertial frame of reference. The mission is continued as long as the computer resources permit. The mission can be stopped at any moment using the End Mission button.

A.6.16 Saving pictures as graphics files

Unfortunately, DR Orbits has no abilities to save a drawn picture as a graphic file. Use **Alt-Print Screen** to put the whole window into the copy-paste Windows buffer (or any screen grabber) and any graphic editor like Paint to process the picture and save it in a graphic format of your choice.

A.6.17 Additional features

The graphical user interface is doubled by the **F2** - **F11** functional keys.

F2 - switches background color white(by default)/black.

F3 - switches on/off(by default) stability option.

F4 - switches axes of the coordinate system and has three states: - axes at origin (by default); - axes in the corner of the picture; - no axes. For two-dimensional pictures this options has also three states.

F5 - switches step for the drawing of the orbit family:

F6 - switches thickness of the orbits, with 5 gradations.

F7 - switches the colors of coordinate axes: color or black for white background; color or white for black background.

F8 - switches the color scheme of an orbit family except for bifurcation orbits: gradient color scheme from red to blue (by default); nine other schemes.

F9 - goes through bifurcation orbits consecutively, and is used to choose one of them for changing its color.

F10 - changes the color of the chosen bifurcation orbit in accordance with 10 defined colors.

F11 - switches the lines/three-dimensional tubes graphics.

A.6.18 Pop-up menu

Click on the picture window using the left mouse button for appearance of pop-up menu (Fig. A.11 and Table A.3).

Most of the menu items are doubled by keys or key combinations and their actions were described above. Some additional menu items have no corresponding keys or key combinations and permit to switch on/of drawing of primaries (the Moon and the Earth), the semi-transparent disk (the Moon orbit) or libration points (Lagrange points).

Table A.3: The pop-up menu of DR Orbits

Menu item	Submenu items	Key or key combinations
3D graphs		
	XYZ	**do**
	UVW	**ds**
	XY	**xy**
	XZ	**xz**
	YZ	**yz**
	X(t)	**xt**
	Y(t)	**yt**
	Z(t)	**zt**
	UV	**uv**
	UW	**uw**
	VW	**vw**
	U(t)	**ut**
	V(t)	**vt**
	W(t)	**wt**
3D Settings		
	Background White/Black	**F2**
	Stability Off/On	**F3**
	Frame 1/2/3	**F4**
	Orbit Step 1/2/4..	**F5**
	Line Width (pixels)	**F6**
	Frame Axes Color/Monochrome	**F7**
	Orbits color scheme 1..10	**F8**
	Choice of Bifurcation Orbit	**F9**
	Color of Bifurcation Orbit	**F10**
	Tube Orbits	**F11**

	Moon orbit On/Off	
	Lagrange points On/Off	
	Moon On/Off	
	Earth On/Off	
2D Settings		
	Stability Off/On	**F3**
	Frame 1/2/3	**F4**
	Orbit Step 1/2/4..	**F5**
	Line Width (pixels)	**F6**

	Moon orbit On/Off	
	Lagrange points On/Off	
	Moon On/Off	
	Earth On/Off	
Help		**F1**
About		**F12**
Quit		

A.6.19 Brief help

If you press **F1** functional key, you can see in the separate black DOS window the short help of DR Orbits as below:

```
*****************************************************************
* DR Orbits program HELP *
*****************************************************************
* MAIN WINDOW:
* Arrow keys or left mouse button drag&drop - rotation.
* Insert/Delete - scaling -/+.
* PgUp - goes trough each single orbit/choose orbit.
* Home - shows the range of orbits.
* End - shows all the orbits of the family.
* Right mouse button - main pop-up MENU.
*---------------------------------------------------------------
* FUNCTIONAL KEYS:
* F1 - shows program help.
* F2 - switches background color (black/white) for 3D picture.
* F3 - shows stability of different orbits using colors.
* F4 - switches frames.
* F5 - changes steps to show orbits.
* F6 - changes line width for orbits.
* F7 - changes color of axes.
* F8 - changes color scheme of orbits.
* F9 - chooses bifurcation orbit.
* F10 - changes color of chosen bifurcation orbit.
* F11 - draws orbits as 3D tubes.
* F12 - shows info about the program.
* SOME OF THESE OPTIONS ARE DOUBLED IN THE MENU ITEMS
* 3D Options and 2D Options.
*---------------------------------------------------------------
* KEYS COMBINATIONS: SWITCH PICTURE/PROJECTION
* Press two keys one after another:
* do - 3D orbits in XYZ space.
* ds - 3D velocities in phase UVW space.
* xy - 2D orbits projection on XY plane.
* xz - 2D orbits projection on XZ plane.
* yz - 2D orbits projection on YZ plane.
* uv - 2D velocities projection on UV plane.
* uw - 2D velocities projection on UW plane.
* vw - 2D velocities projection on VW plane.
* xt - shows X(t).
* yt - shows Y(t).
* zt - shows Z(t).
* ut - shows U(t).
```

```
* vt - shows V(t).
* wt - shows W(t).
* ALL THESE ABILITIES ARE DOUBLED IN THE MENU ITEMS
*-------------------------------------------------------------
* Use lists from the panel to choose mu value, orbits family
* and single orbits to see mission in the system
* when the Moon(2nd primary) is rotating around the Earth/(1st).
* (Orbit can be chosen using PgUp key as well)
* Click Start mission to see the mission and End mission
* to stop mission.  Use arrow keys for rotating the picture in
* mission window.
* Attention!  You need to be careful about which window is
* the current window.  To avoid unpredictable behavior of the
* program switch the windows by mouse click.
*************************************************************
* DR Orbits program HELP *
*************************************************************
```

Appendix B

How to use AUTO 2000 for solving the CR3BP

B.1 Description of the AUTO 2000 files r3b.c, c.r3b and s.start

The CR3BP AUTO demo files can be found in the directory auto/2000/demos/r3b/. There are three subdirectories under it. Demo files for the Earth-Moon system are in the subdirectory em. Demo files for the Sun-Earth system are in the subdirectory se. Demo files for the Sun-Jupiter system are in the sub-directory **sj**. Each other subdirectory contains similar files.

The file r3b.c defines the differential equations of the CR3BP and defines AUTO parameters. Here is a listing of r3b.c:

```
/*----------------------------------------------------------------------*/
/*----------------------------------------------------------------------*/
/*---- The restricted 3-body problem: periodic solutions----------*/
/*----------------------------------------------------------------------*/
/*----------------------------------------------------------------------*/
#include        "auto_f2c.h"
/*----------------------------------------------------------------------*/
int func (integer ndim, const double *u, const integer *icp,
          const double *par, integer ijac, double *f, double *dfdu,
          double *dfdp)
{
        double x, y, z, xp, yp, zp, dE, dM, dE3, dM3, p, mu, mc;
        int i;

        x  = u[0];      y  = u[1];      z  = u[2];
        xp = u[3];      yp = u[4];      zp = u[5];

        mu = par[1];
        p  = par[2];
```

```
        dE = sqrt((x+mu)*(x+mu) + y*y + z*z);
        dM = sqrt( (x-1+mu)*(x-1+mu) + y*y + z*z );
        mc = 1 - mu;
        dE3 = 1/(dE*dE*dE);
        dM3 = 1/(dM*dM*dM);

        f[0] = xp;
        f[1] = yp;
        f[2] = zp;
        f[3] =  2*yp + x - mc*dE3*(x+mu) - mu*dM3*(x-1+mu);
        f[4] = -2*xp + y - mc*dE3*y      - mu*dM3*y;
        f[5] =           - mc*dE3*z      - mu*dM3*z;

        f[3] += p*xp;
        f[4] += p*yp;
        f[5] += p*zp;

        return 0;
} /*============================================================*/
/*============================================================*/
int pvls (integer ndim, const double *u, double *par) {
  extern double getp();
  double x, y, z, xp, yp, zp, d1, d2, mu, U, E, det;

        mu = par[1];
        x  = getp("BV0", 1, u);
        y  = getp("BV0", 2, u);
        z  = getp("BV0", 3, u);
        xp = getp("BV0", 4, u);
        yp = getp("BV0", 5, u);
        zp = getp("BV0", 6, u);

        d1 = sqrt((x+mu)*(x+mu) + y*y + z*z);
        d2 = sqrt( (x-1+mu)*(x-1+mu) + y*y + z*z );

        U = (x*x + y*y)/2 + (1-mu)/d1 + mu/d2;
        E = (xp*xp + yp*yp + zp*zp)/2 - U - mu*(1-mu)/2;
        par[3] = E;

        det     = getp("BIF", 1, u);
        par[4]  = log10(10+abs(det)) * atan(det);
        par[5]  = getp("STA", 1, u);
        par[21] = getp("INT", 1, u);
        par[22] = getp("INT", 2, u);
        par[23] = getp("NRM", 3, u);
```

```
        return 0;
}
/*======================================================*/
/*======================================================*/
int stpnt() {} int bcnd () {} int icnd () {} int fopt () {}
/*======================================================*/
/*======================================================*/
```

Function func() defines the equations, and function pvls() defines calculated parameters of the problem (Table. B.1). Other functions are not used in calculations.

Table B.1: Parameters defined in the file r3b.c

Parameter	Description
par[1]	the μ value (mass ratio)
par[2]	the unfolding parameter λ
par[3]	the energy (Jacoby constant) E
par[10]	the period T
par[21]	$\int_0^1 x(t)\ dt$
par[22]	$\int_0^1 y(t)\ dt$
par[23]	$\sqrt{\int_0^1 z^2(t)\ dt}$

The file c.r3b contains which are needed for the calculations. The structure of this file and a role of each constant are described in details in the **AUTO 2000 Guide** (E.J. Doedel, R.C. Paffenroth, A.R. Champneys, T.F. Fairgrieve, Yu.A. Kuznetsov, B.E. Oldeman, B. Sandstede, X. Wang *AUTO 2000: Continuation and bifurcation software for ordinary differential equations (with HomCont)*, 2000, available from http://www.aem.caltech.edu/~redrod/auto2000/distribution/). Here, we only describe a few parameters, namely those that play an important role in calculations for the CR3BP.

The parameter IRS (first line) is the label of the starting point for the calculations. Its values containing in the starting file are presented in Table B.2. The value of this label can be changed by the command cc("IRS", Label), where Label is an integer number - the label of bifurcation point (see below).

The parameter NTST (third line) is the number of mesh intervals. To obtain more accurate results for some orbit families, especially near abnormal terminations, one may need to increase this parameter up to 100 - 500. The calculation time will increase accordingly.

```
6 2 11 0                NDIM,IPS,IRS,ILP
7 2 10   21 22 3 4      5NICP,(ICP(I),I=1,NICP)
50 4 3 3 -1 15 0 0      NTST,NCOL,IAD,ISP,ISW,IPLT,NBC,NINT
300 -1e9 1e9 -3 3       NMX,RL0,RL1,A0,A1
 10 -5 2 15 5 3 0       NPR,MXBF,IID,ITMX,ITNW,NWTN,JAC
1e-8 1e-8 1e-4          EPSL,EPSU,EPSS
1e-2 1e-5 2e-2 1        DS,DSMIN,DSMAX,IADS
1                       NTHL,((I,THL(I)),I=1,NTHL)
10 0 0
0                       NTHU,((I,THU(I)),I=1,NTHU)
3                       NUZR,((I,UZR(I)),I=1,NUZR)
```

The parameter ISW is equal to -1, if we want to go switch to a new orbit family from a bifurcation orbit: it is the case of "branch switching". If ISW = 1, we can continue to go along the same orbit family (no "branch switching").

The parameter NMX defines the maximum number of the steps, *i.e.*, maximum number of orbits we want to compute (the calculation may finish earlier in case of abnormal termination). For the small continuation step size (parameter DS) the value of NMX may need to be increased.

The parameter NPR defines the step size for orbit calculations. If NMX is large, the value of NPR could be in the rang 25 - 50.

Parameters DS, DSMIN, DSMAX define the value of pseudo-arclength step size. For some orbit families, especially abnormally terminated, the values DS and DSMAX may need to be decreased in 5 - 10 times.

The AUTO 2000 starting file can be generated automatically by the program stgen (E. Doedel, V. Romanov). This program calculates for any selected input μ value ($0 \leq \mu \leq 0.5$) coordinates of all libration points, all eigenvalues, and starting periods

Table B.2: Labels of starting points used in the AUTO file c.r3b.. Labels 41, 43, and 51, 53 does not exist for $\mu \geq 0.03852089$.

Label	Libration point	Orbit family
11	L1	**L1**
12	L1	**V1**
21	L2	**L2**
22	L2	**V2**
31	L3	**L3**
32	L3	**V3**
41	L4	**L4**
42	L4	**V4**
43	L4	**S3**
51	L5	**L5**
52	L5	**V5**
53	L5	**S3**

for each existing family of orbits arising from each libration point for this μ value. The program can be started as: stgen mu ext, where mu is any real number representing μ value and ext is the extension of the starting file: it will be named as s.ext.

B.2 Some AUTO2000 commands

Here we describe briefly a sequence of actions and corresponding **AUTO 2000** commands used for the Circular Restricted 3-Body Problem. How to install and start **AUTO 2000** is described in above-mentioned **AUTO 2000** guide.

It is better to copy the files `r3b.c`, `c.r3b` and `s.start` into a special separate directory. The program Orbit_4.exe can be also copied in this directory. If we want to start with the orbit family **L1** we need to be sure that the parameter IRS of the file `c.r3b` is equal to 11.

Start the calculations with the sequential AUTO 2000 commands:

load("r3b", c="r3b")

load(s="start")

run()

On the Linux System Monitor, a brief summary of the calculations will be printed:

```
 BR    PT  TY LAB    PAR(2)      L2-NORM U(3)     PERIOD       PAR(21)     ...
-11     3      54   1.43046E-14   0.00000E+00  2.692090E+00  8.369559E-01 ...
-11    10  BP  55  -1.37474E-15   0.00000E+00  2.743033E+00  8.406718E-01 ...
-11    20      56   1.36952E-12   0.00000E+00  3.301425E+00  8.704122E-01 ...
-11    25  BP  57   1.75486E-11   0.00000E+00  3.950086E+00  8.890280E-01 ...
-11    30      58  -1.26545E-10   0.00000E+00  4.877751E+00  8.992548E-01 ...
-11    40      59   9.44442E-12   0.00000E+00  6.354205E+00  8.810780E-01 ...
-11    50      60  -1.64688E-09   0.00000E+00  7.091095E+00  8.331280E-01 ...
-11    60      61  -3.39537E-09   0.00000E+00  7.385340E+00  7.682688E-01 ...
-11    70      62  -2.35269E-08   0.00000E+00  7.450533E+00  6.919871E-01 ...
-11    80      63  -5.37535E-08   0.00000E+00  7.394414E+00  6.084152E-01 ...
-11    90      64  -1.39024E-07   0.00000E+00  7.272618E+00  5.220438E-01 ...
-11   100      65  -2.48596E-07   0.00000E+00  7.118165E+00  4.379401E-01 ...
-11   110      66  -6.52471E-07   0.00000E+00  6.953890E+00  3.610491E-01 ...
-11   120      67  -2.21016E-06   0.00000E+00  6.863585E+00  3.224062E-01 ...
-11   130      68  -2.45289E-06   0.00000E+00  6.844038E+00  3.143288E-01 ...
-11   140      69  -2.48997E-06   0.00000E+00  6.824740E+00  3.064488E-01 ...
-11   148  MX  70  -1.13452E-06   0.00000E+00  6.811366E+00  3.010420E-01 ...

 Total Time    6.532E+00
r3b ... done
```

The complete results of the calculation are saved in three temporary files: fort.7, fort.8, fort.9. The command

save("L1")

saves them permanently in the files: b.L1, d.L1, and s.L1. To see the picture we

can use the Red Hat command to start Orbit_4.exe:

./Orbit_4 s.L1

(Fig. B.1). As can be seen, this orbit family has two bifurcation orbits marked **BP** (branch point). The bifurcation orbits have the numbers **55** and **57**.

Figure B.1: Linux variant of DR Orbits: Program Orbits_4 used for plotting of the results of calculation. This program was compiled under Linux Red Hat 9.0. I.

If we want to calculate the orbit family that bifurcates from the **BP** with label 57 we need to load the saved file s.L1 as the starting file with the AUTO 2000 command

load(s="L1")

and change the starting point **11** by the number of bifurcation orbit **57** using AUTO 2000 command

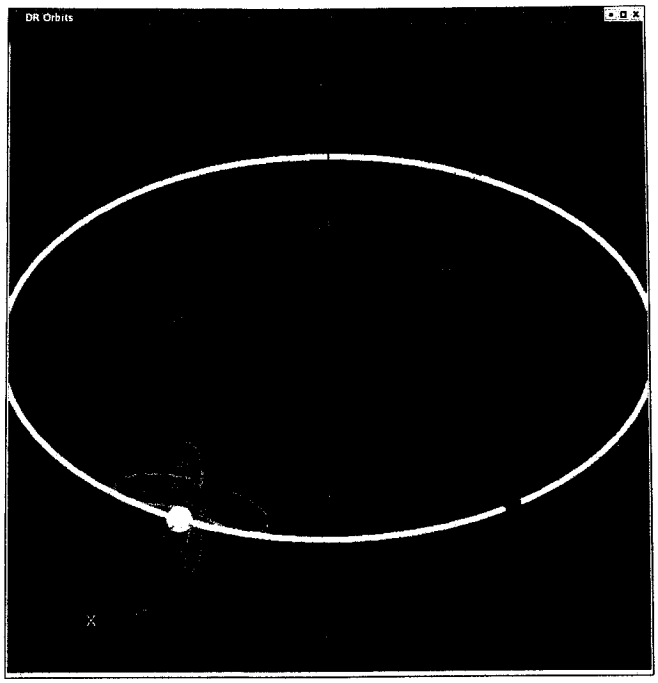

Figure B.2: Lighted variant of DR Orbits: Program Orbits_4 used for plotting of the results of calculation. II.

cc("IRS",57)

After that we can start the calculation of the new orbit family by the run() command. If we save our new orbit family using save("A1") we can see this family with the command ./Orbit_4 s.A1 (Fig. B.2). After that we can calculate the orbit family that bifurcates from the BP 55 of the family L1 and from the BP's of the new families, and so on.

We can also continue our calculation of **L1** trying to obtain a few orbits after previous **MX 70** point. For this continuation we need to change the file c.r3b as follows:

- ISW = 1;
- NTST = 150;

- DS = 5E-3, DSMAX 1E-2

and repeat the commands

```
load("r3b", c="r3b)
```

```
load(s="start")
```

```
run()
```

The additional orbits (saved in temporary files fort.*) can be appended to the previously saved files b.L1, d.L1, and s.L1 using command

```
app("L1")
```

Now we need to relabel the orbits so they will be numbered connectively:

```
rlb("L1")
```

To see the new labels use the command

```
llb("L1")
```

The above-described commands are sufficient for practical calculations of the most of the orbit families described in Chapter 4. The average time for an orbit family is about half a minute or even less, undoubtably a merit of the numerical method described in Chapter 3. For a graphical representation of the solutions one can also use the new AUTO 2000 graphic tool Plaut04. (See: Chenghai Zhang *Computation and Visualization of Periodic Orbits in the Circular Restricted Three-Body Problem*, M. Comp. Sci. Thesis, Concordia University, 2004.)